THE UNIVERSITY OF HULL

DESIGN OF NOISE ATTENUATING DEVICES INCORPORATING ELASTIC POROUS STRUCTURES

being a Thesis submitted for the degree of Doctor of Philosophy

in the University of Hull

by

Haydar Aygun, MSc

February/2006

Abstract

The deflection of a non-porous (aluminium) plate has been theoretically and numerically studied for clamped and simply supported boundary conditions. Measurements of the deflection of poroelastic plates subject to mechanical vibration have been made and the results compared with predictions based on previously published theory. The agreement between measurements and predictions is fairly good. The radiation impedance matrix has been defined, and computed including direct terms and cross-coupling terms. Three vibroacoustic indicators of porous and non-porous plates have been calculated. To extend previous work, the effects of fluid loading on the vibration of rectangular, clamped, porous, elastic plates and on their radiated sound power are considered. This requires an extra term in the equations of the plate vibration, corresponding to the additional external force acting on the plate. For vibrating rectangular plates, fluid-structure coupling is a very complex phenomenon since the plate modes are coupled by the fluid.

Two contributions have been made to studies of the usefulness of poroelastic plates for noise control in ducts containing mean flow. Measurements of the acoustic insertion loss of poroelastic plates with different perforations, mounted transversely across a flow duct, are presented. The insertion losses of two such poroelastic plates are compared to those of a similar but non-porous plate. It is demonstrated that the insertion losses of the porous and non-porous plates are very similar without mean airflow but slightly different in the presence of air flow. The sound transmission loss of a porous plate mounted in the flow duct and separated from the walls by an air cavity is calculated from sound pressure measurements in flow duct. The results show that introduction of air flow increases the transmission loss and shifts the maximum in the TL to lower frequency. Introducing the air flow in the flow duct has been found to increase the plate deflection.

Finally, a porous plate has been tested in a large impedance tube to investigate the effects of structural vibration and sound radiation from a porous plate on its acoustic surface impedance. The resonant frequencies observed in the surface acoustic impedance are close to those predicted by the theory of the deflection of poroelastic plates which in turn are close to those observed in the measured deflection spectrum.

Acknowledgements

Firstly, I would like to thank to my parents and brothers for their financial support and encouragement, right from the days of college study. I would like to thank to my wife, Fulya, for all the love and encouragement that she has given to me and for giving birth to our baby, Ronas. I would like to thank to my supervisor, Professor Keith Attenborough, for his guidance during the preparation of this Thesis, and his support during PhD study. I would like to thank to my co-supervisors, Professor Alan Cummings, and Dr P. Leclaire for their important assistance. I would also like to thank to Dr Q. Qin and Dr H. Shin for their help with using equipment in Laboratory. I would like to thank Professor Kirill V. Horoshenkov of the University of Bradford for his many useful suggestions.

Finally thanks go to the E.P.S.R.C for their financial support through grant number GR/R43761.

Table of Notation

a	dimension of the plate in direction x
A_D	area of the test section in the duct rig
Amn	unknown coefficient of plates
a_m	frequency parameter
b	dimension of the plate in direction y
B^2	Prandtl number
b_n	frequency parameter
c	shape factor
c_o	speed of sound in air
c_p	complex sound speed in the porous plate
D	flexural rigidity
d	diameter of the hole
E	Young's modulus
ε	velocity transfer coefficient
$F(x, y, t)$	excitation force
f_c	cut-off frequency
Fmn	expansion coefficients
(f_{mn})	vector of excitation force
$G(x,y,0;x',y',0)$	Green function
g	gravitational acceleration, 9.81 m/s^2
h	thickness of the plate
$H_0^{(1)}$	Hankel function of the first kind of order zero
H	measured transfer function of the two microphone signals corrected for microphone response mismatch

Δh_{ij}	difference of head measured in terms of the fluid flowing
$H(w)$	Hamilton's operator
IL	insertion loss of the plate
$\lfloor K_{mnpq} \rfloor$	stiffness matrix
k_p	complex wave number of the porous plate
K	bulk modulus for the air in the porous material
$\overline{L}_{pI}$	spatial average sound pressure level in the frequency band in the test duct, when the test silencer is installed
$\overline{L}_{pII}$	spatial average sound pressure level in the frequency band in the test duct, when the silencer out
M	Biot's elastic coefficients
$m(\omega)$	frequency dependent mass parameter
m_{dry}	dry mass
m_{wet}	wet mass
$\lfloor M_{mnpq} \rfloor$	mass matrix
n_m	number of measurements
P_a	atmospheric pressure
$P(x,y,0,t)$	surface acoustic pressure
P_0	stagnation pressure
P_r	reflected sound pressure
ΔP	pressure difference between two surfaces in the fluid
(p_{mn})	pressure difference in the fluid between two surfaces
P_S	sound pressure on the source side
P_{st}	static pressure

P_t	transmitted sound pressure
q	external force applied on the plate
Q_{ij}	volume flow rate in the duct
R	distance between vectors
r_b	reflection coefficient of the receiver side of the plate
R_c	complex reflection coefficient for plane waves
S	surface area of the plate
T	kinetic energy of the plate
t_0 and t_1	arbitrary times
V	strain energy
v	Poisson's ratio
v_f	spatially averaged velocity of the hole on the plate
V_{ij}	velocity of the flow in the duct
$\bar{v}_m$	mean particle velocity
v_p	velocity of a perforated plate
w	fluid solid relative displacement in the pores
$\ddot{w}$	second order derivatives of the fluid solid relative displacement in the pores
ω	angular frequency of the plate
$W_{excitation}$	work done by the excitation force
W_{fluid}	work due to fluid loading
ω_{ij}	correction factor
$\lvert W^s_{mn} \rvert$	magnitude of solid lateral displacement
$[W_{mn}]$	magnitude of the fluid-solid relative displacement

w_s	plate lateral displacement
$\ddot{w}_s$	second order derivatives of the plate lateral displacement,
$X_r(x)$	beam function
χ_1	specific acoustic admittance of the source side of the plate surface
χ_2	specific acoustic admittance of the receiver side of the plate surface
$Y_n(y)$	beam function
Z_a	acoustic impedance of the fluid half-space
Z_{in}	front specific acoustic impedance of the plate
$\lfloor Z_{mnpq} \rfloor$	radiation impedance matrix
Z_p	characteristic impedance of the porous plate
Zs	normalized acoustic impedance at the front surface of the porous medium
Z_0	impedance of the hole on the plate
α	Biot's elastic coefficients
α_{abs}	absorption coefficient of the plate
α_∞	tortuosity
γ	fluid specific heat ratio
∇	vector operator
λ	ratio of perforation
η_0	air viscosity
ρ	density of the solid-fluid mixture
ρ_0	air density
ρ_f	density of the fluid

ρ_m	density of water, 10^3 kg/m^3
ρ_p	effective density of the fluid in porous plate
ρ_s	mass density
ϕ	porosity
Λ	characteristic dimension for viscous forces
Λ'	characteristic dimension for thermal forces
λ_0	wave length

TABLE OF CONTENTS

INTRODUCTION

Porous plates can be used in applications such as silencers, fuselage structures in the aeronautical industry or double-wall building structures. Clamped porous plates can be used also as sound absorbers in air conditioning ducts. Vibration of porous plates is important in the study of fluid-solid interactions where porous plates are used as sound absorbers.

A brief description of the classical theory of the vibrating plate is given in Chapter 1. The responses of the clamped and simply supported porous and non-porous plates have been calculated at different locations. The deflections of clamped poroelastic plates have been measured and compared to predictions for poroelastic plates and to predictions for a rectangular clamped aluminium plate.

Calculations of the radiation efficiency, the mean square velocity, and the radiated sound power from rectangular, clamped, porous plates and from a rectangular, simply supported, aluminium plate are reported in Chapter 2. In addition, the radiation impedance matrix has been calculated by using the basic equation without interpolation, convergence and without reducing the quadruple integral to a double integral. The results presented here are similar to those obtained by others but have been obtained with less computational demands.

The effects of fluid loading on the vibration of the rectangular, clamped, porous plate and on the radiated sound power are investigated in Chapter 3. The fluid-structure coupling is very complex in the case of the rectangular plates where the plate modes are coupled by the fluid. The effect of fluid loading can be incorporated by inserting an extra term in the equations of plate, corresponding to an additional external force acting on the plate. This leads to the calculation of radiation impedance matrices with non-negligible cross terms. A Gaussian quadrature scheme with 20 terms of the Legendre polynomial has been used to compute the fluid loaded plate deflection. To the author's

knowledge this Thesis presents the first theoretical investigation of the effects of the fluid loading on the vibration of porous elastic plates.

The effects of inserting a perforated porous plate on the uniformity of flow and sound absorption in a duct containing mean flow are studied in Chapter 4. To the author's knowledge, this is the first such investigation to have been made. These effects have been assessed by measurements at different locations in the duct. The plate is assumed to be governed by the clamped rectangular porous plate theory. The measured insertion loss of porous plate in the absence of mean air flow has been compared to predictions. The normal incidence absorption coefficient of a perforated poroelastic plate has been calculated.

Measurements of the sound transmission loss of a porous plate mounted on a wall of a flow duct are presented in Chapter 5. The aim is to investigate the effectiveness of introducing a porous plate into the flow duct for attenuating noise. The plate was separated from the walls by an air cavity to allow bending vibration. It was excited by lateral components of the air flow and by an acoustic plane waves. The sound transmission loss has been calculated from sound pressure measurements made at several locations in a flow duct. The results show that the introduction of air flow increases the transmission loss and shifts the maximum in the TL to lower frequency. Introducing the air flow in the flow duct has been found to increase the plate deflection. To the author's knowledge this is the first such investigation.

A large impedance tube has been built to study the effects of frame vibration on the acoustic properties of poroelastic plates. Calibrations have been carried out for three different configurations of the empty impedance tube with a rigid backing and are reported in Chapter 6. The aim of these calibrations was to determine the variation of the relative pressure with distance (in the x direction) at the plane wave frequency and at the standing wave frequency, and also, to confirm plane waves in the duct.

Measurements of the absorption coefficient and the acoustic surface impedance have been carried out in the large impedance tube and are reported in Chapter 7. These have allowed exploration of the effects of structural vibration and sound radiation from a porous panel on its surface impedance. The data for the absorption coefficient and the surface impedance of poroelastic plates exhibit obvious resonances. The resonance frequencies observed in the surface acoustic impedance are close to the theoretical and experimental values for the deflection of poroelastic plates. However the results reported here are different from those obtained by others. These differences might be because the result of different clamping conditions, or the use of a different length air gap or the use of an impedance tube made of different material.

Chapter 1

VIBRATION OF POROUS AND NON-POROUS PLATES

1.1 INRODUCTION

A number of works on the vibrating plates have been carried out. Most of these works are based on the investigation of behaviours of non-porous plates. The vibration of elastic porous structures has become an important subject in the study of noise control, in the aeronautical industry and in the study of fluid-solid interactions. Theodorakopoulos and Beskos [1] and Leclair [2, 3, 4] have studied vibrations of porous plates rigorously. Theodorakopoulos and Beskos have described the vibration of porous plates by two coupled equations which are based on Biot's stress-strain relations [5, 6] and which introduce two types of compressional waves ('fast' and 'slow') and a shear wave. They assumed that the thickness of plate is smaller than the wavelength and that interaction can take place between the slow waves and the bending waves in the plate. They also ignored the amplitude of the fast wave. Leclaire has applied Galerkin's variational methods to porous plates where a classical set of trial functions obtained from the linear combination of trigonometric and hyperbolic functions is chosen. This method can be applied for any boundary condition such as clamped, simply supported and free. An overview of the classical theory of plates can be found in Szilard's book [7]. Leissa [8] has presented comprehensive and accurate analytical results for the free vibration of rectangular plates. D. Young [9] has solved the equations for non-porous plates by the Ritz method.

In the present chapter a brief description of the classical theory of the vibrating plate is given. The responses of the clamped and simply supported porous and non-porous plates have been calculated at different locations. The deflection of clamped poroelastic

plates has been measured and compared to predictions, and the deflection of rectangular clamped aluminium plate.

1.2 VIBRATION OF NON-POROUS PLATES

A thin, baffled rectangular plate of dimension a x b and uniform thickness h, excited by a force density $F(x, y, t)$ is considered. The geometry of the plate is shown in Figure 1.1. The equation of dynamic equilibrium for non-porous plates is deduced from Leclaire [2] and Rayleigh [10];

$$D\nabla^4 w_s + \rho_s h \ddot{w}_s = \begin{Bmatrix} 0, \ free \ \ vibration \\ F(x,y), forced \ \ vibration \end{Bmatrix} \qquad (1.1, a, b)$$

Where w_s is the plate deflection, $\ddot{w}_s$ is the second order derivative of the plate deflection, $D = Eh^3/12(1-v^2)$ is the flexural rigidity, $\nabla^4 = \nabla^2(\nabla^2)$ and $\nabla^2 = \partial^2/\partial x^2 + \partial^2/\partial y^2$ in the system of coordinates *(x, y)* with x and y parallel to the plate sides of length a and b respectively, ρ_s is the mass density, E is Young's modulus, and v is Poisson ratio. w_s [7] is given by:

$$w_s(x, y) = \sum_{m=0}^{\infty} \sum_{n=0}^{\infty} A_{mn} \ X_m(x) Y_n(y) \qquad (1.2)$$

Where A_{mn} is the unknown coefficients to be determined, $m, n = 0, 1, 2, 3$ ..... and X_m and Y_n are the beam functions in x and y direction respectively.

An appropriate trigonometric function for vibrating beams will be used for X_m and Y_n. For simply supported plates, the beam functions are $X_m(x) = \sin(m\pi x/a)$, and $Y_n(y) = \sin(n\pi y/b)$ which must satisfy the equations of equilibrium. The boundary conditions for simply supported edges of the plate are $w = 0, \frac{\partial^2 w}{\partial x^2} = 0$, for $x = 0$ and $x = a$

and $w = 0, \frac{\partial^2 w}{\partial y^2} = 0$, for $y = 0$ and $y = b$. The shape of each mode of vibration of plate can be determined from Equation (1.2) by knowing the relative values of A_{mn} and the values of X_m and Y_n functions. In the static and dynamic analysis, Function $F(x, y)$ is expanded into sine series of variables x, y, by using the equation below [7];

$$F(x,y) = \sum_{m=0}^{\infty}\sum_{n=0}^{\infty} F_{mn} \sin(m\pi x / a) \sin(n\pi y / b). \tag{1.3}$$

where F_{mn} are the expansion coefficients. By inserting (1.2) and (1.3) into (1.1), we can obtain that:

$$A_{mn} = F_{mn} / [D\nabla^4 - \omega^2 \rho_s h] \tag{1.4}$$

where ω is the angular frequency of the plate.

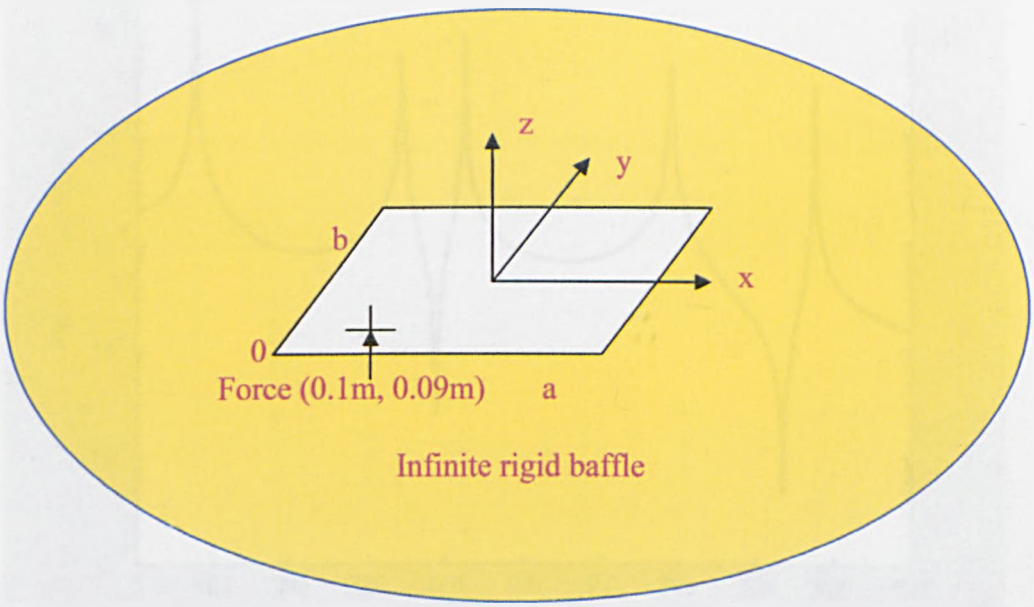

Figure1.1: The geometry of a baffled plate.

1.3 NUMERICAL RESULTS FOR NON-POROUS PLATES

1.3.1 Simply supported non-porous plate

Definitions, boundary conditions, frequency equations and eigenfunctions of simply supported, clamped and free edges of the plate can be found in [7]. A simply supported,

baffled, rectangular aluminium plate is excited by a point force applied at $x_0 = 0.08$ m, and $y_0 = 0.07$ m from a corner of the plate. The responses are calculated at the locations given by $x = 0.24$ m and $y = 0.21$ m, $x = 0.15$ m and $y = 0.15$ m, $x = 0.30$ m and $y = 0.30$ m, respectively. The magnitude of the force is 1 N. The properties of the plate are given in the Table1.1. The vibration response of the plate is measured in the 0-1000 Hz frequency range.

Table1.1: Properties of the aluminium plate

Length (m)	Width (m)	Thickness (m)	Density (kg/m3)	Young's Modulus (Pa)	Loss Factor	Poisson Ratio
0.48	0.42	0.00322	2680	6.6×10^{10}	0.005	0.33

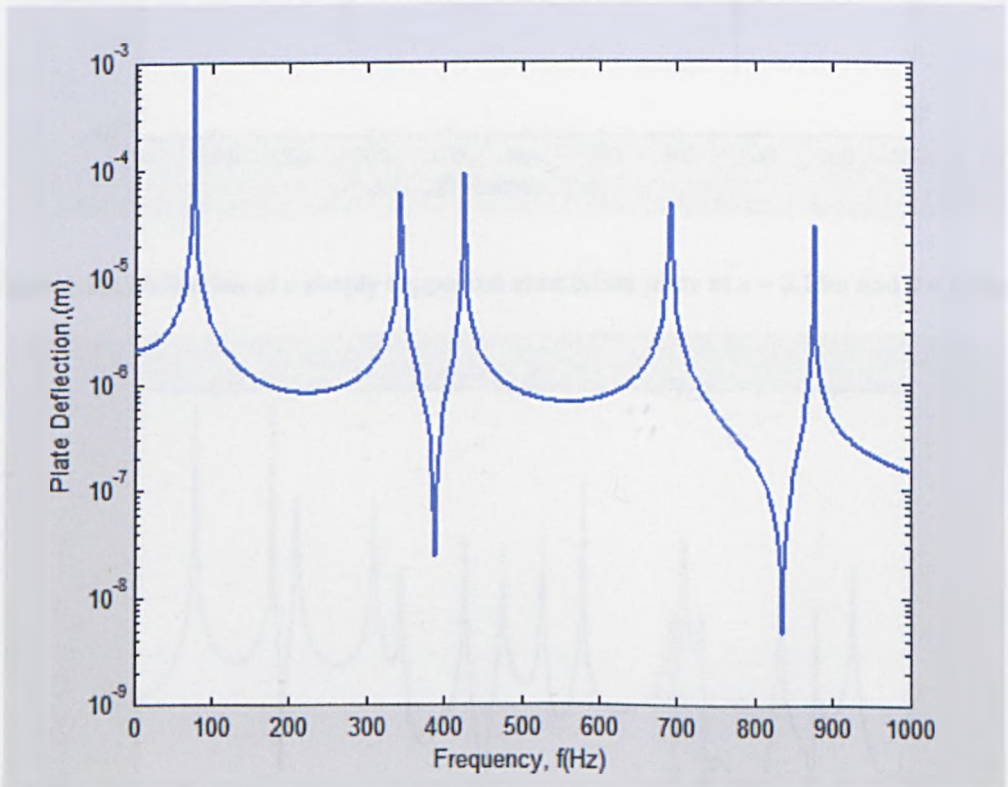

Figure1.2a: Deflection of a simply supported aluminium plate at $x = 0.24$m and $y = 0.21$m.

The curves in Figure1.2 are calculated for values of *(m, n)* up to 30. The vibration responses of a simply supported, aluminium plate plotted against frequency are shown in Figures1.2a, b, c. There are five resonant frequencies in Figure1.2a, and fifteen resonant frequencies in Figure1.2b, c. The first resonance frequency is at about 76.92 Hz for the responses at three different locations. The second resonant frequency is at

about 342.65 Hz for the response at the centre of the plate. The second resonant frequency for the response at the locations given by $x = 0.15$ m and $y = 0.15$m, $x = 0.30$ m and $y = 0.30$ m respectively is shifted to a lower frequency, and is at about 176.82Hz.

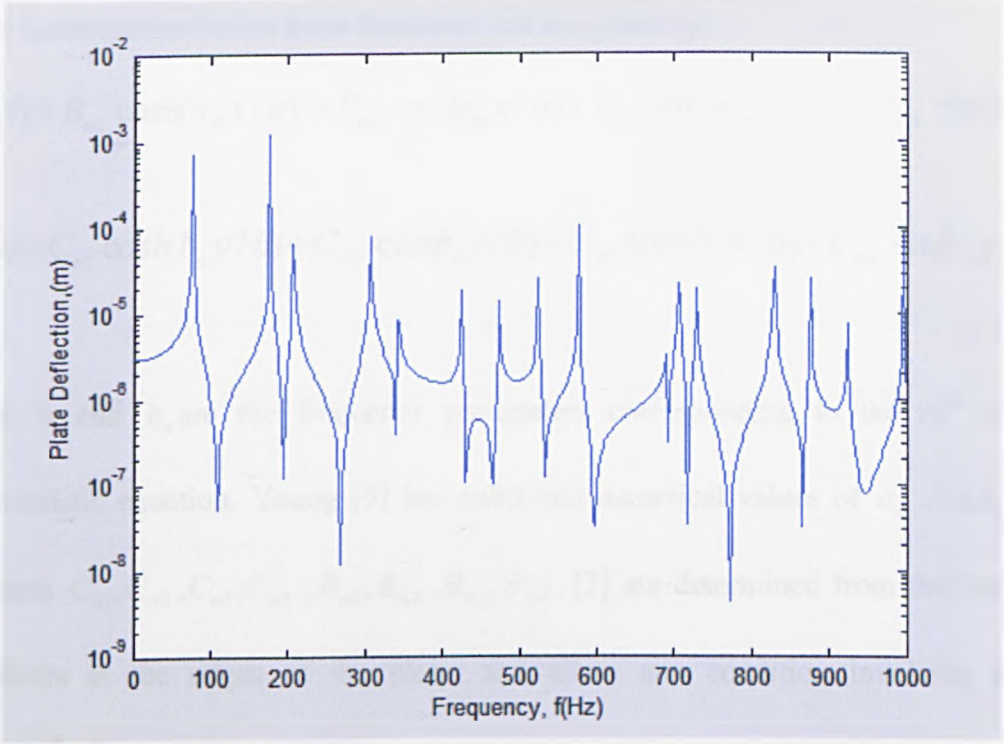

Figure1.2b: Deflection of a simply supported aluminium plate at $x = 0.15$m and $y = 0.15$m

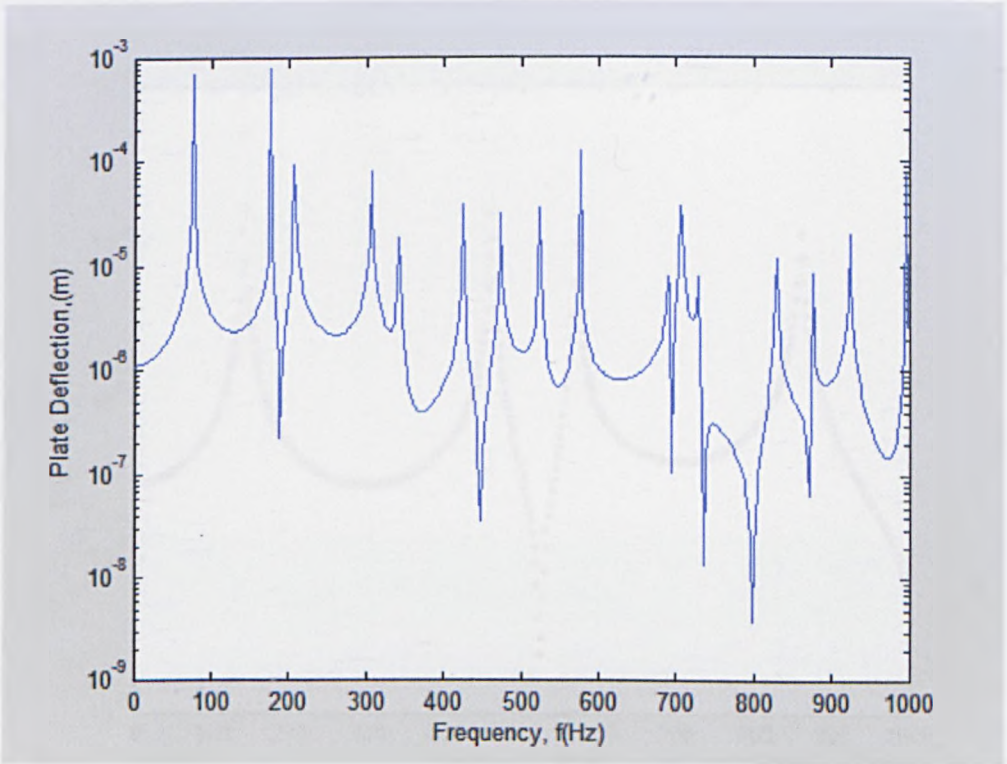

Figure1.2c: Deflection of a simply supported aluminium plate at $x = 0.3$m and $y = 0.3$m

1.3.2 Clamped non-porous plate

Figures1.3a, b, c. show the vibration response of a rectangular aluminium plate clamped along all edges. Trigonometric functions have been used to expand the plate deflection. These functions are called beam functions and are given by;

$$X_m(x) = B_{m1}\cosh(a_m x/a) + B_{m2}\cos(a_m x/a) + B_{m3}\sinh(a_m x/a) + B_{m4}\sin(a_m x/a)$$

$$Y_n(y) = C_{n1}\cosh(b_n y/b) + C_{n2}\cos(b_n y/b) + C_{n3}\sinh(b_n y/b) + C_{n4}\sin(b_n y/b)$$

(1.5-a, b)

where a_m and b_n are the frequency parameters corresponding to the mth and nth characteristic equation. Young [9] has published numerical values of a_m and b_n. The constants $C_{n1}, C_{n2}, C_{n3}, C_{n4}, B_{m1}, B_{m2}, B_{m3}, B_{m4}$ [7] are determined from the boundary conditions at the edges of the plate, and allow any condition involving simply supported, clamped or free edges.

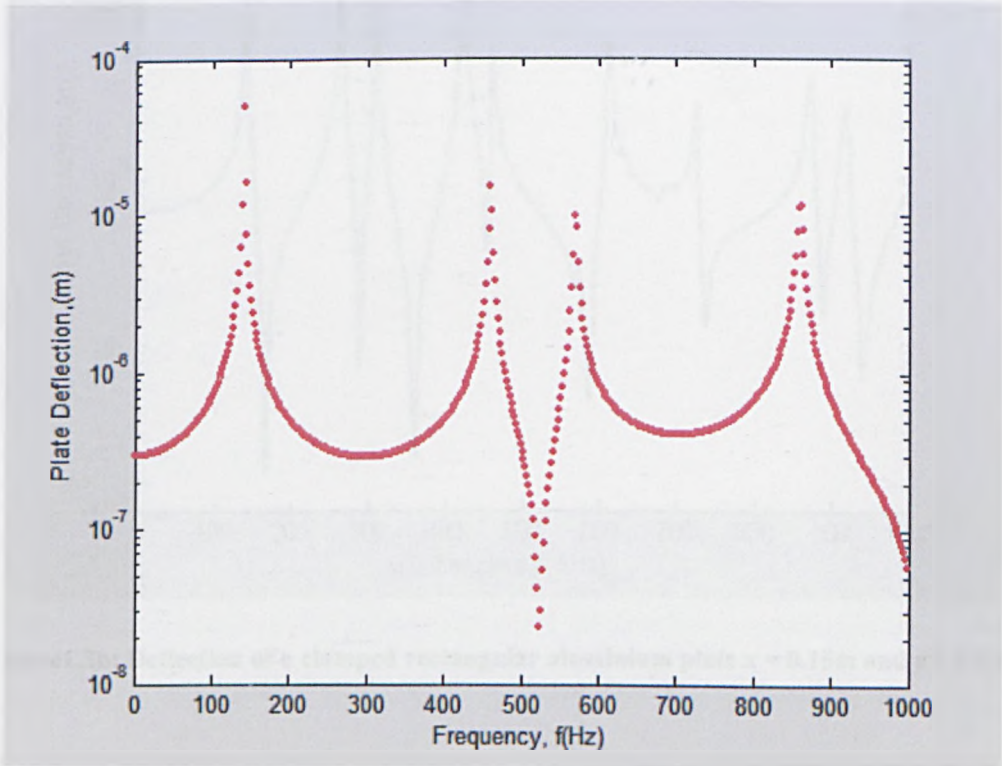

Figure1.3a: Deflection of a clamped rectangular aluminium plate at x = 0.24m and y = 0.21m

Deflections of a clamped rectangular aluminium plate at the different locations of the plate are shown in Figure1.3 (a, b, c). A clamped aluminium plate is excited by a point force, 1N, applied at x_0 = 0.08 m, and y_0 = 0.07 m from a corner of the plate. The responses are calculated at the locations given by x = 0.24m and y = 0.21m, x = 0.15m and y = 0.15m, x = 0.30m and y = 0.30m, respectively. The curves in Figure1.3 (a, b, c) are calculated for values of (m, n) up to 30. The first resonant frequencies at the locations given above for the clamped plate are at 140.86 Hz. The second resonant frequency at the middle of the clamped plate is at 460.54 Hz. The second and third resonant frequencies at the locations closer to the edges of the clamped plate are at 264.73 Hz and 310.69 Hz. The number of resonant frequencies obtained at the middle of the plate is less than obtained at the locations closer to the edges of the plate.

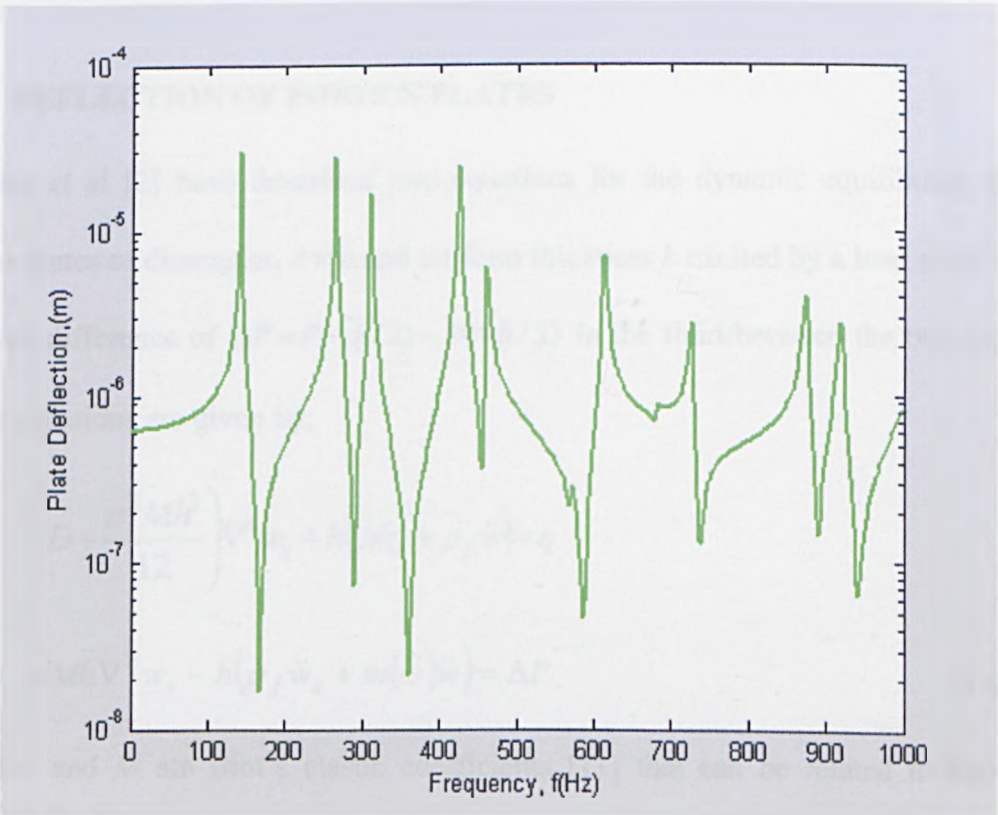

Figure1.3b: Deflection of a clamped rectangular aluminium plate x = 0.15m and y = 0.15m

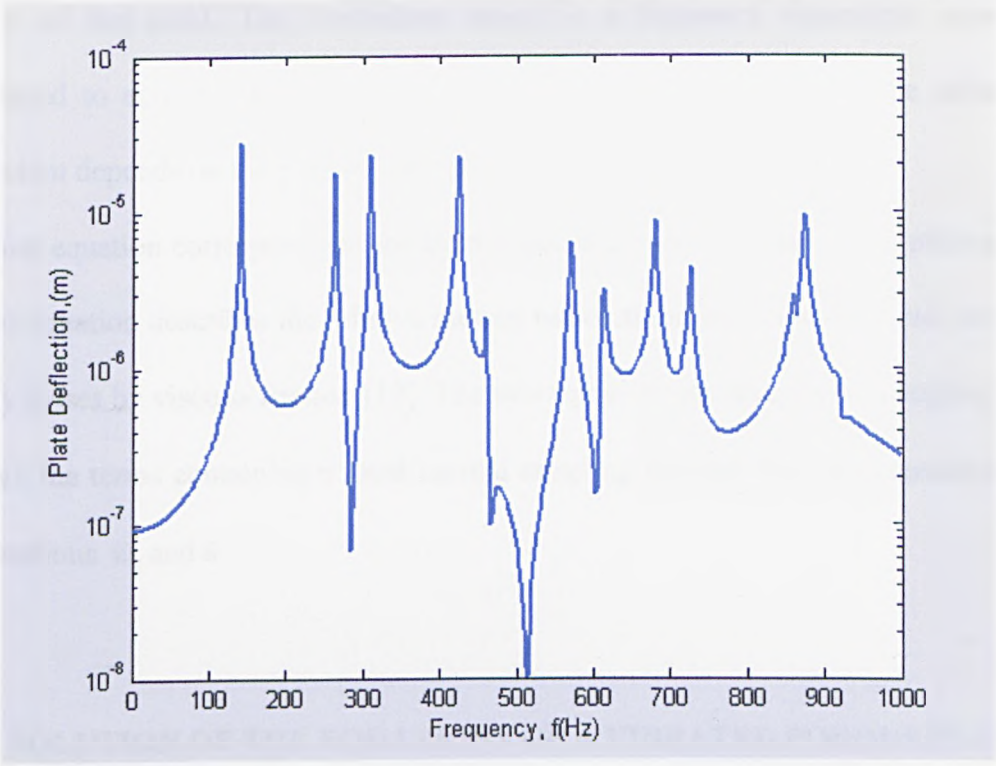

Figure1.3c: Deflection of a clamped rectangular aluminium plate $x = 0.30$m and $y = 0.30$m

1.4 DEFLECTION OF POROUS PLATES

Leclaire et al [2] have described two equations for the dynamic equilibrium of thin porous plates of dimension $a \times b$ and uniform thickness h excited by a load q and with a pressure difference of $\Delta P = P(-h/2) - P(+h/2)$ in the fluid between the two surfaces. These equations are given by;

$$\left(D + \frac{\alpha^2 M h^3}{12}\right)\nabla^4 w_s + h\left(\rho \ddot{w}_s + \rho_f \ddot{w}\right) = q$$

$$\alpha M h \nabla^2 w_s - h\left(\rho_f \ddot{w}_s + m(\omega)\ddot{w}\right) = \Delta P \qquad \text{(1.6-a, b)}$$

where α and M are Biot's elastic coefficients [11] that can be related to known or measurable elastic constants, w is the fluid solid relative displacement in the pores, $\ddot{w}$ is the second order derivatives of the fluid solid relative displacement in the pores, ρ is the density of the solid-fluid mixture, ρ_f is the density of the fluid and ρ_s is the

density of the solid. The coefficient $m(\omega)$ is a frequency dependent mass [12] introduced to account for the viscous friction between the fluid and the solid. This coefficient depends on the porosity, the permeability and the tortuosity.

The first equation corresponds to the instantaneous elastic response of the plate and the second equation describes the relative motion between the solid and the fluid, including energy losses by viscous friction [13]. The two equations involve elastic coupling factor through the terms containing α, and inertial coupling through the terms containing the accelerations $\ddot{w}_s$ and $\ddot{w}$.

1.5 SOLUTION OF THE EQUATIONS OF A VIBRATED POROUS PLATE

In this part we are going to use the variational method of solution developed by Leclaire et al [3]. The eigenfunctions and their derivatives satisfy the orthogonality requirement. After insertion into equation (1.6-a, b), the solutions can be written as:

$$\sum_{r=1}^{\infty}\sum_{n=1}^{\infty}\left(W_{rn}^{s}\left[\left(D+\frac{\alpha^2 M h^3}{12}\right)\left(I_1 I_2+2I_3 I_4+I_5 I_6\right)-h\rho\omega^2 I_2 I_6\right]\right.$$

$$\left.-W_{rn}h\rho_f\omega^2 I_2 I_6\right)=\sum_{r=1}^{\infty}\sum_{n=1}^{\infty}Q_{rn}I_2 I_6$$

$$\sum_{r=1}^{\infty}\sum_{n=1}^{\infty}\left(W_{rn}^{s}\left[\alpha M h\left(I_2 I_3+I_4 I_6\right)+h\rho_f\omega^2 I_2 I_6\right]\right. \qquad \text{(1.7-a, b)}$$

$$\left.+W_{rn}hm(\omega)\omega^2 I_2 I_6\right)=\sum_{r=1}^{\infty}\sum_{n=1}^{\infty}\Delta P_{rn}I_2 I_6$$

Where (I_1)-(I_6) are the definite integrals:

$$I_1=\int_0^a X_r^{(IV)}(x)X_r(x)dx,\ I_6=\int_0^a X_r(x)X_r(x)dx,\ I_3=\int_0^a X_r^{(II)}(x)X_r(x)dx \qquad \text{(1.8. a,b,c)}$$

$$I_5=\int_0^b Y_n^{(IV)}(y)Y_n(y)dy,\ I_2=\int_0^b Y_n(y)Y_n(y)dy,\ I_4=\int_0^b Y_n^{(II)}(y)Y_n(y)dy \qquad \text{(1.8. d,e,f)}$$

where $X_r(x)$ and $Y_n(y)$ are the beam functions which are given by equation (1.5.a,b). The exponents *(IV)* and *(II)* denote the fourth and second order derivatives, respectively. By solving equation (1.7.a, b) for *r, n modes,* the coefficients W_{rn}^s and W_{rn} can easily be found. Once we find the coefficients W_{rn}^s and W_{rn}, the deflection of porous plates can be calculated by;

$$w_s(x,y) = \sum_{r=1}^{\infty}\sum_{n=1}^{\infty} W_{rn}^s X_r(x).Y_n(y)$$

$$w\ (x,y) = \sum_{r=1}^{\infty}\sum_{n=1}^{\infty} W_{rn} X_r(x).Y_n(y) \qquad \text{(1.10.a, b)}$$

For a simply supported plate, the integrals take a simple form and a solution similar to Navier's algebraic solution [7] for a porous plate [1] is obtained.

The coefficients Q_{rn} and P_{rn} [3] correspond to the external exciting forces. For a load F_0 concentrated at one point (x_0, y_0) of the solid surface (obtained with the help of a shaker for example), the forces $Q_{rn}.I_2I_6$ and $P_{rn}.I_2I_6$ appearing in equation (1.7.a, b) are respectively equal to $F_0 X_r(x_0).Y_n(y_0)$ and *0*. Detailed derivations for Q_{rn} and P_{rn} can be found in reference [14].

1.6 NUMERICAL RESULTS FOR POROUS PLATES

The deflections of three rectangular, clamped, porous plates (G foam, YB10 foam and Coustone) [3] have been computed by using the Gaussian quadrature scheme with 20 terms in the Legendre polynomial. G foam and YB10 foam are fabricated from particles of plastic foam obtained from recycled car dashboard. The Coustone plate contains flint particles with a mean grain size of about 1 mm and an epoxy rubber binder. These clamped porous plates are considered to be excited by a point force, 1N, applied at x_0 =

0.08 m, and $y_0 = 0.07$ m from a corner of the plate. The responses are calculated at the centre of the plates. The curves in Figures1.4, 1.5 and 1.6 are calculated for values of (r, n) up to 16.

The characteristics of the plates taken from [3] are given in Table1.2. The computed shapes of the plate deflection are given in Figures 1.4, 1.5 and 1.6 for G foam, YB10 foam and Coustone, respectively, as a function of the frequency. The resonant frequencies are much affected by the Poisson ratio, the Young's modulus, and the porosity of the porous plates than the other characteristics of porous plates. The first and second resonant frequencies of G foam, YB10 foam, and Coustone are at 10 Hz, and 34 Hz, 20 Hz, and 74 Hz, 46 Hz, and 166 Hz, respectively.

Table1.2: Characteristics of porous plates

	G foam	**YB10**	**Coustone**	**Y foam**
Lx (m) in x direction	0.5	0.5	0.9	0.5
Ly (m) in y direction	0.5	0.5	0.5	0.5
Thickness (m)	0.011	0.0107	0.0115	0.01
Density, $\rho(\text{kg}/m^3)$	348	353	1295	960
Young's modulus, (Pa)	$4\text{x}10^6$	$2.1\text{x}10^7$	$3.4\text{x}10^8$	$29\text{x}10^6$
Loss factor	0.15	0.1	0.15	0.07
The Poisson ratio, ν	0.35	0.35	0.35	0.4
Porosity, ϕ	0.74	0.69	0.36	0.57
Tortuosity, τ_∞	1.2	1.2	1.8	1.4
Permeability, $\kappa(m^2)$	7.0×10^{-10}	2.7×10^{-10}	4.3×10^{-10}	$1.2\text{x}10^6$

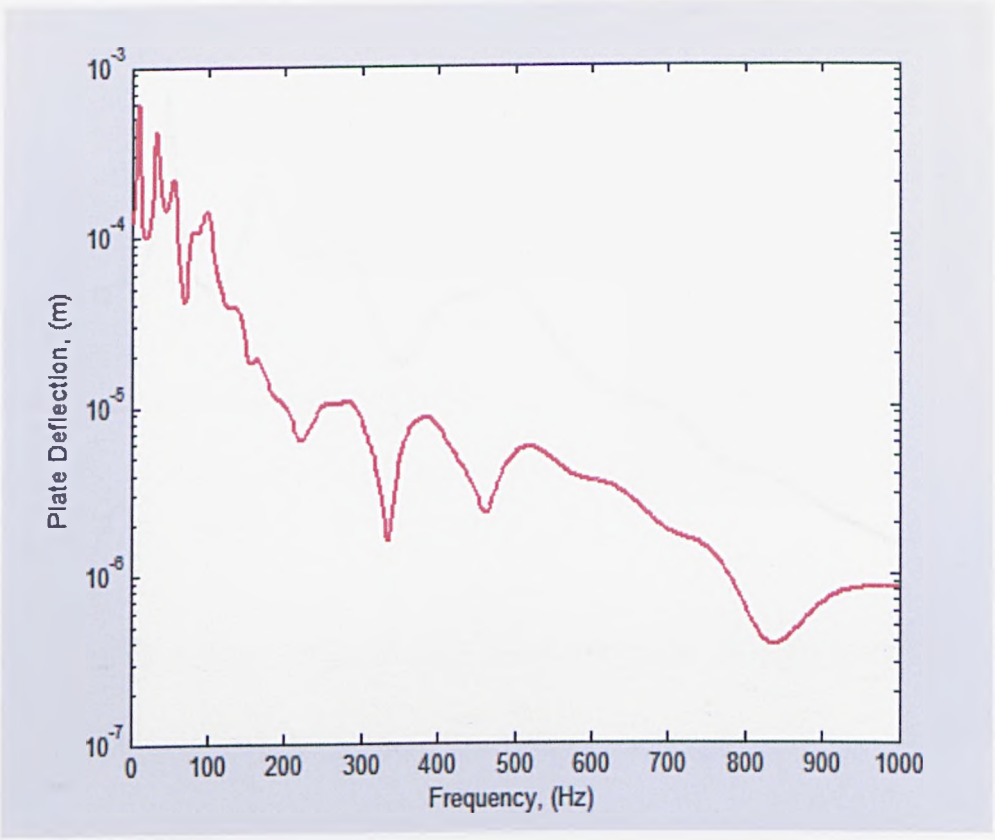

Figure1.4: Predicted deflection of G foam plate

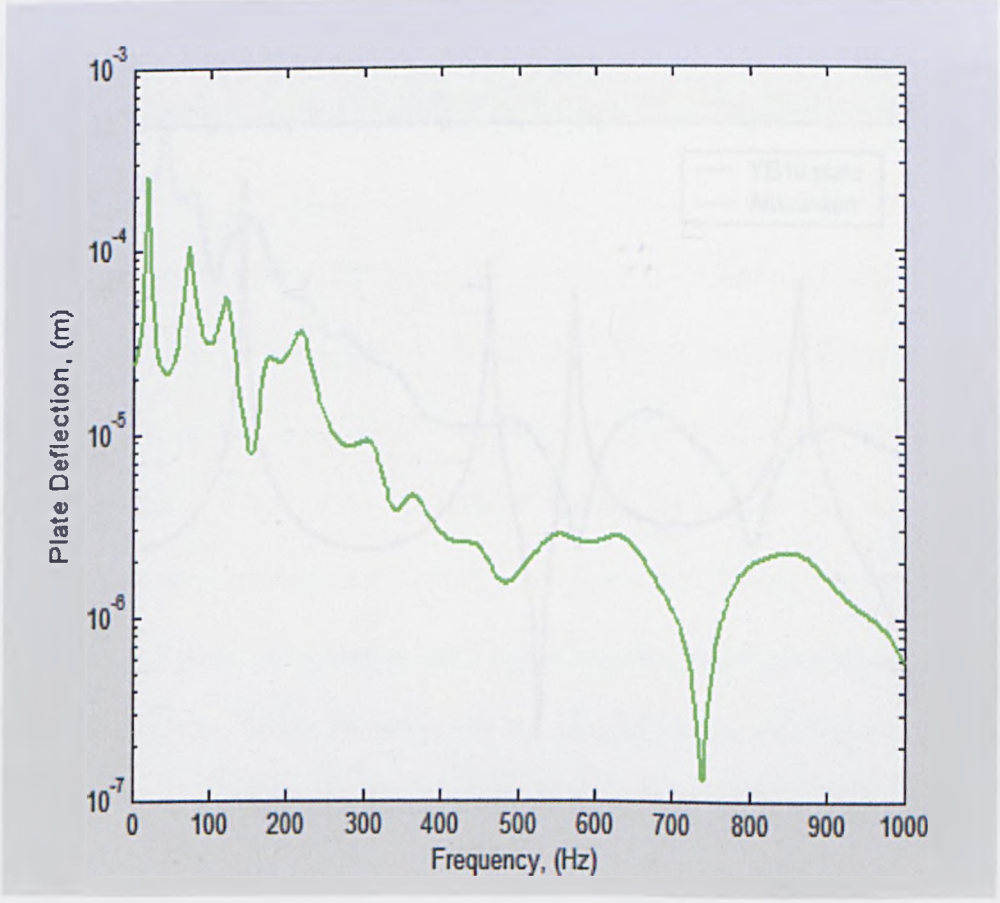

Figure1.5: Predicted deflection of the YB10 foam plate

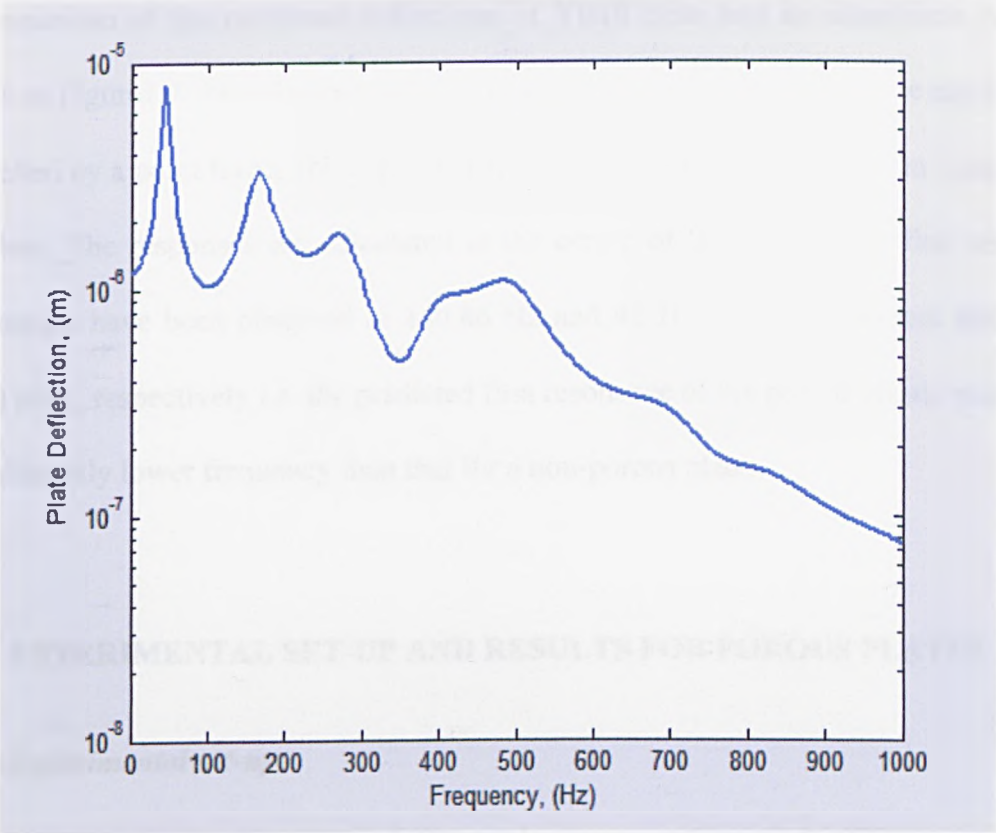

Figure1.6: Predicted deflection of the Coustone plate

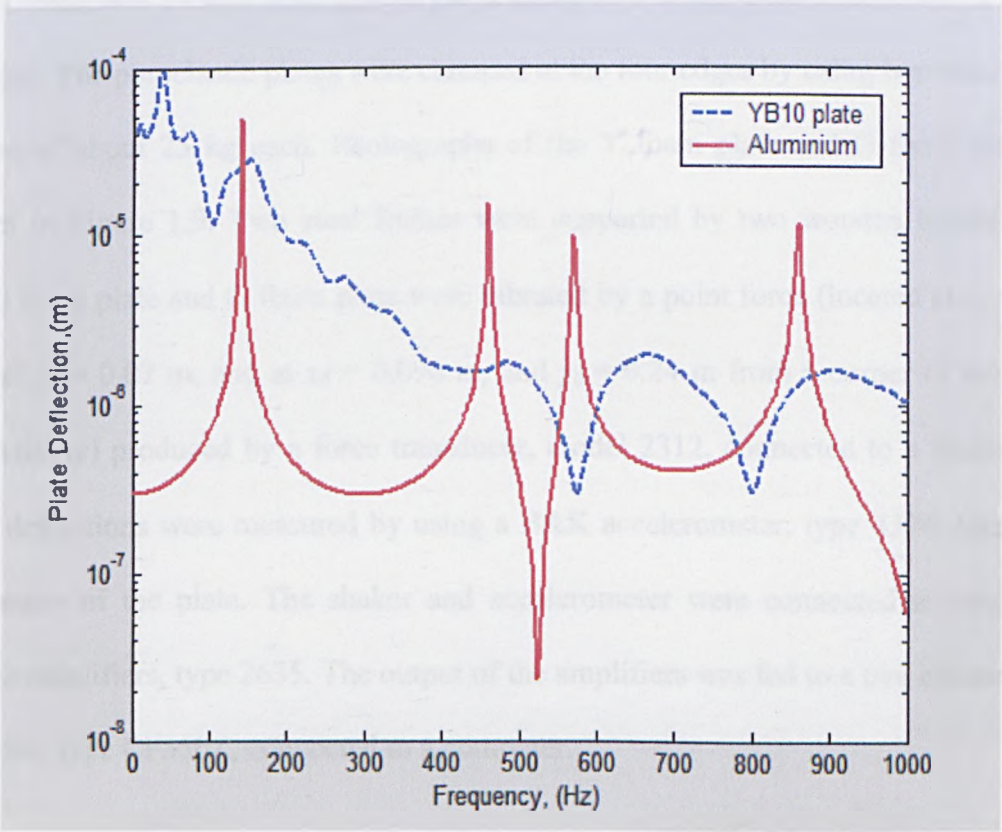

Figure1.7: A comparison of predicted deflections of YB10 plate and an aluminium plate.

A comparison of the predicted deflections of YB10 plate and an aluminium plate is shown in Figure1.7. The clamped porous plate and the non-porous plate are assumed to be excited by a point force, 1N, applied at $x_0 = 0.08$ m, and $y_0 = 0.07$ m from a corner of the plate. The responses are calculated at the centre of the plates. The first resonant frequencies have been observed at 140.86 Hz and 40 Hz for an aluminium plate and YB10 plate, respectively i.e. the predicted first resonance of the porous elastic plate is at a significantly lower frequency than that for a non-porous plate.

1.7 EXPERIMENTAL SET-UP AND RESULTS FOR POROUS PLATES

1.7.1 Experimental set-up

The experimental set-up has been built and is shown in Figure1.8. This arrangement has been used to measure the responses of a 10.7 mm thick porous plate, made of the YB10 foam, and 11 mm thick porous plate, made of G foam, with dimensions of 50 cm x 50 cm. The poroelastic plates were clamped at the four edges by using two heavy steel frames of about 25 kg each. Photographs of the Y foam plate and G foam plate are shown in Figure 1.9. Two steel frames were supported by two wooden holders. The YB10 foam plate and G foam plate were vibrated by a point force (located at $x_0 = 0.09$ m, and $y_0 = 0.07$ m, and at $x_0 = 0.096$ m, and $y_0 = 0.24$ m from a corner of the plate, respectively) produced by a force transducer, model 2312, connected to a shaker. The plate deflections were measured by using a B&K accelerometer, type 4374, located at the centre of the plate. The shaker and accelerometer were connected to two B&K charge amplifiers, type 2635. The output of the amplifiers was fed to a two channel FFT analyzer, type CF350Z, connected to a computer.

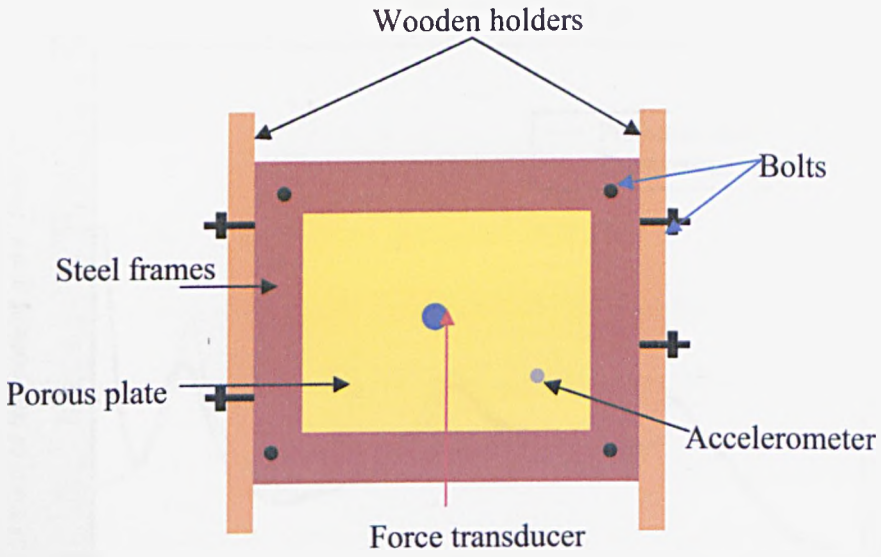

Figure1.8: Arrangement for measurements on porous plate

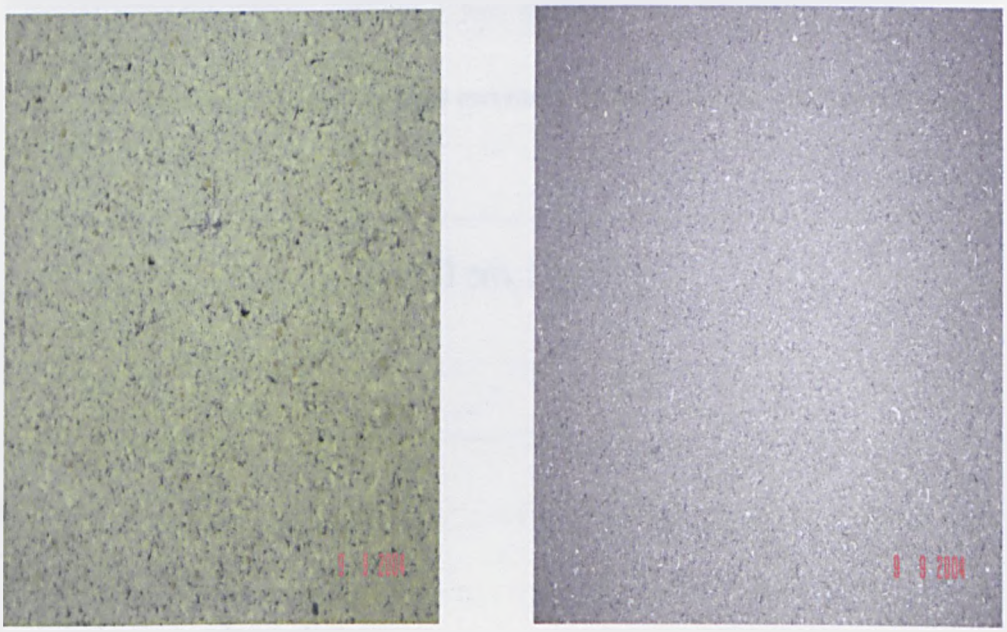

Figure1.9: Pictures of the YB10 foam plate, and G foam plate

1.7.2 Experimental results

The deflections of YB10 foam plate and G foam plate were measured as a function of frequency, and compared to the predictions. A comparison of experimental and predicted results of YB10 foam plate is shown in Figure 1.10.

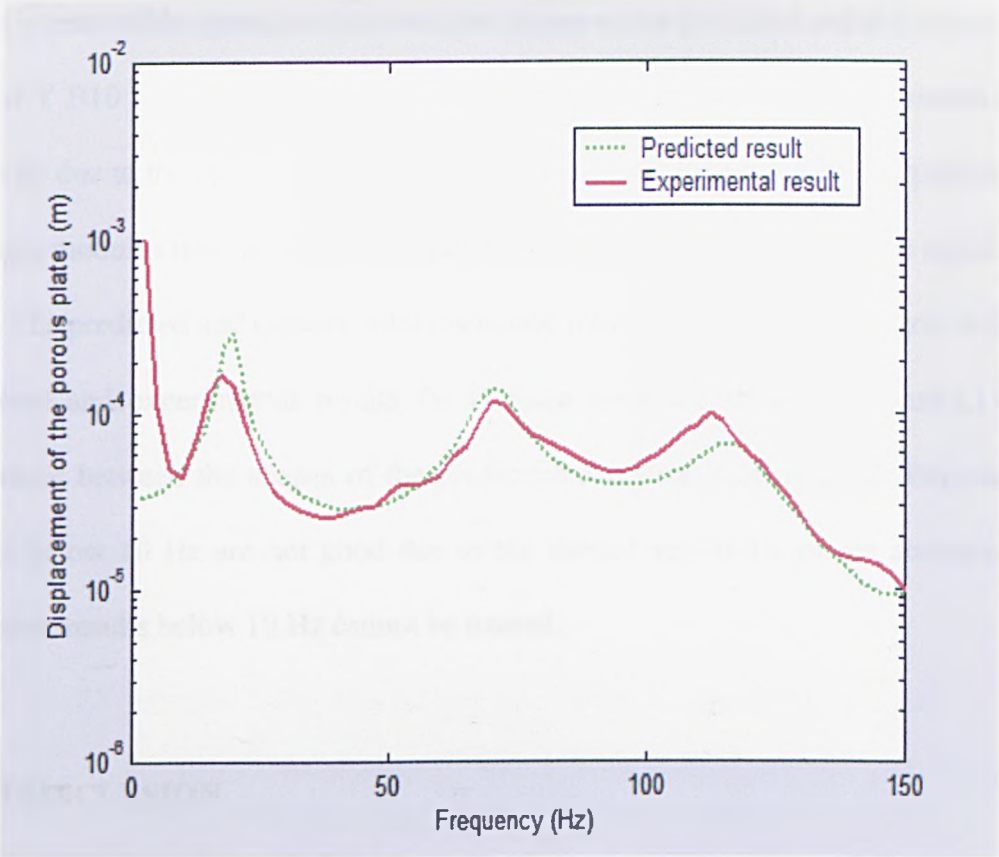

Figure1.10: Predicted and measured deflection of the YB10 foam plate.

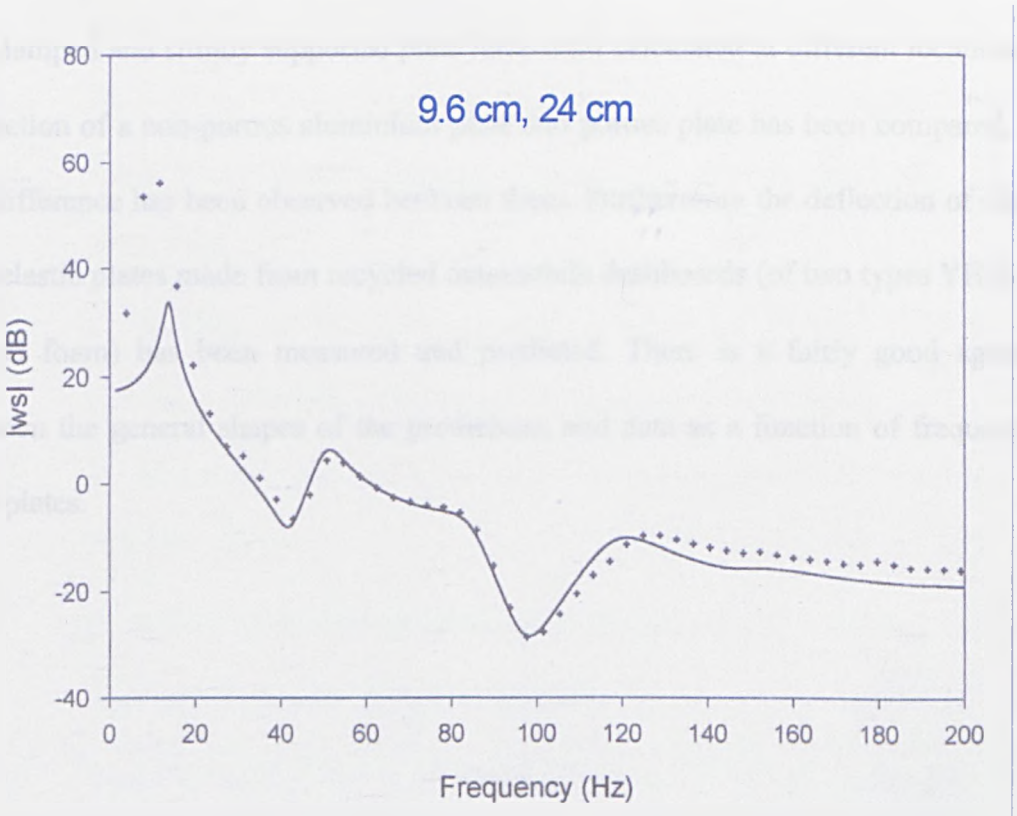

Figure1.11: Predicted (solid line) and measured (dotted line) deflections of the G foam plate [3].

There is reasonable agreement between the shapes of the predicted and the experimental data of Y B10 foam. The discrepancies between the predicted and experimental curves might be due to the imprecision in the calculation of the Poisson ratio, the porosity, and Young's modulus used in the code or due to the boundary conditions at the edges of the plate. The predicted and experimental resonance frequencies of the plate agree well. The predicted and experimental results for G foam plate are shown in Figure1.11. The agreement between the shapes of the prediction and data is fairly good. Experimental results below 10 Hz are not good due to the limited sensitivity of the accelerometer. Therefore results below 10 Hz cannot be trusted.

1.8 CONCLUSION

The deflection of a non-porous (aluminium) plate has been studied theoretically and numerically for clamped and simply supported boundary conditions. The responses of the clamped and simply supported plate have been calculated at different locations. The deflection of a non-porous aluminium plate and porous plate has been compared, and a big difference has been observed between them. Furthermore the deflection of clamped poroelastic plates made from recycled automobile dashboards (of two types YB10 foam and G foam) has been measured and predicted. There is a fairly good agreement between the general shapes of the predictions and data as a function of frequency for both plates.

References:

1. D. D. Theodorakopoulos and D. E Beskos, "Flexural vibration of poroelastic plates," Acta Mechanica, 103, 191-203 (1994).
2. P. Leclaire, A. Cummings and K. V. Horoshenkov, "Transverse vibration of a thin rectangular porous plate saturated by a fluid," J. Sound Vib. 247(1), 1-18(2001).
3. P. Leclaire, K. V. Horoshenkov, M. J. Swift, and D. C. Hothersall, "The vibration response of a clamped rectangular porous plate," J. Sound Vib. 217(1), 19- 31(2001).
4. P. Leclaire, "Vibration of Porous Plates in Structural Acoustic Coupling Applications," 3rd European Congress on Acoustics. 16th –20th September 2002, Spain.
5. M. A. Biot, "Theory of elastic wave propagation in a fluid saturated porous solid. Part I-low frequency range," J. Acoust. Soc. Am. 28,168-178(1956).
6. M. A. Biot, "Theory of elastic wave propagation in a fluid saturated porous solid. Part 2-higher frequency range," J. Acoust. Soc. Am. 28, 179-191(1956).
7. R. Szilard, (1974), "Theory and Analysis of Plates". "Classical and Numerical Methods". Prentice-Hall, Englewood, New Jersey.
8. A. W. Leissa, "the free vibration of rectangular plates" J. Sound Vib. 1(3), 257-293(1973).
9. D. Young, "Vibration of rectangular plates by the Ritz method," Journal of Applied Mechanics 17, 448-453(1950).
10. Lord Rayleigh, *"Theory of Sound"* (London, 1926) Vol.(I), and (Dover, New York, 1945), Vol.(II).

11. M. A. Biot and D. G. Willis, "The elastic coefficients of the theory of consolidation," J. Appl. Mech., 24, 594-601 (1957).

12. M. A. Biot, "Mechanics of deformation and acoustic propagation in porous media," J. Appl. Phys. 33, 1482-1498(1962).

13. M. A. Biot, "Theory of buckling of a porous slab and its thermoelastic analogy," J. Appl. Mech. ASME., 31, 194-198 (1964).

14. H. Deresiewicz, and R. Skalak, "On uniqueness in dynamic poroelasticity," Bulletin of the Seismological Society of America 53, 783-788(1963).

Chapter 2

ACOUSTIC RADIATION FROM A BAFFLED, NON-POROUS AND POROUS PLATE, AND RADIATION IMPEDANCE MATRIX

2.1 INTRODUCTION

Chapter 1 was concerned with measured and predicted deflections of clamped poro-elastic plates. Here the emphasis is on calculations of the vibro-acoustic indicators for poroelastic plates such as radiation efficiency. Important progress in predicting acoustic radiation from baffled structures including plates and beams has been made in the last two decades. Many previous studies have focused on the calculation of the radiation efficiency of these structures.

Initial studies of the radiation impedance of a plane structure in the form of a simply supported rectangular plate were made by Davies [1]. Pope and Leibowitz [2] have proposed a set of formulas corresponding to corner, edge and surface radiation regimes of the plates by developing the solution of Davies. These two studies use a wave number transformation of the fluid and structure governing equations. Davies, and Pope and Leibowitz have also calculated the radiation impedance matrix in the case of a simply supported plate.

Sound radiation from plates carrying one-dimensional or two-dimensional vibration patterns with general boundary conditions has been studied by Gomperts [3, 4]. More recently Berry [5, 6] has analyzed the radiation of sound from a baffled, rectangular plate with edges elastically restrained against deflection and rotation. Atalla and Nicolas [7] have presented a comparison of several models used to evaluate the radiation efficiency of plate-like radiators. They compared models ranged from very simple ones based on modal average expressions to refined calculations of the radiation impedance

matrix with cross-modal coupling. Then they developed a new approach based on Taylor's expansion of the Green's function.

Foin [8] has proposed a variational model solved by the Rayleigh-Ritz method for a baffled, rectangular, simply supported multilayered plate immersed either in a light fluid or in a heavy fluid. Foin has calculated the radiation of sound from the plate with the method of Sandman [9] and Nelisse [10] which makes high frequencies attainable without convergence problems.

The radiation impedance matrix has calculated by Foin, Sandman and Nelisse. Sandman and Nelisse reduced the quadruple integral into a double integral using a specific change of variable. They integrated the double integral with a numerical method using Gaussian quadrature formulae.

Here, vibroacoustic indicators including the radiation efficiency, the mean square velocity, and the radiated sound power, are calculated for rectangular, clamped, porous plates, and for a rectangular, simply supported, aluminium plate. The vibroacoustic indicators of the clamped porous plates are calculated, and compared to each other. Furthermore, the radiation impedance matrix is calculated by using basic equation without interpolation, convergence and without reducing the quadruple integral into a double integral. The direct and cross coupling terms of the radiation impedance matrix are divided by characteristic impedance. The real part of the radiation impedance matrix is the radiation resistance and expresses the radiation damping of the structure. The imaginary part of the radiation impedance matrix is the radiation reactance and expresses the added mass of fluid on the structure.

2.2 MEAN SQUARE VELOCITY

Mean square velocity gives the global behaviour of the vibration of the plate. Mean square velocity is defined as a time-space average of the square vibrational velocity of plate, and is given by [8];

$$V^2 = \frac{1}{abT}\int_0^T \iint_S \left|\frac{\partial w(x,y,t)}{\partial t}\right|^2 dSdt \tag{2.1}$$

where $T = \frac{2\pi}{\omega}$, a and b are the coordinates of plates in x and y direction, respectively. S is the surface area of the plate and ω is the angular frequency of the plate.

If the plate deflection given by Equation (1.2) is solved, mean square velocity of the plate can easily be computed. Three clamped, rectangular porous plates and a simply supported, rectangular aluminium plate are considered herein. The properties of the aluminium plate and of porous plates are given in Table1.1, and in Table1.2, respectively.

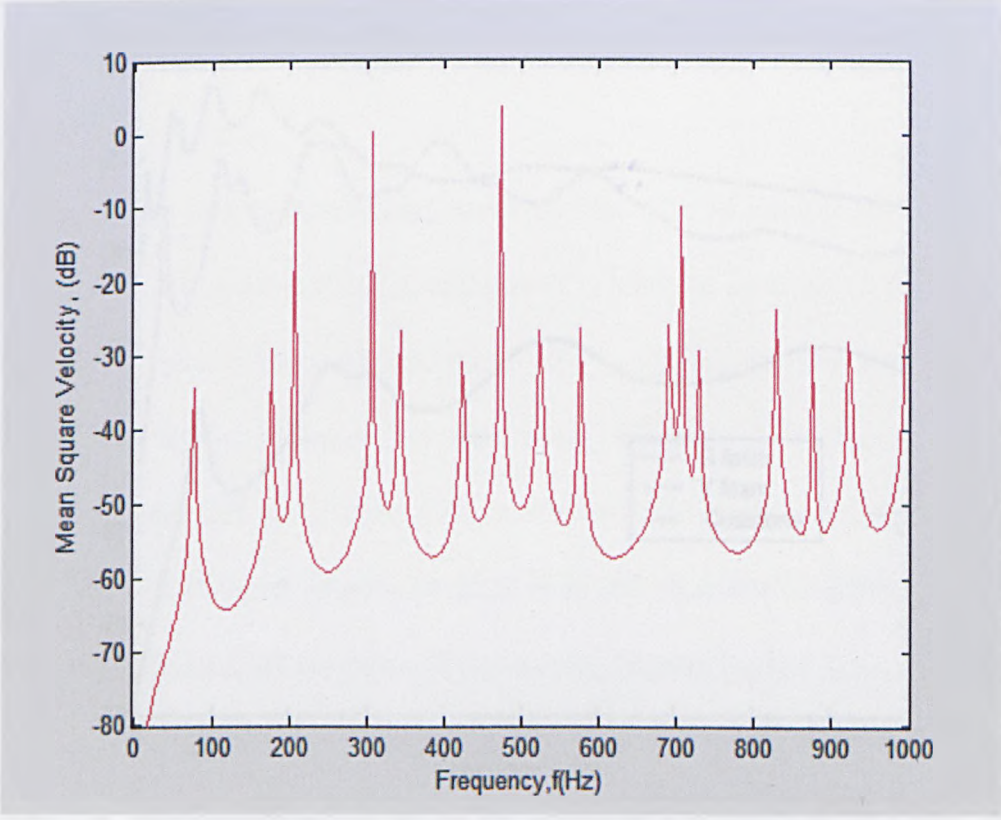

Figure2.1: The mean square velocity of a simply supported, rectangular, aluminium plate

A Gaussian quadrature scheme with 20 terms of the Legendre polynomial is used to expand the deflection of the plate and mean square velocity of the plate with 14 elements in each direction (m, n,). The plate is excited by a point force applied at x_0 = 0.08 m, y_0 = 0.07m from a corner of the plate. The response for all of the plates is calculated at the centre of the plate. The reference velocity is taken to be equal to 1 m/s in this work.

Figure 2.1 shows predicted result of the mean square velocity of an aluminium plate plotted against frequency. A comparison of the mean square velocities of the clamped porous plates are shown in Figure 2.2. The predicted mean square velocity of the G foam plate is higher than Y foam plate or the Coustone plate. As shown in Figure 2.2 the predicted mean square velocity of a Coustone plate is lowest. The reason for this is that the density of the Coustone plate is higher than others. Also the Tortuosity, Young's modulus and density of the Coustone plate are higher than those of the others whereas the porosity is lower.

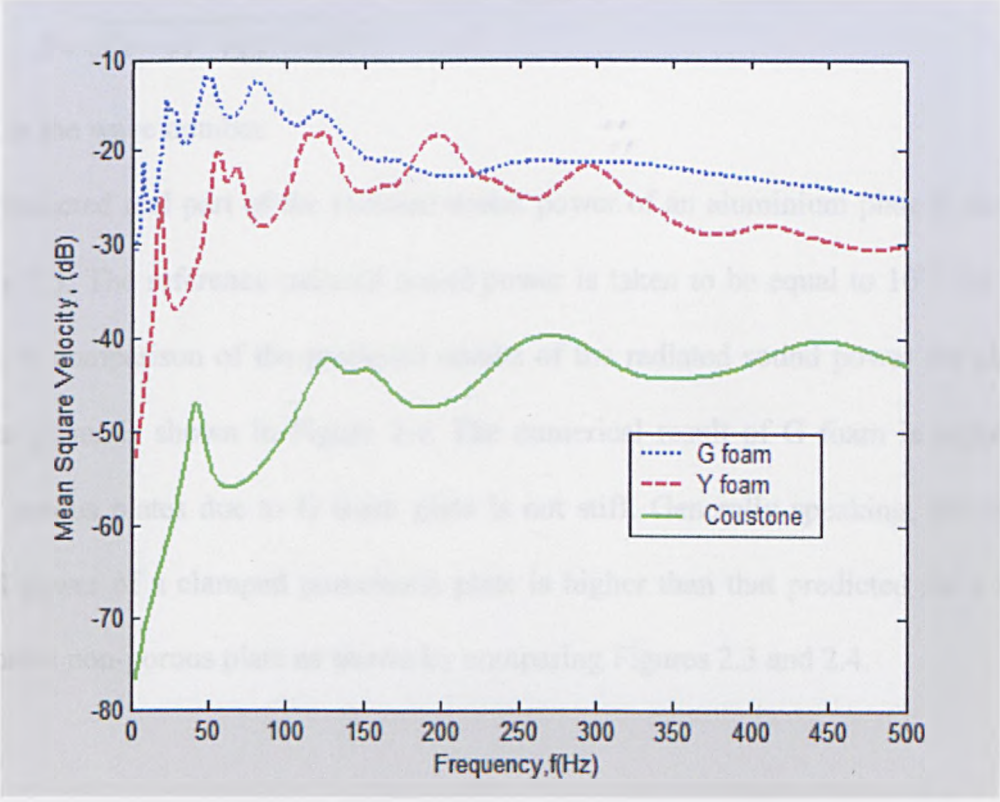

Figure2.2: A comparison of the mean square velocities of the clamped porous plates

2.3 RADIATED SOUND POWER

The radiated sound power expresses the sound energy radiated by the plate. It is obtained from the integration of the intensity over the plate surface. The radiated sound power [8] is given by

$$W = \frac{1}{T}\int_0^T \iint_S P(x, y, 0, t)\frac{\partial w(x, y, t)}{\partial t} dS dt \tag{2.2}$$

where $P(x,y,0,t)$ is the surface acoustic pressure which is often called Rayleigh integral, and is given by the equation (2.3) [11],

$$P(x,y,z) = -\rho\omega^2 \iint_S w(x',y')G(x,y,z;x',y',0)\, dS', \tag{2.3}$$

where $G(x,y,0;x',y',0)$ is the Green function given by Equation (2.4);

$$G(x, y, z; x', y', 0) = \frac{\exp(-jkR)}{2\pi R} \tag{2.4}$$

where R is the distance between points, and is given by Equation (2.5);

$$R = \sqrt{(x-y)^2 + (x'-y')^2}, \tag{2.5}$$

and k is the wave number.

The predicted real part of the radiated sound power of an aluminium plate is shown in Figure 2.3. The reference radiated sound power is taken to be equal to 10^{-12} Pa in this work. A comparison of the predicted results of the radiated sound power for clamped porous plates is shown in Figure 2.4. The numerical result of G foam is higher than other porous plates due to G foam plate is not stiff. Generally speaking, the radiated sound power of a clamped poroelastic plate is higher than that predicted for a simply supported non-porous plate as shown by comparing Figures 2.3 and 2.4.

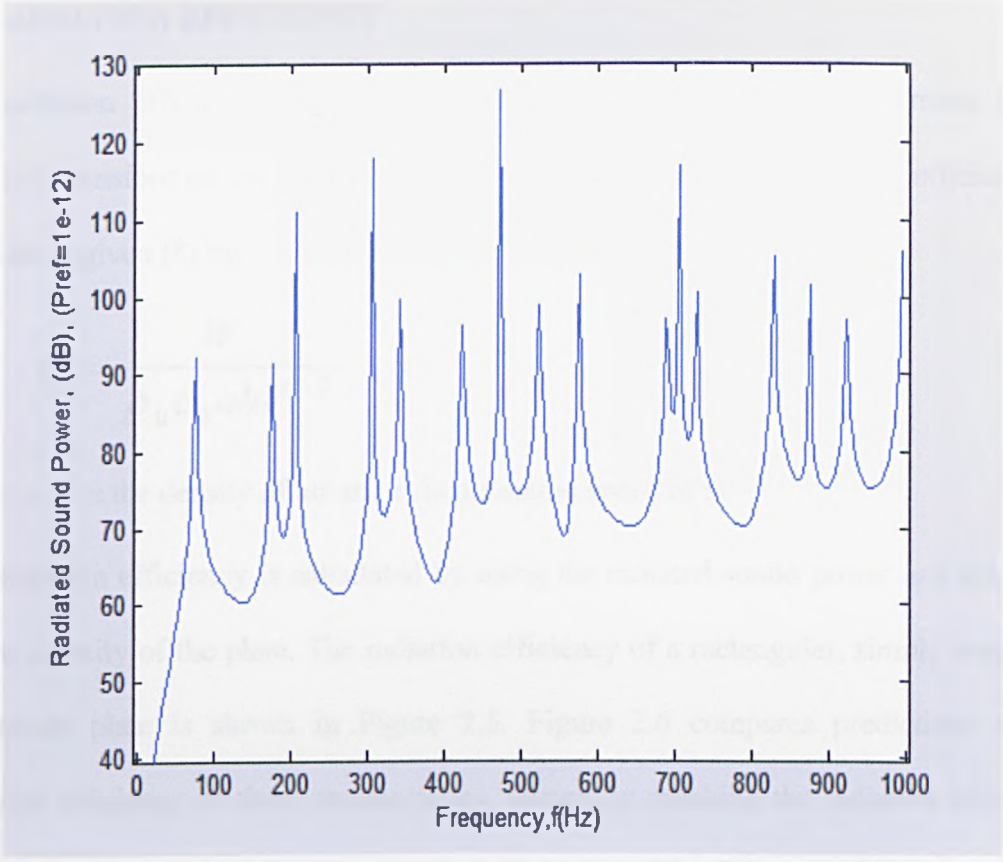

Figure2.3: The real part of radiated sound power of an aluminium plate

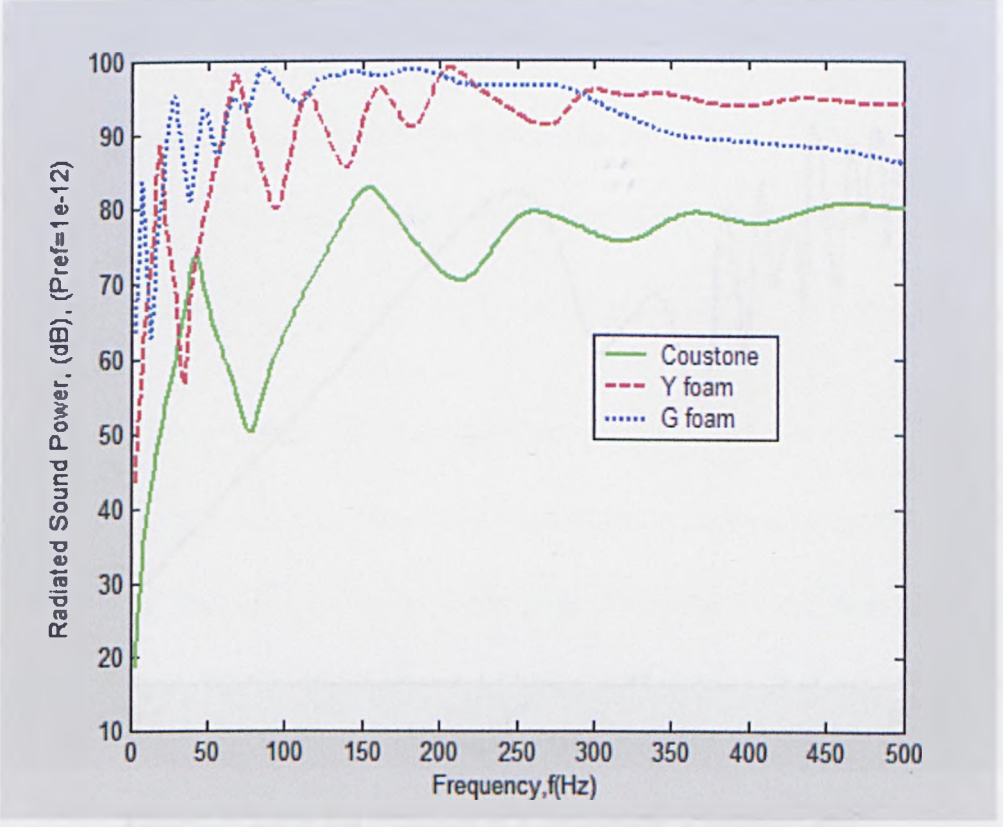

Figure2.4: A comparison of the real parts of radiated sound powers of the porous plates

2.4 RADIATION EFFICIENCY

The radiation efficiency expresses the ratio of the vibration energy (mean square velocity) transformed into acoustic energy (sound power). The radiation efficiency of the plate is given [8] by;

$$\eta = \frac{W}{\rho_0 c_0 abV^2} \tag{2.6}$$

where ρ_0 is the density of air and c_0 is the sound speed of air.

The radiation efficiency is calculated by using the radiated sound power and the mean square velocity of the plate. The radiation efficiency of a rectangular, simply supported aluminium plate is shown in Figure 2.5. Figure 2.6 compares predictions of the radiation efficiency of three porous plates. Generally speaking the radiation efficiency of Coustone plate is predicted to be higher than those of the G foam and Y foam plate.

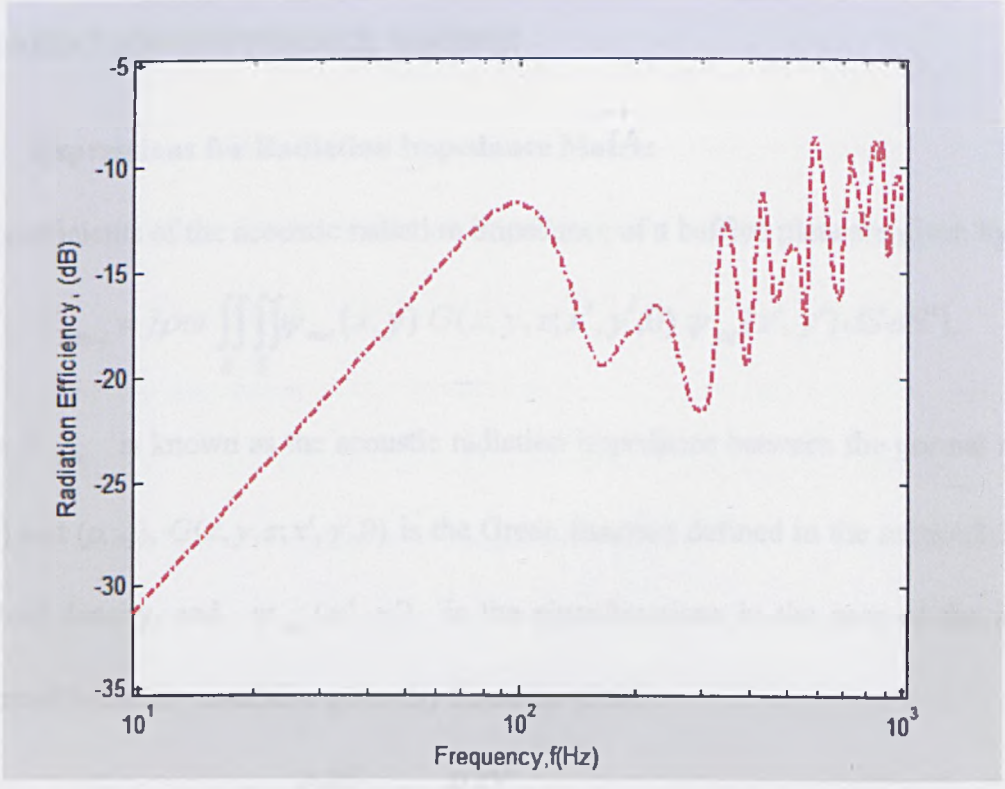

Figure2.5: Radiation efficiency of a rectangular aluminium plate

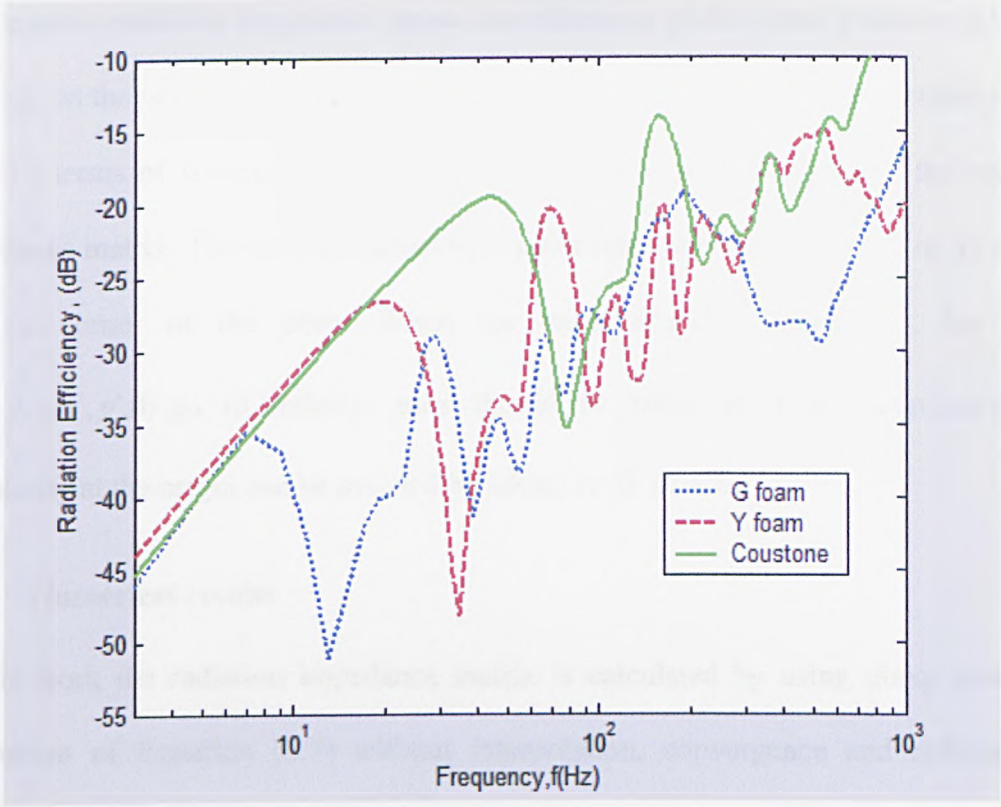

Figure2.6: A comparison of radiation efficiency of rectangular, clamped porous plates

2.5 RADIATION IMPEDANCE MATRIX

2.5.1 Expressions for Radiation Impedance Matrix

The coefficients of the acoustic radiation impedance of a baffled plate are given by [8]:

$$Z_{mnpq} = j\rho\omega \int_S \int_S \psi_{mn}(x,y)\, G(x,y,z;x',y',0)\, \psi_{pq}(x',y')\, dS\, dS'), \qquad (2.7)$$

where Z_{mnpq} is known as the acoustic radiation impedance between the normal modes (m, n) and (p, q), $G(x,y,z;x',y',0)$ is the Green function defined in the section2.3, ρ is the fluid density, and $\psi_{pq}(x',y')$ is the eigenfunctions in the case of the simply supported boundary condition given by Equation (2.8);

$$\psi_{pq}(x',y') = \sin\left(\frac{p\pi x'}{a}\right)\sin\left(\frac{q\pi y'}{b}\right) \qquad (2.8)$$

The acoustic radiation impedance shows the influences of the sound pressure in the (*m, n*) mode on the plate system vibrating in the (*p, q*) mode. A Gaussian quadrature scheme with 13 terms of functions in each direction (*x, y*) is used to compute the radiation impedance matrix. The plate is excited by a point force applied at $x_0 = 0.1$ m, $y_0 = 0.1$m from a corner of the plate. When the variables $x = x'$ and $y = y'$, for which $G(x, y, z; x', y', 0)$ go to infinity, care should be taken to avoid singularity. The singularity at the origin can be avoided by taking *G (0, 0) = 0*.

2.5.2 Numerical results

In this work the radiation impedance matrix is calculated by using direct numerical integration of Equation (2.7) without interpolation, convergence and reducing the quadruple integral into a double integral. The direct and cross coupling terms of the radiation impedance matrix are normalized by the characteristic impedance ($\rho_0 c_0$), where ρ_0 is the air density and c_0 is the sound speed in the air.

The direct terms ($Z_{mnmn} / \rho_0 c_0$) of the impedance matrix are shown in Figures 2.7 (a, b, c). When higher values of (*m, n*) are used in the calculations, the radiation impedance matrix is equal to zero at low frequency as seen in Figure 2.7c. The cross coupling terms ($Z_{mnpq} / \rho_0 c_0$) are shown in Figures2.8 (a, b, c). If the values of ($m + p$) or ($n + q$) is odd the radiation impedance matrix is equal to zero. The values of *m, n, p,* and *q* vary between *0* and *N*. These figures show that the predicted radiation impedance matrix exhibits a smooth variation in terms of frequency.

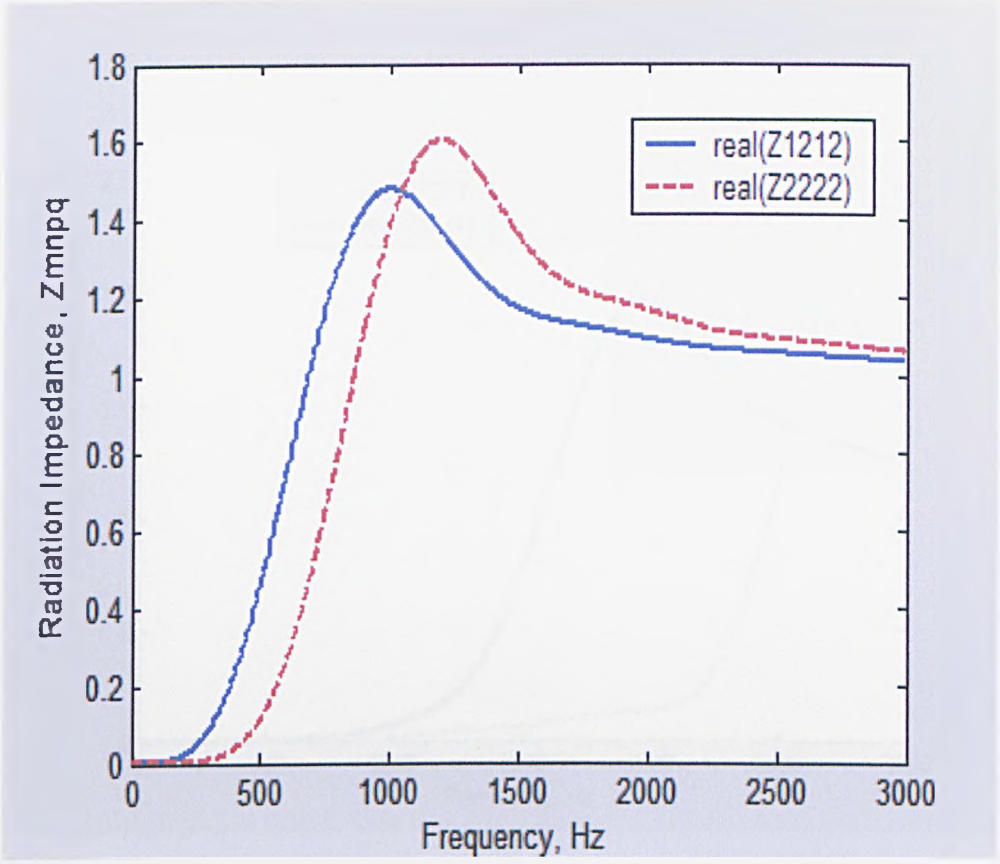
real(Z1212)
real(Z2222)
Radiation Impedance, Zmnpq
Frequency, Hz
0
0.2
0.4
0.6
0.8
1
1.2
1.4
1.6
1.8
0
500
1000
1500
2000
2500
3000

(a)

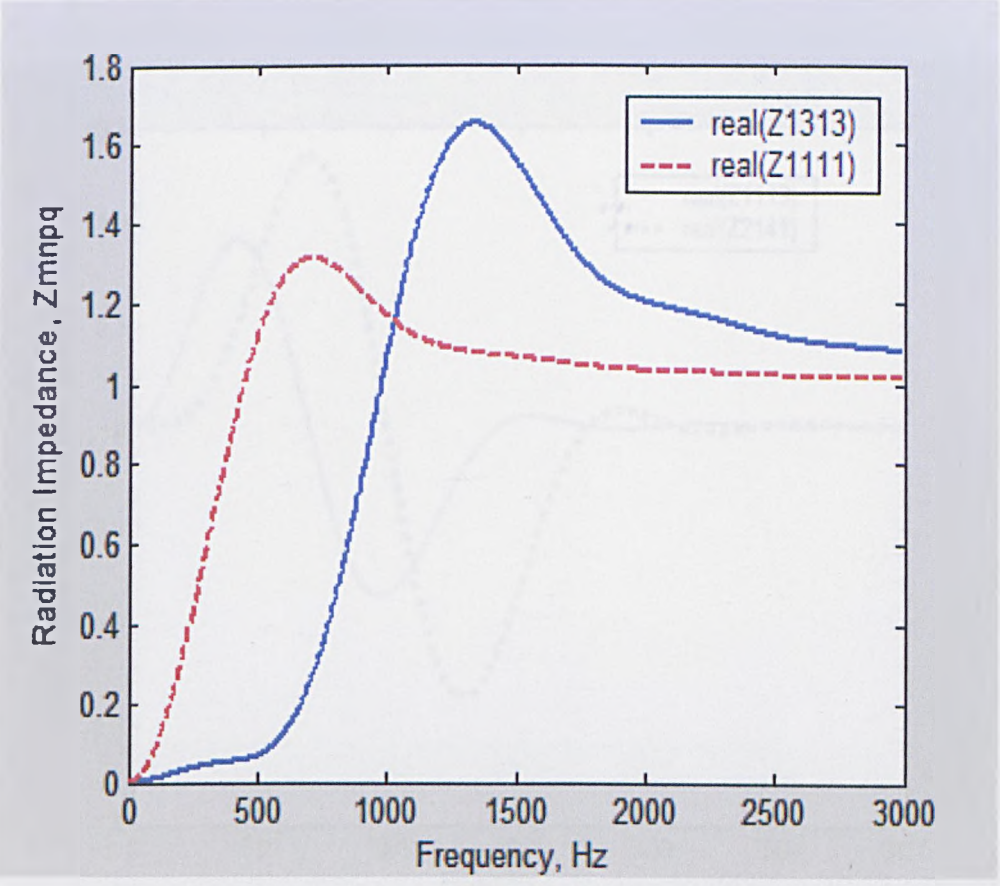
real(Z1313)
real(Z1111)
Radiation Impedance, Zmnpq
Frequency, Hz
0
0.2
0.4
0.6
0.8
1
1.2
1.4
1.6
1.8
0
500
1000
1500
2000
2500
3000

(b)

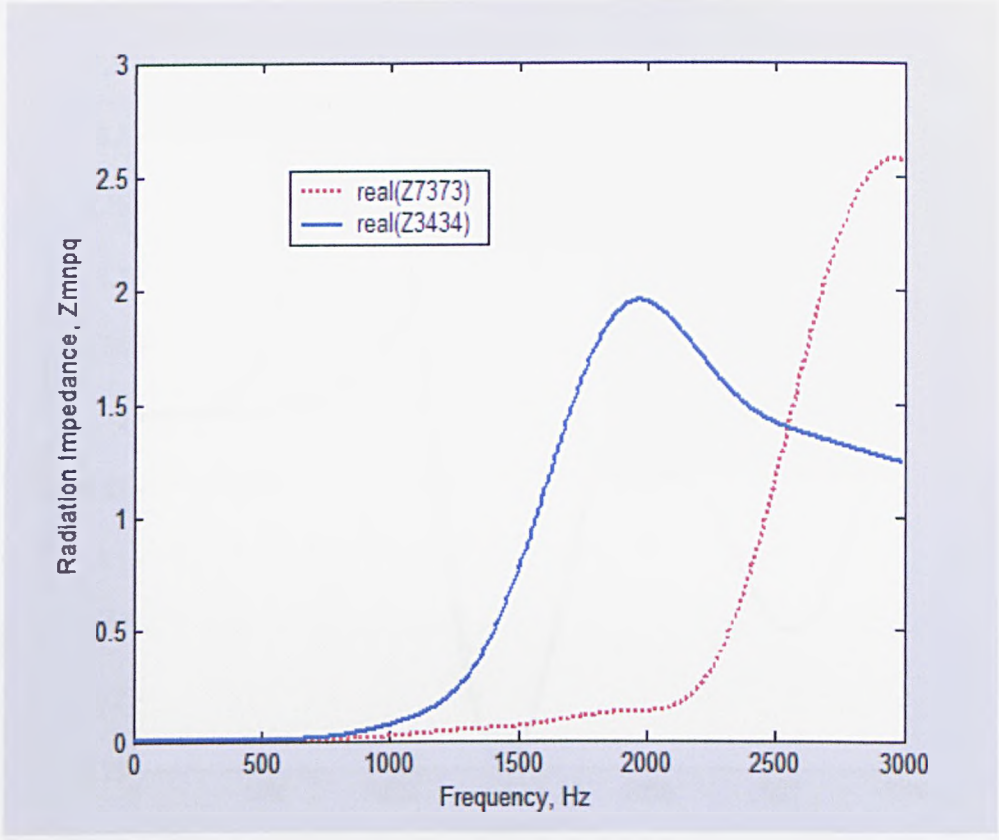

(c)

Figure2.7 (a, b, c): Direct terms of the real part of the radiation impedance matrix

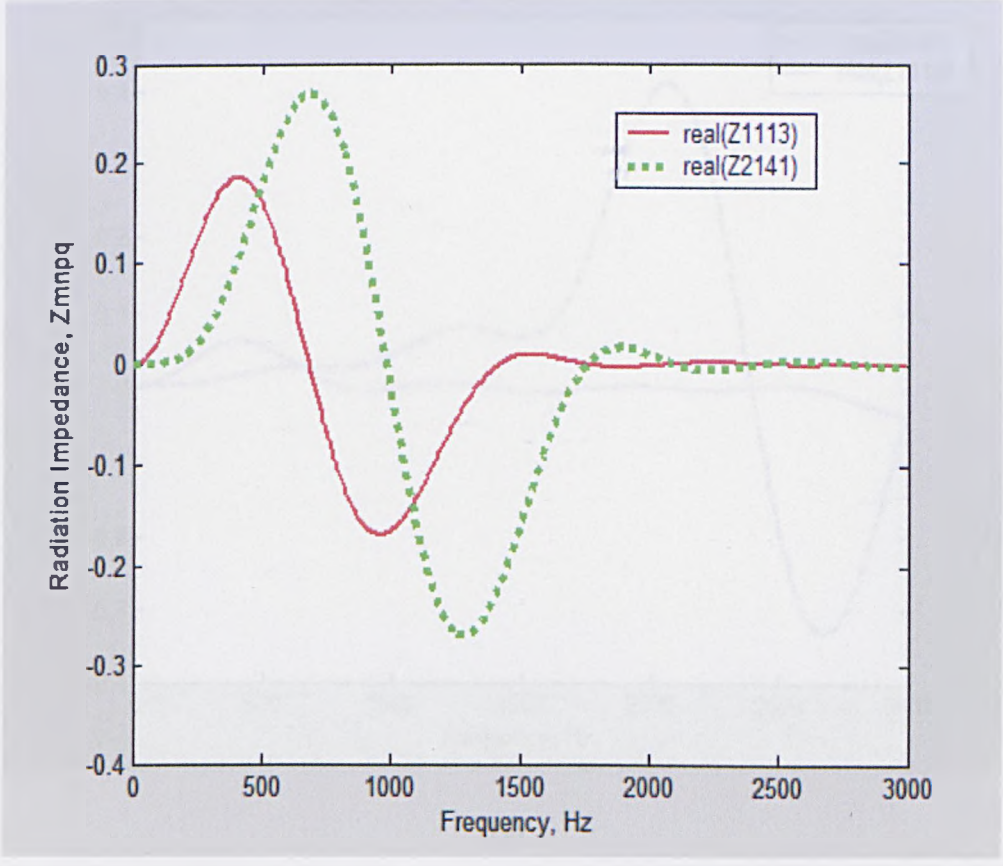

(a)

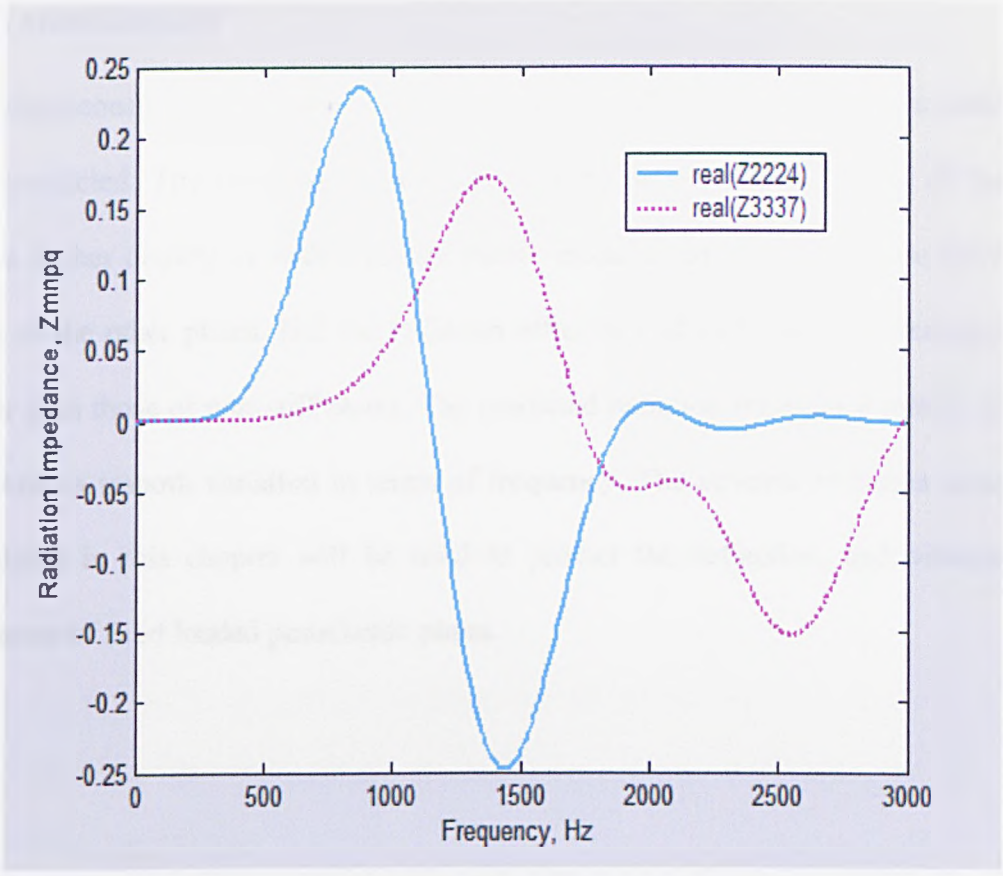

(b)

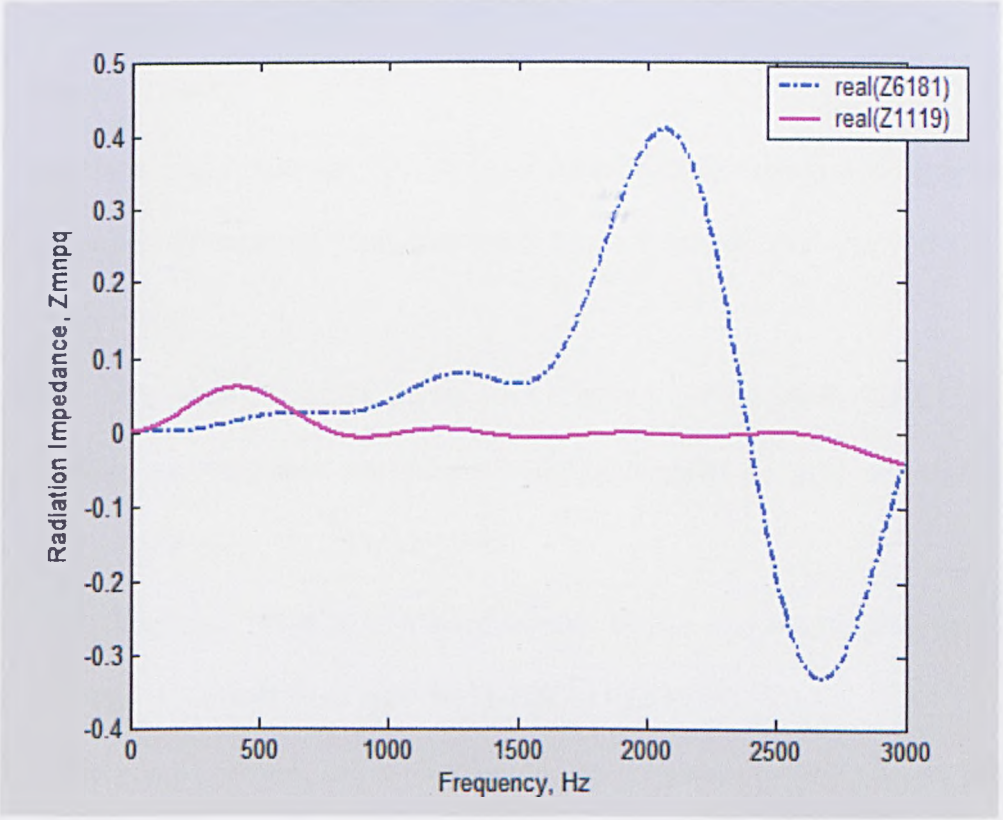

(c)

Figure2.8a, b and c: Cross coupling terms of the real part of the radiation impedance matrix

2.6 CONCLUSION

The vibroacoustic indicators of a simply supported and clamped poroelastic plates have been predicted. The mean square velocity and the radiated sound power of the plate with a higher density or with a higher elastic modulus are predicted to be lower than those of the other plates. But the radiation efficiency of stiff plates is predicted to be higher than those of non-stiff plates. The predicted radiation impedance matrix is found to exhibit a smooth variation in terms of frequency. The acoustic radiation impedance calculated in this chapter will be used to predict the deflection, and vibroacoustic indicators of fluid loaded poroelastic plates.

References:

1. H. G. Davies, "Low frequency random excitation of water-loaded rectangular plates," *J. Sound Vib.* 15. 107-126 (1971).
2. L. D. Pope and R. C. Leibowitz, "Intermodal coupling coefficients for a fluid-loaded rectangular plate," J. Acoust. Soc. Am.56, 408-414 (1974)
3. M.C. Gomperts, "Radiation from rigidly baffled rectangular panels with general boundary conditions," *Acustica* , 30, 320-327 (1974).
4. M.C. Gomperts, "Sound radiation from baffled, thin, rectangular plates," *Acustica,* 37, 93-102 (1977).
5. A. Berry, "A general formulation for the sound radiation from rectangular, baffled plates with arbitrary boundary conditions," J. Acoust. Soc. Am. 88(6), 2792-2802 (1990).
6. A. Berry, "A new formulation for the vibrations and sound radiation of fluid-loaded plates with elastic boundary conditions," J. Acoust. Soc. Am. 96((2), 889-901 (1994).
7. N. Atalla and J. Nicolas. "A new tool for predicting rapidly and rigorously the radiation efficiency of plate-like structures," J. Acoust. Soc. Am. 95 (6), 3369-3378(1994).
8. O. Foin, J. Nicolas, and N. Atalla, "An efficient tool for predicting the structural acoustic and vibration response of sandwich plates in light or heavy fluid," *Applied Acoustics*, 57, 213-242(1999).
9. B. E. Sandman, "Motion of a three-layered elastic-viscoelastic plate under fluid loading," J. Acoust. Soc. Am. 57(5), 1097-1107(1975).
10. H. Nelisse, O. Beslin, and J. Nicolas, "Fluid –structure coupling for an unbaffled elastic panel immersed in a diffuse field," J. Sound Vib. 198(4), 485-506(1996).

11. H. Nelisse, O. Beslin, and J. Nicolas, "A generalized approach for the acoustic radiation from a baffled or unbaffled plate with arbitrary boundary conditions, immersed in a light or heavy fluid," J. Sound Vib. 211(2), 207-225(1998).

EFFECTS OF FLUID LOADING ON POROUS ELASTIC PLATE VIBRATION

3.1 INTRODUCTION

The vibrational response of fluid loaded, infinite plates has been studied by numerous authors [1-5]. Sandman [5] has described the fluid loaded, simply supported plate carrying a concentrated mass by the solution of the governing equations of motion in terms of the normal modes of free vibration. Sandman has presented extensive examples to illustrate in the basic characteristics of fluid-loaded vibration and radiation of a plate with a discrete mass discontinuity. In order to calculate the vibrational response of a plate and sound radiation the magnitude and location of mass loading should be chosen carefully for centre-point excitation.

Recently, A. Berry [6] has studied the vibrations and sound radiation of fluid-loaded plates with elastic boundary conditions. Berry has suggested a new approach for the acoustic radiation of baffled rectangular plates coupled to a dense fluid medium. His approach is based on a variational formulation of the fluid-loaded plate motion and a Rayleigh-Ritz method using polynomial displacement functions. The selection of such polynomial functions leads to a new method of solution of the plate's radiation impedance.

The formulation for a porous plate was firstly rigorously studied by Theodorakopoulos and Beskos [7] in the case of a simply supported rectangular plate. The solutions of Theodorakopoulos and Beskos were developed by P. Leclaire [8, 9, 10], who described a set of equations corresponding to any type of plate.

Foin [11] has evaluated the acoustic pressure exerted by fluid on the baffled plate by using the Rayleigh integral.

An overview of the most common theoretical and numerical methods of plates can be found in the book by Szilard [12]. Freedman [13] has studied the associated phase velocity or wave-number spectra for free plates for positive Poisson ratios.

The effects of the fluid loading on the vibration of the rectangular, clamped, porous plate and on the radiated sound power are considered in here. The fluid-structure coupling is very complex in the case of rectangular plates where the plate modes are coupled through the fluid. The effect of fluid loading can be incorporated by inserting an extra term in the equations of plate, corresponding to an additional external force acting on the plate. This will lead to the calculation of radiation impedance matrices with non-negligible cross terms.

3.2 VARIATIONAL EQUATIONS OF THE FLUID-LOADED POROUS PLATE MOTION

The geometry of a baffled plate is shown in Figure3.1. For baffled plate the upper half-space above the plate, $z>0$, is filled with a fluid, while lower half-space, $z<0$, is assumed to be a vacuum. The work done by excitation force is given by [11];

$$W_{excitation} = \int_0^a \int_0^b F(x,y,0,t)w(x,y,t)dxdy \tag{3.1}$$

where $F(x,y,0,t)$ is the excitation force.

The work done by fluid loading is given by [11];

$$W_{fluid} = \int_0^a \int_0^b P(x,y,0,t)w(x,y,t)dxdy, \tag{3.2}$$

where $P(x,y,0,t)$ is the acoustic pressure exerted by the fluid on the plate.

By using the Hamilton's variation method [11]:

$$H(w) = \int_{t_1}^{t_0} \delta(T - V + W_{excitation})dt + \int_{t_1}^{t_0} \delta W_{fluid}\, dt \tag{3.3}$$

Where $H(w)$ is the Hamilton's operator, T is the kinetic energy of the plate, V is the strain energy, w is the displacement of the plate, and t_0 *and* t_1 are arbitrary times.

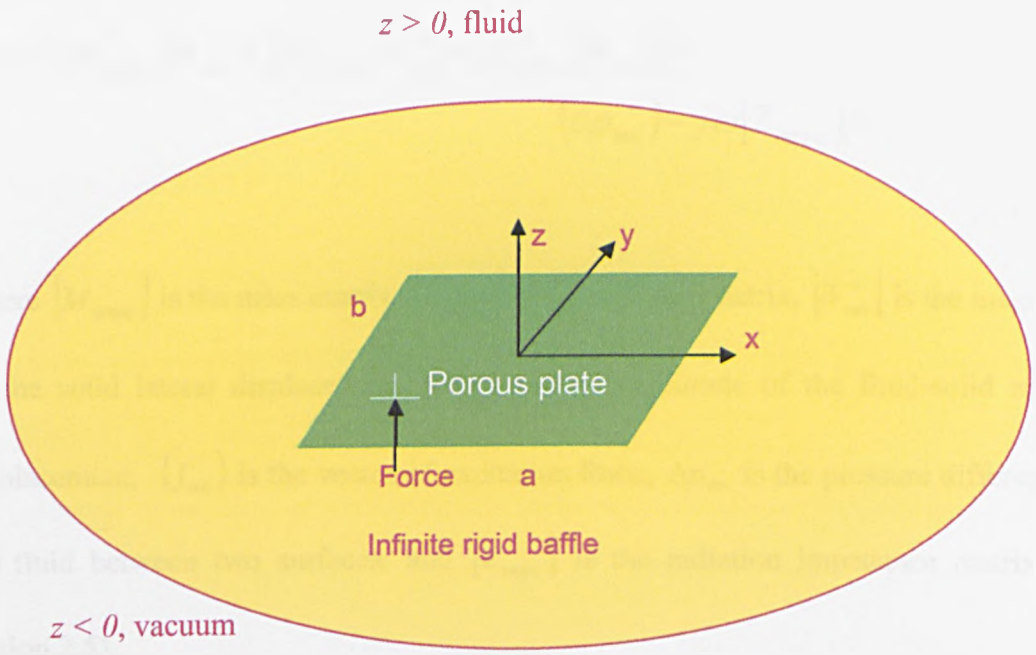

Figure3.1: The geometry of a baffled plate

The formulation for the porous plate motion can be written in terms of the Lagrange's equations by using the stationary condition for the Hamilton's method, and is given by;

$$\frac{d}{dt}\frac{\partial T}{\partial A_{mn}} + \frac{\partial V}{\partial A_{mn}} = \frac{\partial W_{excitation}}{\partial A_{mn}} + \frac{\partial W_{fluid}}{\partial A_{mn}}, \tag{3.4}$$

The equations for the porous plate motion are described in section 1.5. Details of their derivation can be found in the references [7, 8, 9, 10].

The vibrational response of the fluid-loaded porous plate can be obtained by inserting an additional external force $(-j\omega[Z_{mnpq}][W^s_{mn} + W_{mn}])$ acting on the plate in Equations1.7(a, b). At a given angular frequency ω, in the frequency domain (i.e. Fourier transform of the equation (3.4)), the equation of porous plate motion can be written in matrix form. The matrix form of the equation of fluid loaded porous plate motion is given by;

$$\left(-\omega^2\left[M^1_{mnpq}\right]W^s_{mn}+\left[\left[K^{s_1}_{mnpq}\right]W^s_{mn}+\left[K^1_{mnpq}\right]W_{mn}\right]\right)=$$
$$\left(f_{mn}\right)-j\omega\left[Z_{mnpq}\right]\left[W^s_{mn}+W_{mn}\right]$$

$$\left(-\omega^2\left[M^2_{mnpq}\right]W^s_{mn}+\left[\left[K^{s_2}_{mnpq}\right]W^s_{mn}+\left[K^2_{mnpq}\right]W_{mn}\right]\right)=$$
$$\left(\Delta p_{mn}\right)-j\omega\left[Z_{mnpq}\right]\left[W^s_{mn}+W_{mn}\right]$$

(3.5- a, b)

where $\left[M_{mnpq}\right]$ is the mass matrix, $\left[K_{mnpq}\right]$ is the stiffness matrix, $\left[W^s_{mn}\right]$ is the magnitude of the solid lateral displacement, $\left[W_{mn}\right]$ is the magnitude of the fluid-solid relative displacement, $\left(f_{mn}\right)$ is the vector of excitation force, Δp_{mn} is the pressure difference in the fluid between two surfaces, and $\left[Z_{mnpq}\right]$ is the radiation impedance matrix (see section 2.5).

The coefficients of the mass matrix are defined by:

$$\left[M^1_{mnpq}\right]=\sum_{m=1}^{\infty}\sum_{n=1}^{\infty}\sum_{p=1}^{\infty}\sum_{q=1}^{\infty}\left[\left(D+\frac{\alpha^2 Mh^3}{12}\right)\left(I_1I_2+2I_3I_4+I_5I_6\right)\right]$$

$$\left[M^2_{mnpq}\right]=\sum_{m=1}^{\infty}\sum_{n=1}^{\infty}\sum_{p=1}^{\infty}\sum_{q=1}^{\infty}\left[\alpha\, Mh\,\left(I_2I_3+I_4I_6\right)\right] \qquad \text{(3.6-a, b)}$$

The coefficients of the stiffness matrices are defined by;

$$\left[K^{s_1}_{mnpq}\right]=\sum_{m=1}^{\infty}\sum_{n=1}^{\infty}\sum_{p=1}^{\infty}\sum_{q=1}^{\infty}-h\rho\omega^2I_2I_6$$

$$\left[K^1_{mnpq}\right]=\sum_{m=1}^{\infty}\sum_{n=1}^{\infty}\sum_{p=1}^{\infty}\sum_{q=1}^{\infty}-h\rho_f\omega^2I_2I_6$$

$$\left[K^{s_2}_{mnpq}\right]=\sum_{m=1}^{\infty}\sum_{n=1}^{\infty}\sum_{p=1}^{\infty}\sum_{q=1}^{\infty}h\rho_f\omega^2I_2I_6$$

$$\left[K^2_{mnpq}\right]=\sum_{m=1}^{\infty}\sum_{n=1}^{\infty}\sum_{p=1}^{\infty}\sum_{q=1}^{\infty}hm(\omega)\omega^2I_2I_6 \qquad \text{(3.7-a,b,c,d)}$$

Where (I_1)-(I_6) are the simple definite integrals described in section 1.5.

3.3 NUMERICAL RESULTS

The effects of the fluid loading have been obtained by successive recalculations of the solutions and of the fluid loading term. The effects of the fluid loading have been calculated for three different plates. By solving equation (1.7. a, b) for *r, n modes,* the coefficients W_{rn}^{s} and W_{rn} can easily be found. Once we find the coefficients W_{rn}^{s} and W_{rn}, the deflection of porous plates can be calculated by the Equation (1.10. a, b). The modes (r, n) are taken to be equal to 16 in each direction. The characteristics of the plates are given in the Table 1.2.

A Gaussian quadrature scheme with 20 terms of the Legendre polynomial is used to expand and calculate the mean square velocity and fluid loaded plate deflection. The plates are excited by a point force applied at $x_0 = 0.1$ m, $y_0 = 0.09$ m from a corner of the plates. The plate responses are calculated at locations given by $x = 0.24$ m and $y = 0.24$ m, $x = 0.15$ m and $y = 0.15$ m, $x = 0.35$ m and $y = 0.35$ m. The fluids assumed in these calculations are water and air.

Figures 3.2, (a, b, c) show the predicted deflections of a clamped YB10 foam plate at the different locations of the plate as a function of the frequency. The responses of YB10 foam are calculated in-vacuo, in-air, and in-water. There is only a very small difference between the predicted response in-air and in-vacuo response throughout frequency range. The predicted deflection of the plate in water is less than those predicted in-vacuo and in air. The resonant frequencies are shifted to a lower frequency by about 40 Hz. The shape of the curves is not affected very much by the fluid loading but the values of the curves are changed by the fluid loading.

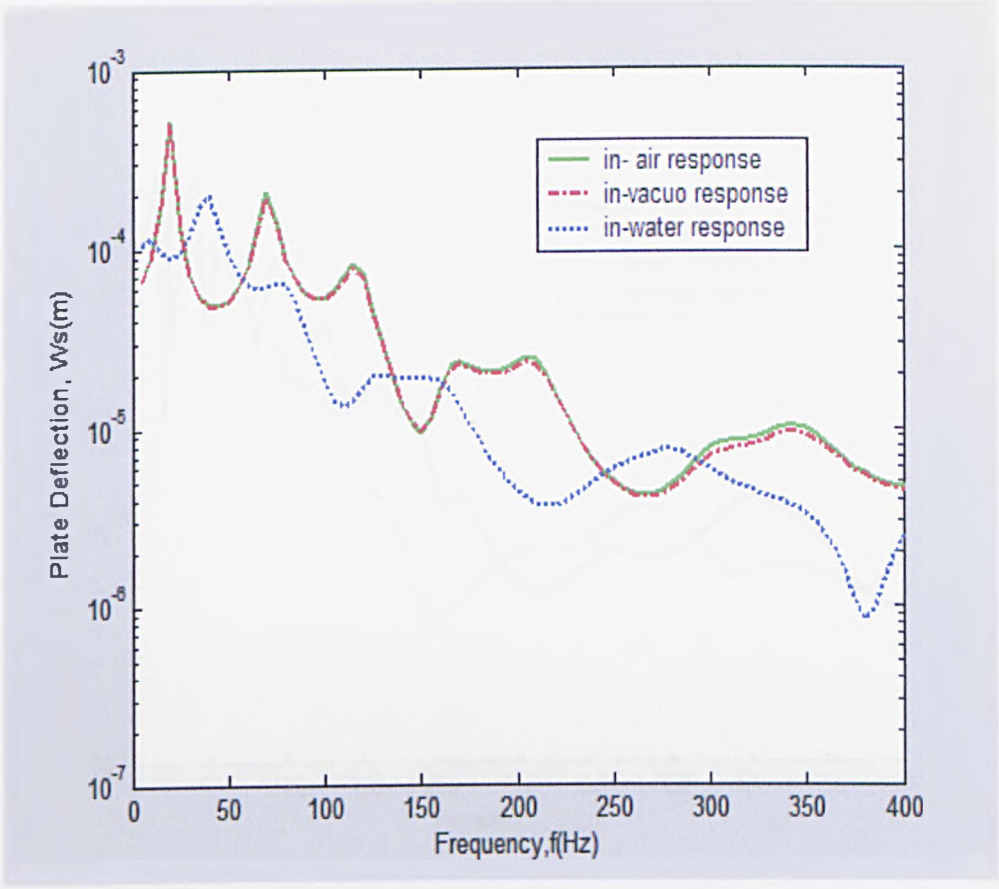

a-) at the centre of the plate

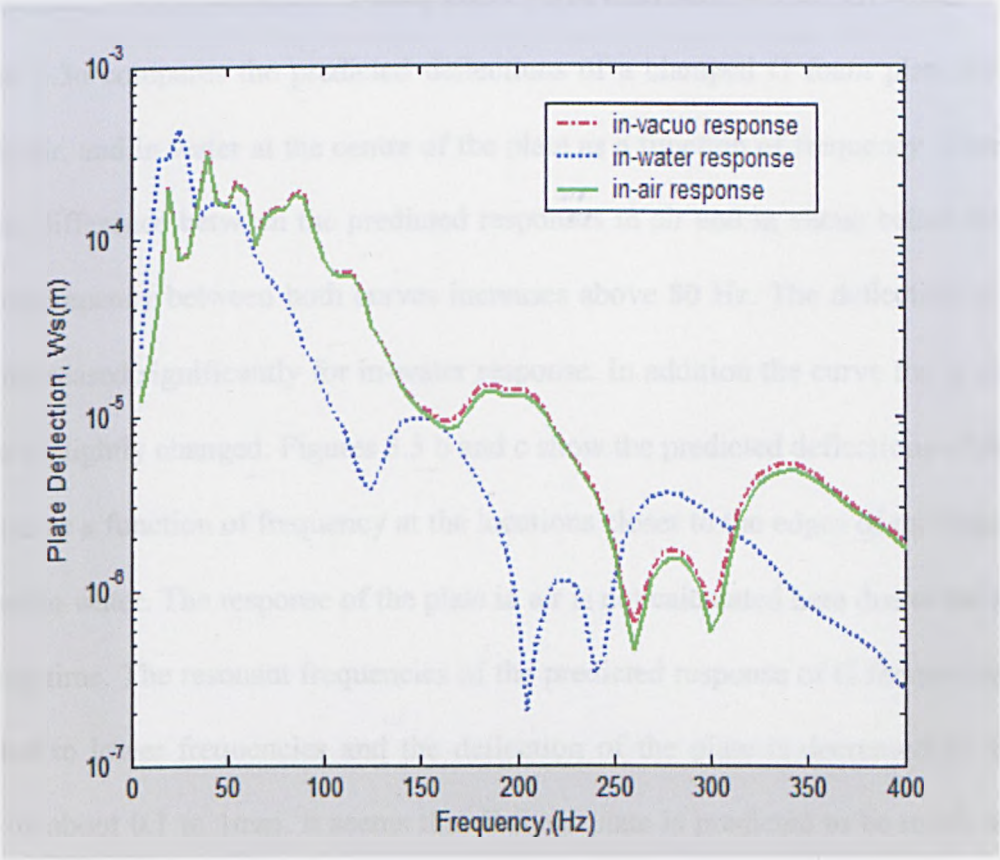

b-) at x=0.35m and y=0.35m

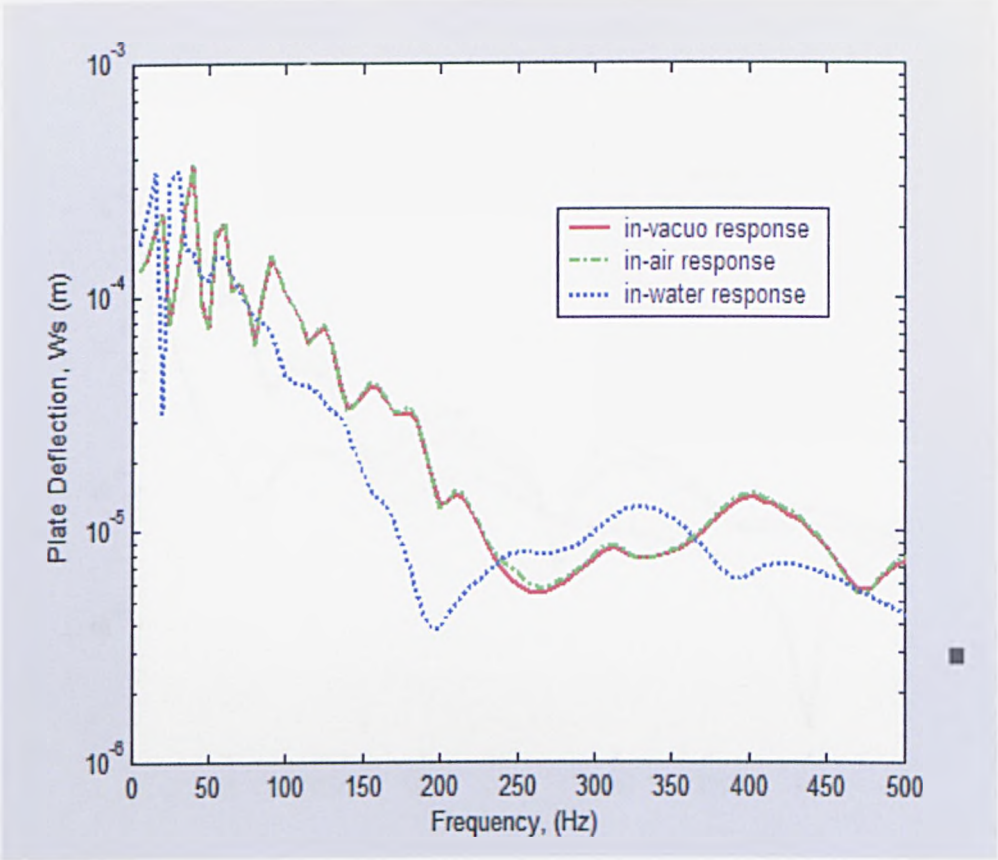

c-) at x=0.15m and y=0.15m

Figure3.2. Predicted deflections of fluids loaded YB10 foam and in-vacuo YB10 foam

In Figure 3.3a compares the predicted deflections of a clamped G foam plate for in-vacuo, in air, and in water at the centre of the plate as a function of frequency. There is negligible difference between the predicted responses in air and in vacuo below 80 Hz but the discrepancy between both curves increases above 80 Hz. The deflection of the plate is decreased significantly for in-water response. In addition the curve for in water response is slightly changed. Figures 3.3 b and c show the predicted deflections of the G foam plate as a function of frequency at the locations closer to the edges of the plate in-vacuo and in water. The response of the plate in air is not calculated here due to the long computing time. The resonant frequencies of the predicted response of G foam in water are shifted to lower frequencies and the deflection of the plate is decreased by fluid loading by about 0.1 to 1mm. It seems that G foam plate is predicted to be much more affected plate by fluid (water) loading.

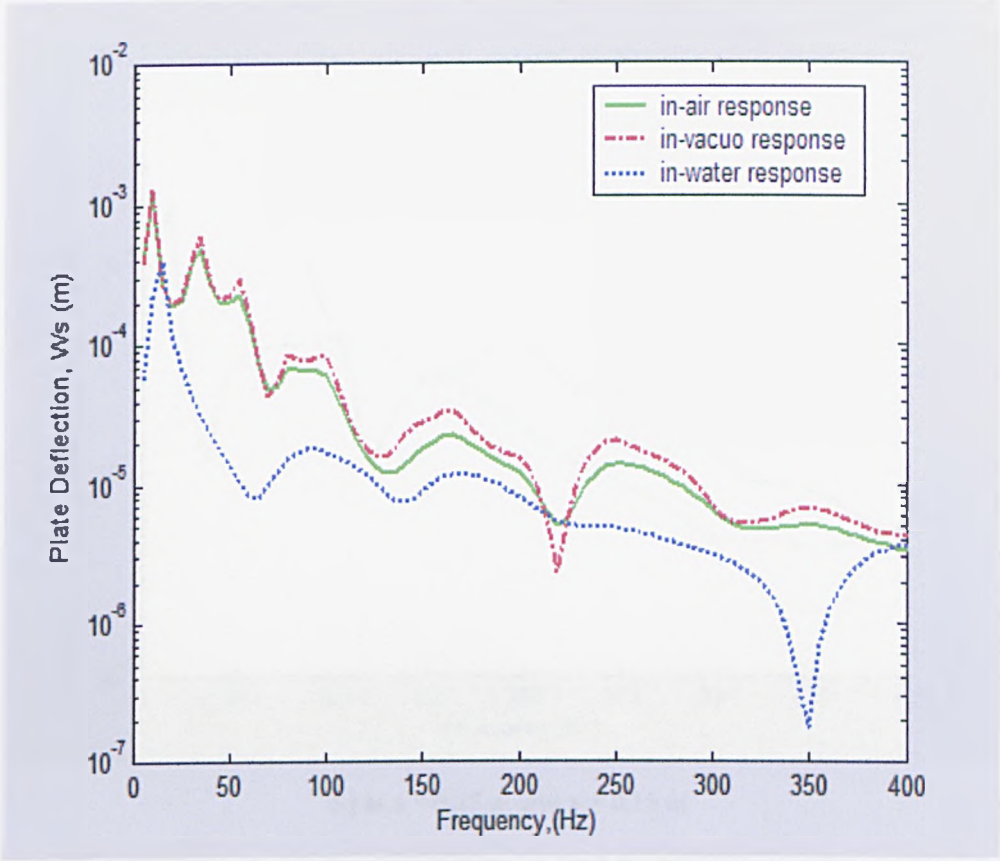

a-) at the centre of the plate

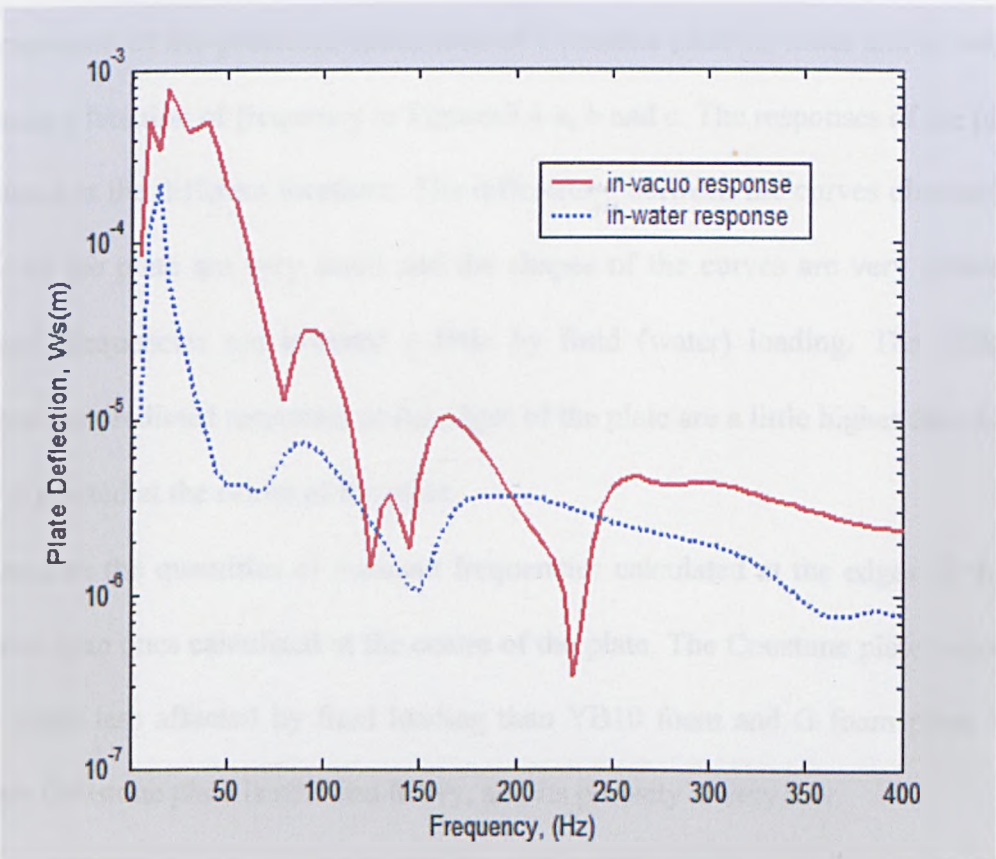

b-) at x = 0.35 m and y = 0.35 m

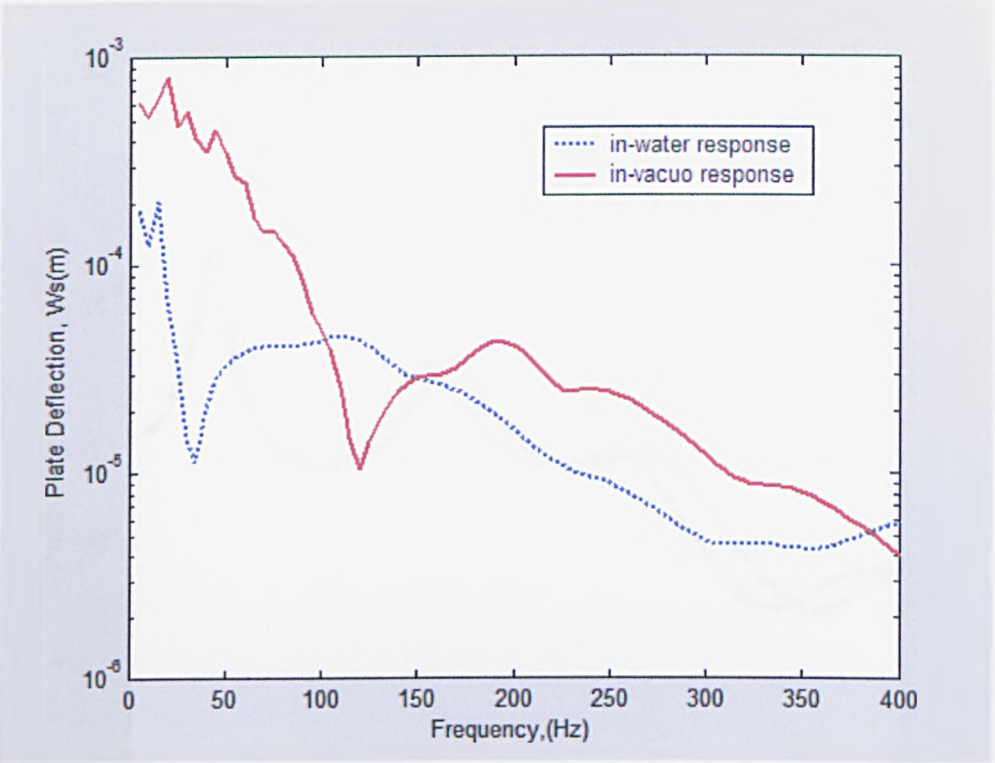

c-) at x = 0.15 m and y = 0.15 m

Figure3.3 (a, b, c): Predicted deflections of fluid loaded G foam and in-vacuo G foam

A comparison of the predicted deflections of Coustone plate in water and in vacuo are shown as a function of frequency in Figures3.4-a, b and c. The responses of the plate are calculated at the different locations. The differences between the curves obtained at the centre of the plate are very small and the shapes of the curves are very similar. The resonant frequencies are lowered a little by fluid (water) loading. The differences between the predicted responses at the edges of the plate are a little higher than between those predicted at the centre of the plate.

Furthermore the quantities of resonant frequencies calculated at the edges of the plate are more than ones calculated at the centre of the plate. The Coustone plate is predicted to be much less affected by fluid loading than YB10 foam and G foam plate. This is because Coustone plate is stiff and heavy, and its porosity is very low.

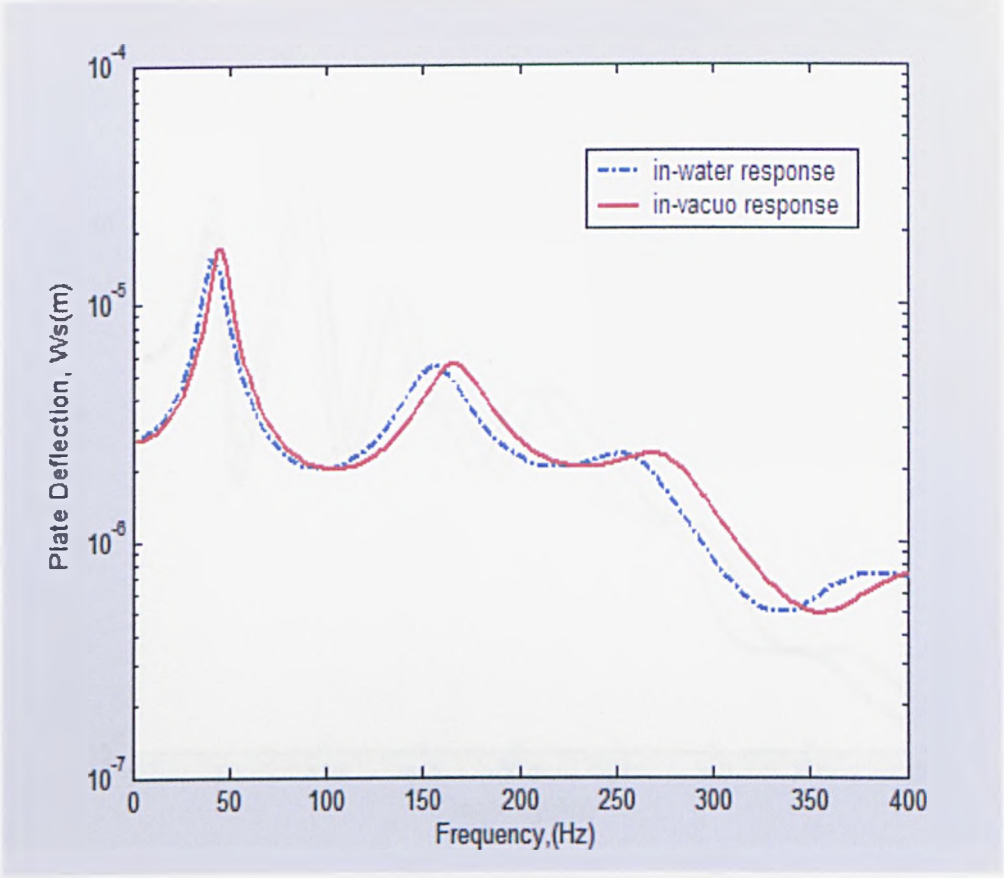

a-) at the centre of the plate

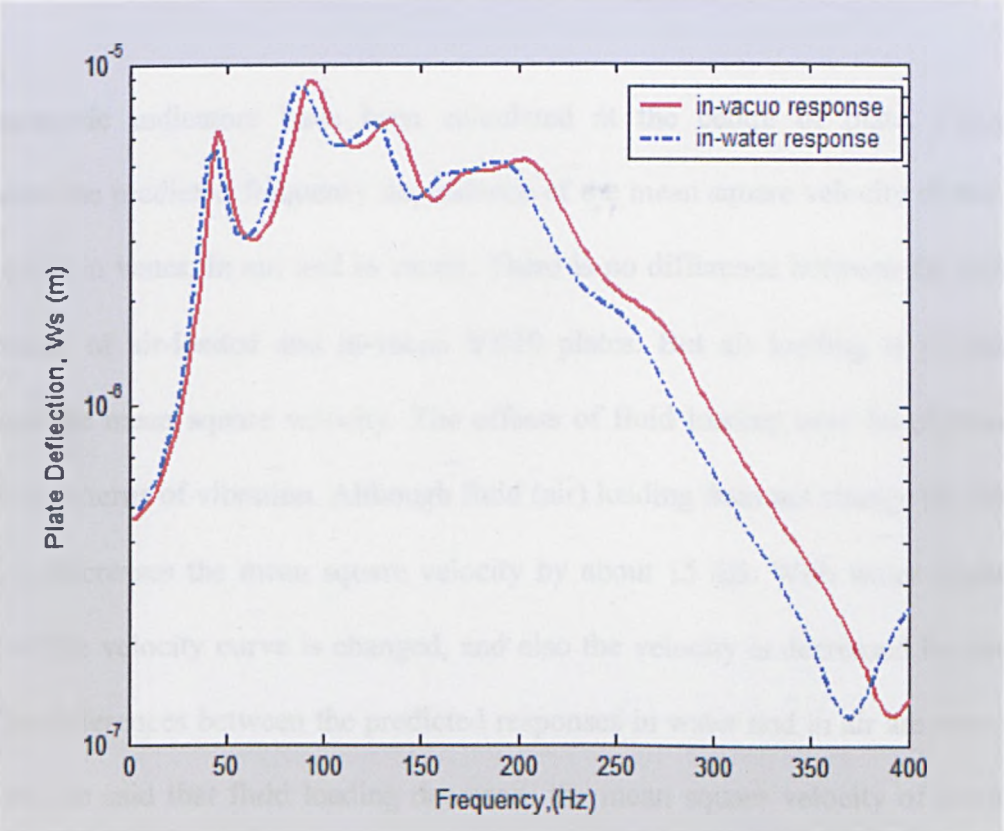

b-) at x=0.35m and y=0.35m

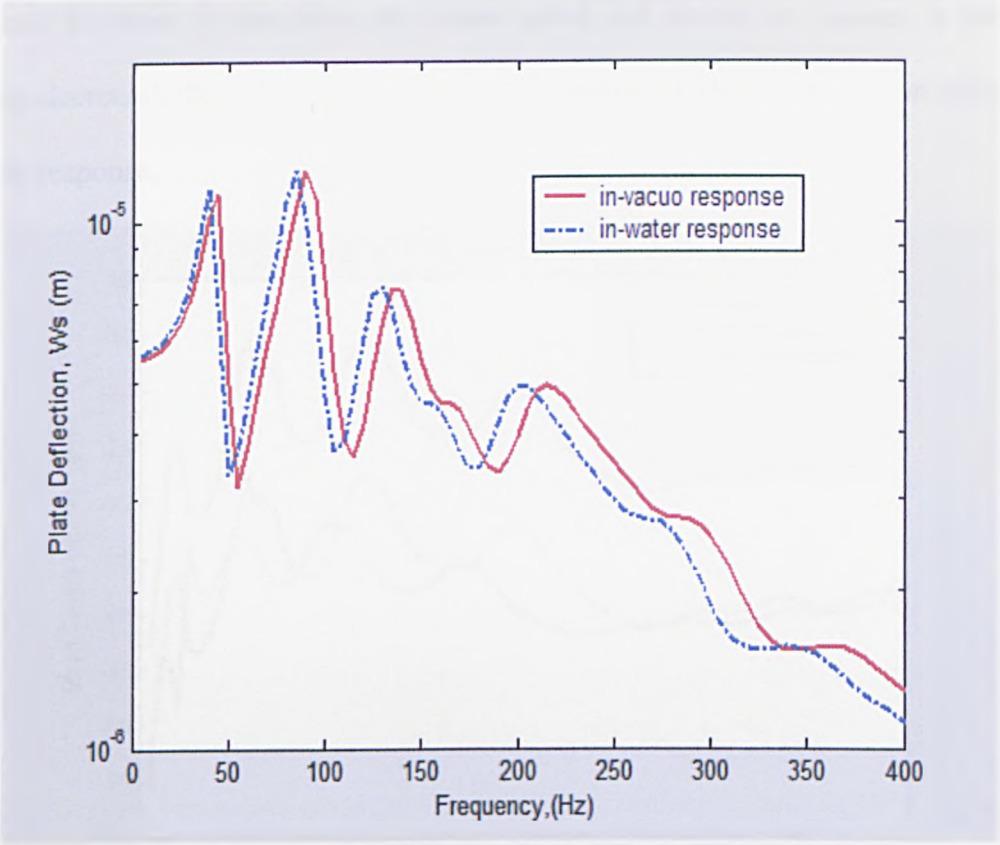

c-) at x = 0.15 m and y = 0.15 m

Figure3.4: Predicted deflections of the fluid loaded Coustone plate and in-vacuo Coustone plate

Vibroacoustic indicators have been calculated at the centre of plate. Figure 3.5 compares the predicted frequency dependence of the mean square velocity of the YB10 foam plate in water, in air, and in vacuo. There is no difference between the predicted deflections of air-loaded and in-vacuo YB10 plates. But air loading is predicted to decrease the mean square velocity. The effects of fluid loading may be explained by different patterns of vibration. Although fluid (air) loading does not change the shape of curve, it decreases the mean square velocity by about 15 dB. With water loading the shape of the velocity curve is changed, and also the velocity is decreased by about 20 dB. The differences between the predicted responses in water and in air are very small. So it can be said that fluid loading decreases the mean square velocity of poroelastic materials. The frequency dependence of the radiated sound power of the YB10 foam plate predicted in air and in water is shown in Figure 3.6. The radiated sound power

predicted in-vacuo is zero since the sound speed and density in vacuum is zero. Air loading decreases the radiated sound power by about 30 dB in comparison with water loading response.

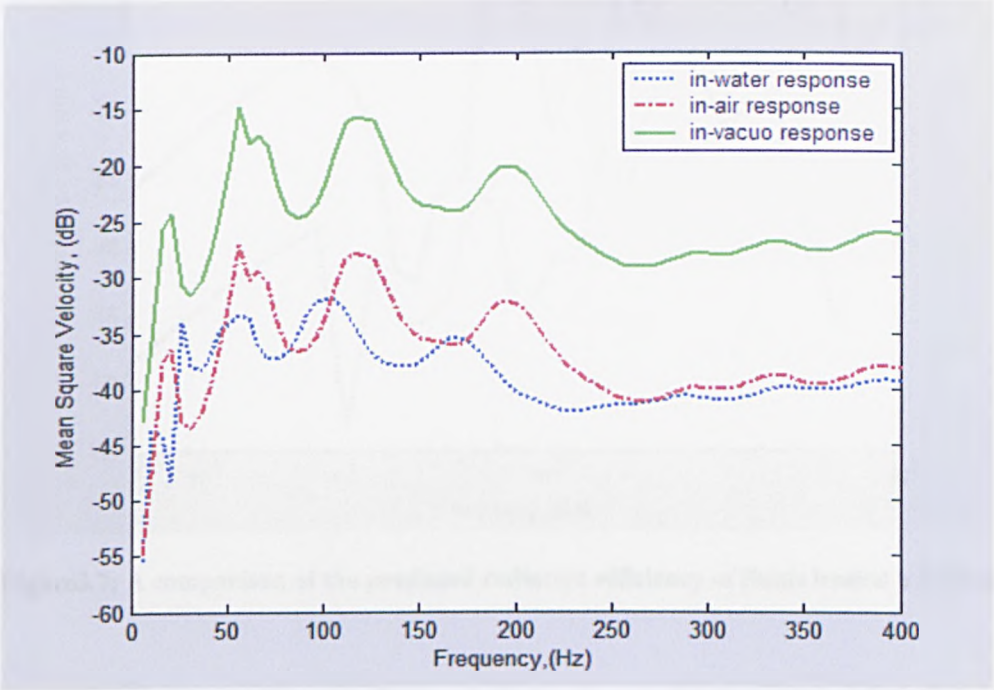

Figure3.5: Comparison of the mean square velocities of fluids loaded YB10 plate and in-vacuo YB10 plate.

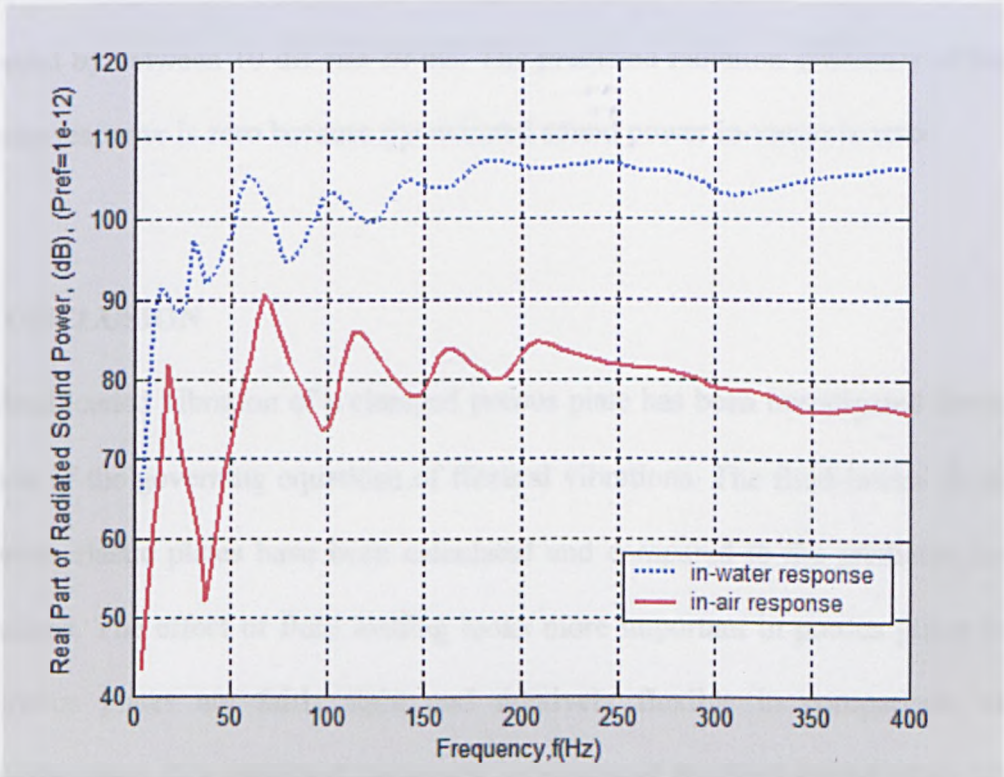

Figure3.6: A comparison of the radiated sound powers of fluids loaded YB10 plate.

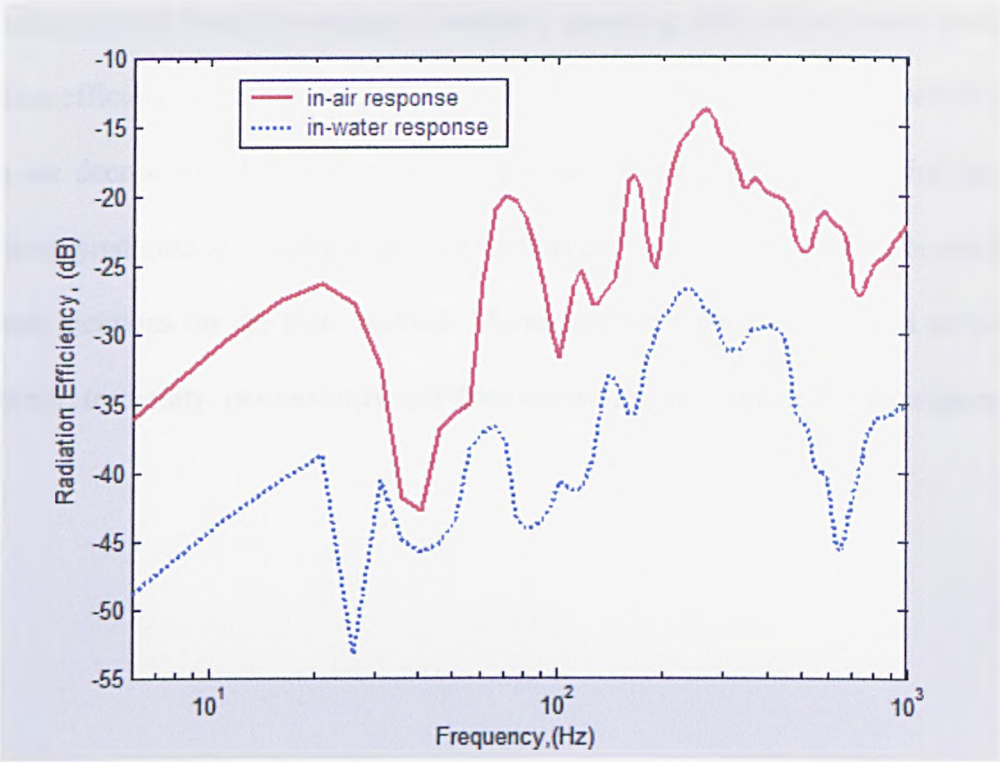

Figure3.7: A comparison of the predicted radiation efficiency of fluids loaded YB10 plate.

A comparison of the predicted radiation efficiencies of the fluid-loaded YB10 plate is shown in Figure 3.7. The predicted radiation efficiency of the plate in air is higher than that predicted in water. With water loading the radiation efficiency of the porous plate is decreased by between 10 dB and 20 dB. The predicted radiation efficiency of the plate in-vacuo response is zero because the radiated sound power in-vacuo is zero.

3.4 CONCLUSION

The fluid-loaded vibration of a clamped porous plate has been investigated through the solution of the governing equations of flexural vibrations. The fluid-loaded deflections of porous elastic plates have been calculated and compared to the predicted in-vacuo deflections. The effect of fluid loading looks more important in porous plates because the porous plates are fairly light and relatively flexible in comparison with an aluminium plate. The predicted frequency responses of the fluid-loaded plate vibration

and radiation have been investigated. Generally speaking, with air and water loading the radiation efficiency, the mean square velocity, and the radiated sound power of porous plates are decreased. The location and magnitude of the force during point excitation have been predicted to be very important. Different responses have been observed at the different locations on the plate surface. Micro-structural parameters, such as porosity, loss factor, tortuosity, permeability and flow resistivity, are expected to be important.

References:

1. G. Madianik, and E. M. Kerwin, "Influence of fluid loading on the radiation from infinite plates below the critical frequency," J. Acoust. Soc. Am. 40, 1034-1038(1966).
2. G. Maidanik, "Influence of fluid loading on the radiation from orthotropic plates," J. Sound Vib. 3, 288-299 (1966).
3. D. Feit, "Pressure radiated by a point-excited elastic plate," J. Acoust. Soc. Am. 40, 1489-1494(1966).
4. B. E. Sandman, "Motion of a three-layered elastic-viscoelastic plate under fluid loading," J. Acoust. Soc. Am. 57(5), 1097-1107(1975).
5. B. E. Sandman, "Fluid loaded vibration of an elastic plate carrying a concentrated mass," J. Acoust. Soc. Am. 61(6), 503-1510(1977).
6. Berry, "A new formulation for the vibrations and sound radiation of fluid-loaded plates with elastic boundary conditions," J. Acoust. Soc. Am. 96((2), 889-901(1994).
7. D. D Theodorakopoulos and D. E Beskos, "Flexural vibration of poroelastic plates," Acta Mechanica, 103, 191-203 (1994).
8. P. Leclaire, K. V. Horoshenkov, M. J Swift, and D. C. Hothersall, "The vibration response of a clamped rectangular porous plate," J. Sound Vib. 217(1), 19-31(2001).
9. P. Leclaire, A. Cummings and K. V. Horoshenkov, "Transverse vibration of a thin rectangular porous plate saturated by a fluid," J. Sound Vib. 247(1), 1-18(2001).
10. P. Leclaire, "Vibration of Porous Plates in Structural Acoustic Coupling Applications," 3rd European Congress on Acoustics. 16th –20th September 2002, Spain.

11. O. Foin, J. Nicolas, N. Atalla, "An efficient tool for predicting the structural acoustic and vibration response of sandwich plates in light or heavy fluid," *Applied Acoustics*, 57, 213-242(1999).

12. R. Szilard, 1974, "Theory and analysis of plates: classical and numerical methods," Englewood cliffs, NJ: Prentice-Hall.

13. A. Freedman, "Effects of fluid-loading on Lamb mode spectra," J. Acoust. Soc. Am. 99(6), 3488-3496(1996).

INSERTION LOSS OF PERFORATED POROELASTIC PLATES IN THE DUCT

4.1 INTRODUCTION

As Rayleigh [1] has explained, 'the fundamental characteristic of porous materials treated to reduce noise is that the produced fluid flow through poroelastic material is opposed because of the frictional force produced by the fibres or the cell walls on the fluid. This mechanism allows the energy to be absorbed from the acoustic wave and to be converted into heat.'

Horoshenkov [2] has used the Helmholtz integral equation formulation to produce the solution for the acoustic field reflected from a finite, thin, poroelastic plate in a rigid baffle with simply supported edges. He has predicted the acoustic properties of the porous material by using the effective fluid assumption.

Takahashi, Sakagami and Morimoto [3] have presented an analytical model of sound absorption in and sound transmission through a single permeable membrane. They carried out a theoretical investigation of the sound absorption of structures composed of air layers, absorptive layers and permeable membrane facings and compared predictions with the experimental data measured by using the reverberation-room method. Takahashi and Tanaka [4] have presented a new method for analyzing acoustic coupling due to flexural vibration of perforated plates and plates of poroelastic materials. The analytical model they presented is developed by introducing flow continuity at the plate surface in a spatially mean sense and air-solid interaction within the plate material. They have analyzed some acoustic problems based on a classical thin-plate theory in relation

to the interactive effect of flexural vibration and plate permeability to demonstrate the method of application.

Cummings [5-8] has carried out a series of investigations into the transmission of an internally propagated sound wave through single-layer ventilation ducts. Cummings and Astley [9] described a FE formulation for sound attenuation in "bar-silencers", consisting of rectangular prisms of sound-absorbing material placed in a rectangular lattice arrangement within a rigid-walled duct. They took a uniform mean gas flow in the "airway" of the silencer into account. Cummings [10] has analyzed the transmission of complex periodic and transient acoustic signals through orifice plates at high amplitude, and in the absence of mean fluid flow. He numerically solved the equation of motion for the air in the orifice numerically in the time domain.

Ingard [11] has studied the absorption and scattering from resonators in a free field as well as in walls.

Morfey [12] has extended the theory of sound transmission and generation in hard-walled ducts to include axial and swirling mean flow. The theory presented is based on the idea of a single-frequency mode response function rather than a Green function. Wendoloski [13] has examined the acoustic behaviour of a constricted duct when a mean flow is presented. The constriction considered in his work is in the form of a concentrically placed orifice (or aperture) plate.

The purpose of the present chapter is to study the effects of inserting a perforated porous plate on the uniformity of flow and sound absorption in the duct. These effects are assessed by measuring insertion loss at different locations in the duct. A parallel impedance model is used for the effects of perforation. The role of perforation is to increase the permeability and to decrease the pressure drop associated with the insertion of the layer. The plate is assumed to be governed by the clamped rectangular porous plate theory developed by Leclaire [14]. The measured insertion loss of porous plate in

the absence of mean air flow is compared to predicted data. The absorption coefficient of a perforated poroelastic plate is calculated for normal incidence.

4.2 THEORETICAL ANALYSIS

4.2.1 Acoustical coupling for perforated porous plate

A conceptual model of a perforated poroelastic plate is given in Fig.4.1. In present work we assume that perforated porous plate and the baffle separate two fluid half-spaces.

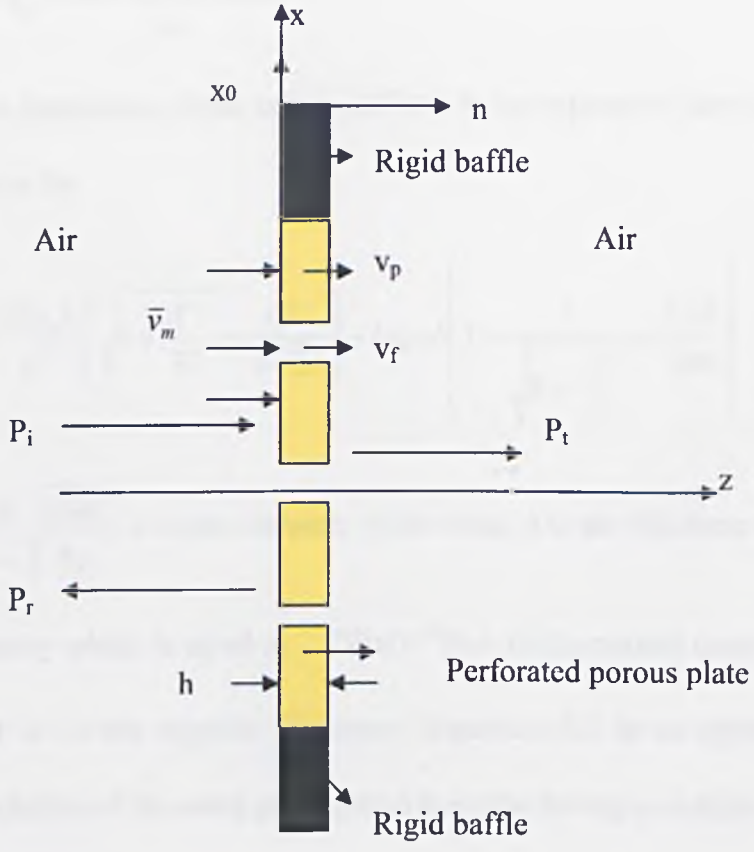

Figure4.1: Analytical model of a perforated porous plate in rigid baffle

The pressure difference ∇P on both sides of the plate causes plate vibration in a flexural mode with velocity v_p. The mean particle velocity $\bar{v}_m$ is given by [4];

$$\bar{v}_m = v_p + (v_f - v_p)\,\tilde{\lambda} \tag{4.1}$$

where v_f is the spatially averaged velocity of the hole and λ is the ratio of perforation.

Let Z_0 be the impedance of the hole which is given by

$$Z_0 = Z_{resist} + Z_{react} = \nabla P / v_f \,. \tag{4.2}$$

The real part of the impedance Z_0 is related to air-solid interaction in the hole. The relative velocity between the hole and the porous plate is given by [4];

$$v_f - v_p = \frac{\nabla P}{Z_0} - \frac{Z_{react}}{Z_0} v_p \tag{4.3}$$

by inserting Eq. (4.3) into Eq. (4.1), the mean particle velocity becomes

$$\bar{v}_m = v_p - \frac{(Z_{react} v_p + \nabla P)\lambda}{Z_0} \tag{4.4}$$

The acoustic impedance of the hole is defined by an expression developed by Maa [15], which is given by

$$Z_0 = \frac{32\eta_0 h}{d^2}\left(\sqrt{1+\frac{X^2}{32}} + \frac{dX}{4\sqrt{2}h}\right) - i\rho_0\omega h\left(1 + \frac{1}{\sqrt{9+\frac{X^2}{2}}} + \frac{17d}{20h}\right) \tag{4.5}$$

where $X = \frac{d}{2}\sqrt{\frac{\rho_0\omega}{\eta_0}}$, d is the diameter of the hole, h is the thickness of the plate, η_0 is the air viscosity which is equal to $1.839x10^{-5}$Pa.s in the normal condition, ρ_0 is the air density and ω is the angular frequency. Equation 4.5 is an approximation for the analytical solution of the wave propagation in a tube having a circular cross section, and a given end correction.

The boundary conditions for the acoustic velocities at the source side of the perforated porous plate are given by

$$\frac{\nabla P_S}{i\omega\rho_0} = \xi v_p + \frac{P_S}{Z_{in}}\lambda \tag{4.6}$$

where Z_{in} is the front specific acoustic impedance of the plate, P_S is the sound pressure on the source side, and $\xi = 1 - (Z_{react} / Z_0)\lambda$.

The boundary conditions for the acoustic pressures and velocities at the receiver side of the plate are given by

$$P_t = P_b^+ e^{i\gamma_b} + P_b^- e^{-i\gamma_b} \tag{4.7}$$

$$\frac{\nabla P_t}{i\omega\rho_0} = \xi v_p + \frac{\nabla P_b}{Z_{in}}\lambda \tag{4.8}$$

where P_t is the transmitted sound pressure, $\gamma_b = k_p h$ and k_p is the complex wave number of the porous medium.

When the plate is loaded by a fluid half-space, the front surface acoustic impedance is given by [16];

$$Z_{in} = Z_p \frac{Z_a - jZ_p \cot g(k_p h)}{Z_p - jZ_a \cot g(k_p h)} \tag{4.9}$$

where $Z_p = \rho_p c_p$ is the characteristic impedance of the porous medium, c_p is the complex sound speed in the porous medium and ρ_p is the effective density of the fluid in porous medium. $Z_a = \rho_0 c_0$ is the acoustic impedance of the fluid half-space.

4.2.2 Formulation for the effective density and the bulk modulus

Several methods have been developed to calculate the effective density and the bulk modulus in rigid-porous materials by Attenborough [17], Allard [16], and Horoshenkov *et al* [18]. The effective density in the porous material with rigid frame is given by [16];

$$\rho_p = \alpha_\infty \rho_0 \left[\frac{\sigma\phi}{j\omega\rho_0\alpha_\infty} G_j(\omega) \right] \tag{4.10}$$

where α_∞ is the tortuosity, ϕ is the porosity, and $G_j(\omega)$ is given by

$$G_j(\omega)=\left(1+\frac{4j\alpha_\infty^2\eta\rho_0\omega}{\sigma^2\Lambda^2\phi^2}\right)^{1/2} \tag{4.11}$$

where Λ is the characteristic dimension for viscous forces and given by

$$\Lambda=\frac{1}{c}\left(\frac{8\alpha_\infty\eta}{\phi\sigma}\right)^{1/2} \tag{4.12}$$

where c is the shape factor.

The bulk modulus for the air in the porous material is given [16];

$$K=\frac{\gamma P_0}{\gamma-(\gamma-1)\left[1+\frac{8\eta}{j\Lambda'^2B^2\omega\rho_0}\left(1+j\rho_0\frac{\omega B^2\Lambda'^2}{16\eta}\right)^{1/2}\right]^{-1}} \tag{4.13}$$

where γ is the fluid specific heat ratio, B^2 is the Prandtl number, P_0 is the ambient atmospheric pressure, and Λ' is the characteristic thermal dimension and given by

$$\Lambda'=\frac{1}{c'}\sqrt{\frac{8\alpha_\infty\eta}{\phi\sigma}} \tag{4.14}$$

where c' is a coefficient that should be equal to or smaller then c, because of Λ' being equal to or larger then Λ.

4.2.3 Reflected sound pressure for a perforated porous plate

A plate as shown in Figure 4.1 is vibrating under a plane wave with the sound pressure P_i which is given by e^{izk_0}. According to the Helmholtz integral formulation for a two-dimensional problem, the sound pressure $P_s(x)$ on the surface of the source side of the plate can be expressed as follows [19]:

$$P_s(x)=2\left[P_i(x)\right]_{z=0}-2\int\left(P_s(x_0)\frac{\partial G(x\mid x_0)}{\partial n}-G(x\mid x_0)\frac{\partial P_s(x_0)}{\partial n}\right)_{z=0}dx_0 \tag{4.15}$$

where $G(x \mid x_0)$ is the two-dimensional free-space Green's function, which is given by $G(x \mid x_0) = (i/4)H_0^{(1)}(k_0 \mid x - x_0 \mid)$. $H_0^{(1)}$ is the Hankel function of the first kind of order zero, which is given by $H_0^{(1)}(k_0 \mid x - x_0 \mid) = \int_0^a \frac{e^{ik_0(x-x_0)}}{\pi i k_0} dx_0$. n is the normal taken outward, perpendicular to the surface of the plate.

In the case of a plane surface, the term involving $\frac{\partial G(x \mid x_0)}{\partial n}$ vanishes. Then equation (4.15) becomes

$$P_s(x) = 2[P_i(x)]_{z=0} + 2\int \left(G(x \mid x_0) \frac{\partial P_s(x_0)}{\partial n} \right)_{z=0} dx_0 \tag{4.16}$$

The normal gradient of the pressure at the boundary is $\partial P_s(x_0)/\partial n = i\rho_0 \omega v(x_0)$.

Then equation (4.16) becomes

$$P_s(x) = 2P_i(x) + \frac{i}{2}\int_0^a \rho_0 \omega v(x_0) H_0^{(1)}(k_0 \mid x - x_0 \mid) dx_0 \tag{4.17}$$

Using the boundary condition (4.6) the acoustic pressure on the surface of the source side of the plate can be expressed as

$$P_s(x) = 2P_i(x) + \frac{i}{2}\int_0^a \left[\omega^2 \rho_0 \xi w + ik_0 \chi_1 P_s(x_0)\right] H_0^{(1)}(k_0 \mid x - x_0 \mid) dx_0 \tag{4.18}$$

where χ_1 is the specific acoustic admittance of the source side of the plate surface which is given by $(\rho_0 c_0 \lambda / Z_m)$, and w is the displacement of the plate.

The solution of the equation of a poroelastic plate is given by Equation (1.10.a, b). Equation (4.18) can be solved analytically by using the Fourier transform technique. The detailed procedures are given in Horoshenkov's work [2] and in Takahashi's works [3-20]. Finally, the solution for the acoustic pressure can be expressed as

$$P_s = \frac{i\rho_0 w \xi / k_0 + 2(1 + \chi_1)}{1 + 2\chi_1} \tag{4.19}$$

The reflected sound pressure P_r can be calculated by using the Helmholtz integral equation for a two-dimensional problem at a certain point (x, z) and by substituting the boundary value P_s. Then P_r becomes

$$P_r(z) = \frac{i\rho_0 w\xi / k_0 + e^{-ik_0 z}}{1 + 2\chi_1} \tag{4.20}$$

The absorption coefficient of the plate can be calculated from

$$\alpha_{abs} = 1 - \left| P_r / P_i \right|^2 \tag{4.21}$$

4.2.4 Sound transmission through a perforated porous plate

In an analogous manner, by using the boundary condition (4.8) and the Helmholtz integral formulation the surface acoustic pressure P_t on the receiver side can be expressed as follows [2];

$$P_t(x) = -\frac{i}{2}\int_0^a \left[\rho_0\omega^2\xi w + ik_0\chi_2\varepsilon P_b(x_0)\right] H_0^{(1)}(k_0 \mid x - x_0 \mid) dx_0 \tag{4.22}$$

where χ_2 is the specific acoustic admittance of the receiver side of the plate surface, which is given by $(\rho_0 c_0 \lambda / Z_{in})$, and ε is the velocity transfer coefficient, which is given by

$$\varepsilon = \frac{e^{i\gamma_b} - r_b e^{-i\gamma_b}}{1 - r_b} \tag{4.23}$$

where r_b is the reflection coefficient of the receiver side of the plate, which is given by

$$r_b = \frac{Z_a - Z_p}{Z_p + Z_a} e^{2i\gamma_b} \tag{4.24}$$

By substituting the sound pressure and its normal derivative on the boundary surface into a Helmholtz integral formula, the transmitted sound pressure can be obtained as [4];

$$P_t(z) = \frac{2\chi_2 \varepsilon e^{ik_0 z} - i\rho_0 \omega^2 \xi w / k_0}{1 - 2\chi_2 \varepsilon} \tag{4.25}$$

The insertion loss *IL* is given by

$$IL = 10 \log 10\left(\left|P_i / P_t\right|\right)^2 \tag{4.26}$$

4.3 NUMERICAL RESULTS

The absorption coefficient and the insertion loss have been predicted for two poroelastic plates with two different perforation ratios in the case of rigid baffle separating two air half-spaces as shown in Figure 4.1. The measured characteristics of the plates are given in Table 4.1. The acoustic impedance of the plate Z_p, the complex wave number k_p, the complex sound speed in the porous plate c_p, and the effective density of the fluid in porous plate ρ_p are calculated by using the method of Allard *et al* [16].

Table4.1. The assumed Characteristics of the porous plates

	L_x (m)	L_y (m)	h (m)	ρ (kg/m^3)	E(Pa)	Loss factor	Porosity ϕ	Poission ratio ν	Flow resistivity, Ns/m^4	α_∞
YB10	0.5	0.5	0.01	353	2.1×10^7	0.1	0.69	0.35	68111	1.2
Black plate	1	1	21	223	2.46×10^6	0.35	0.75	0.3	46933	1.85

There is no particular reason for the numerical value chosen for the low perforation ratio. But the higher perforation ratio was chosen such that, in the measurements reported later, the perforations could be made without damaging the plate. Figure 4.2 shows the predicted effects of the perforation on the sound absorption coefficient of the YB10 plate. When the perforation ratio is increased, the absorption coefficient is changed slightly in the low frequency. But as frequency is increased the absorption

coefficient of the more highly perforated plate is predicted to increase up to 0.4 compared with values of less than 0.1 for the less perforated plate.

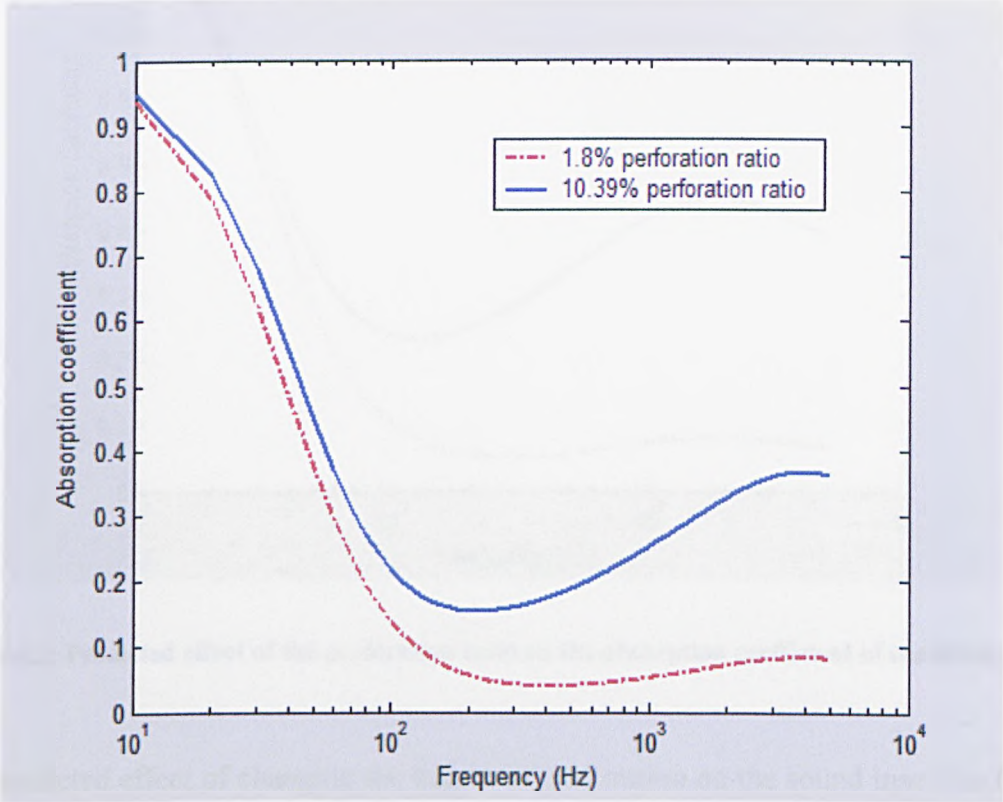

Figure.4.2: Predicted effect of the perforation ratio on the absorption coefficient of the YB10 plate.

The difference between absorption coefficients for the two perforation ratios is at maximum around 4000 Hz. The predicted influence of changing perforation ratios on the absorption coefficient of a black plate is shown in Figure 4.3. The results are similar to those obtained for the YB10 plate. The difference between two curves for the black plate is very small at low frequency. But the difference increases up to 0.35 at high frequency, and is at its maximum between 1000 Hz and 2000 Hz.

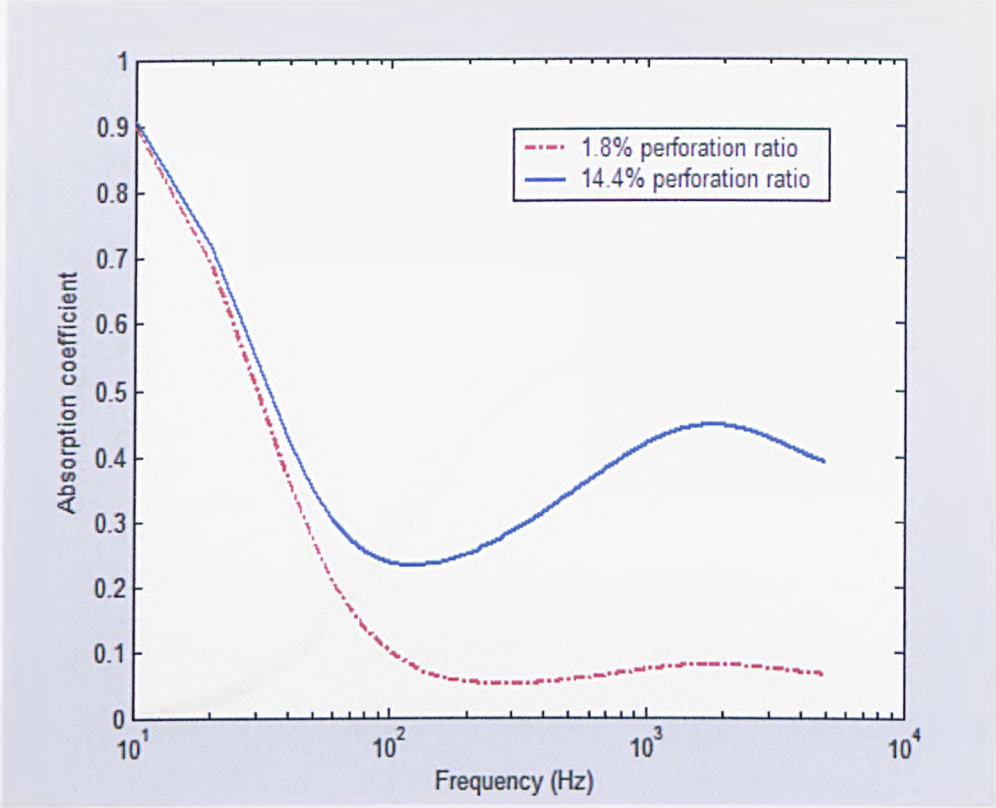

Figure.4.3: Predicted effect of the perforation ratio on the absorption coefficient of the Black plate

The predicted effect of changing the degree of perforation on the sound insertion loss of the YB10 plate is shown in Figure 4.4. The effect is negligible at low frequencies but increased with higher frequencies. At 2 kHz increasing perforation ratio is predicted to decrease the insertion loss of the YB10 plate by about 6dB. The predicted effect of changing perforation ratio on the insertion loss for the black plate is shown in the Figure 4.5. Again it seems that the perforation ratio is predicted to affect the insertion loss significantly at high frequencies, but only slightly affects the insertion loss at low frequencies. The gap between two curves increases above 200 Hz to a maximum near 3000 Hz. As shown in the Figure 4.5, increasing perforation ratio is predicted to decrease the insertion loss by about 7 dB at high frequency. The vibration has the greatest effect at low frequency while the visco-thermal effect has significant effect at higher frequencies.

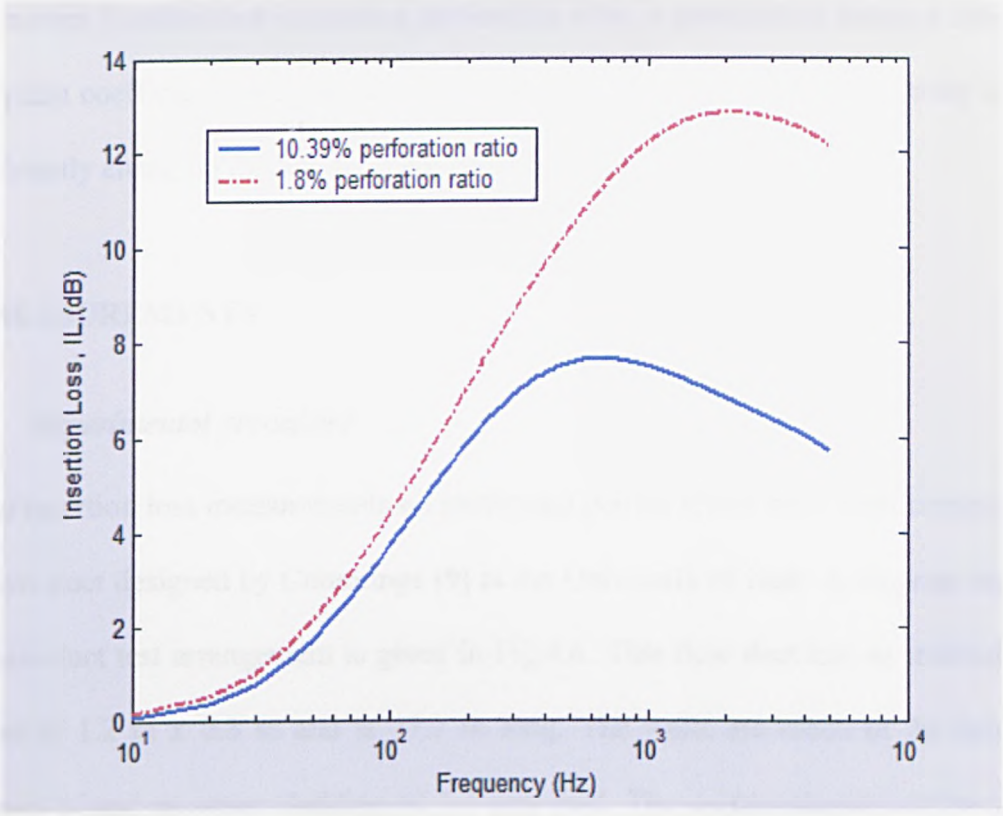

Figure.4.4: Predicted effect of the perforation ratio on the sound insertion loss of the YB10 plate.

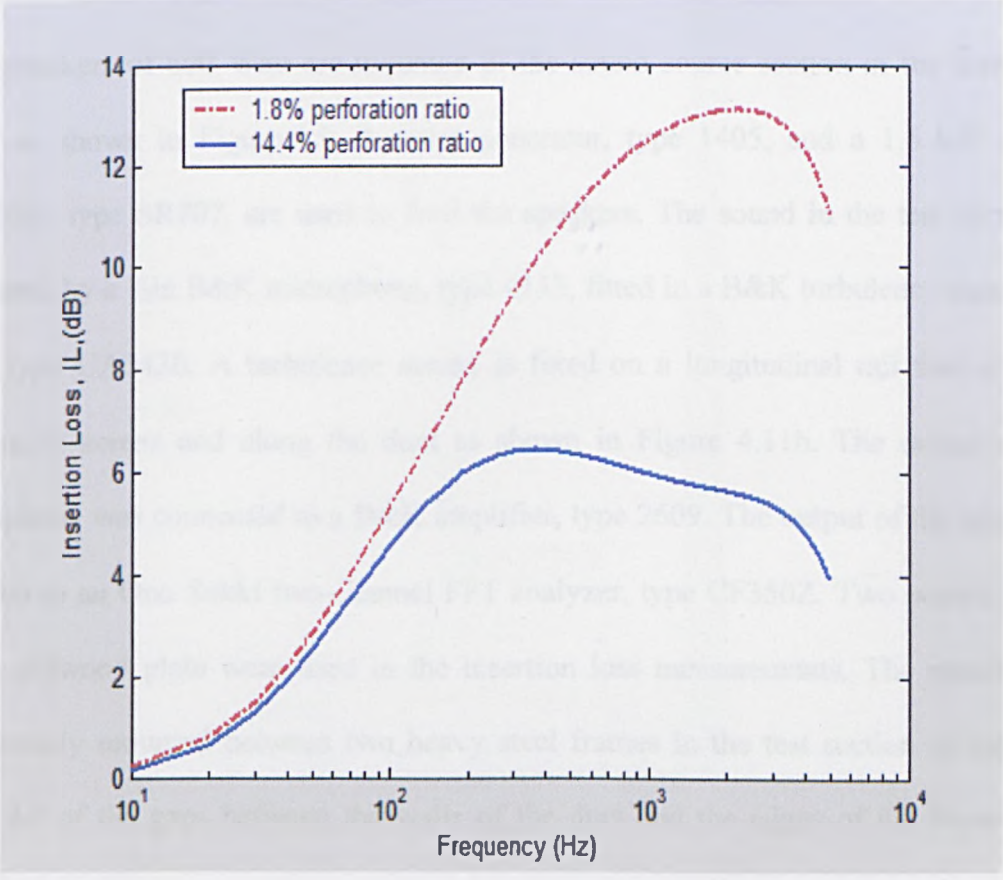

Figure.4.5: Predicted effect of the perforation ratio on the sound insertion loss of the Black plate.

In summary it seems that increasing perforation ratio is predicted to increase the sound absorption coefficient, and decrease the sound insertion loss at high frequency without significantly changing the low frequency performance.

4.4 MEASUREMENTS

4.4.1 Experimental procedure

Sound insertion loss measurements on perforated porous plates have been carried out in the flow duct designed by Cummings [9] at the University of Hull. A diagram showing the flow duct test arrangement is given in Fig.4.6. This flow duct has an internal cross section of 1.2 m x 0.8 m and is 27.7 m long. The walls are made of 24 mm thick plywood of and an outer cladding of 1.3 mm lead. The surface density of the wall is about 32 kg/m^2. The air-flow rate can be changed by varying of the fan blade pitch angle between -2^0 and +24^0.

Four speakers of 600 Watt are mounted in the sound source section in the flow duct walls as shown in Figure.4.5. A noise generator, type 1405, and a 1.6 kW power amplifier, type SR707, are used to feed the speakers. The sound in the test section is measured by a ½in B&K microphone, type 4133, fitted in a B&K turbulence cancelling tube, type UA0436. A turbulence screen is fixed on a longitudinal rail that is fitted diagonally across and along the duct as shown in Figure 4.11b. The output of the microphone was connected to a B&K amplifier, type 2609. The output of the amplifier was fed to an Ono Sokki two-channel FFT analyzer, type CF350Z. Two porous plates and a plywood plate were used in the insertion loss measurements. The plates were transversely mounted between two heavy steel frames in the test section of the flow duct. All of the gaps between the walls of the duct and the edges of the frame were sealed by putty.

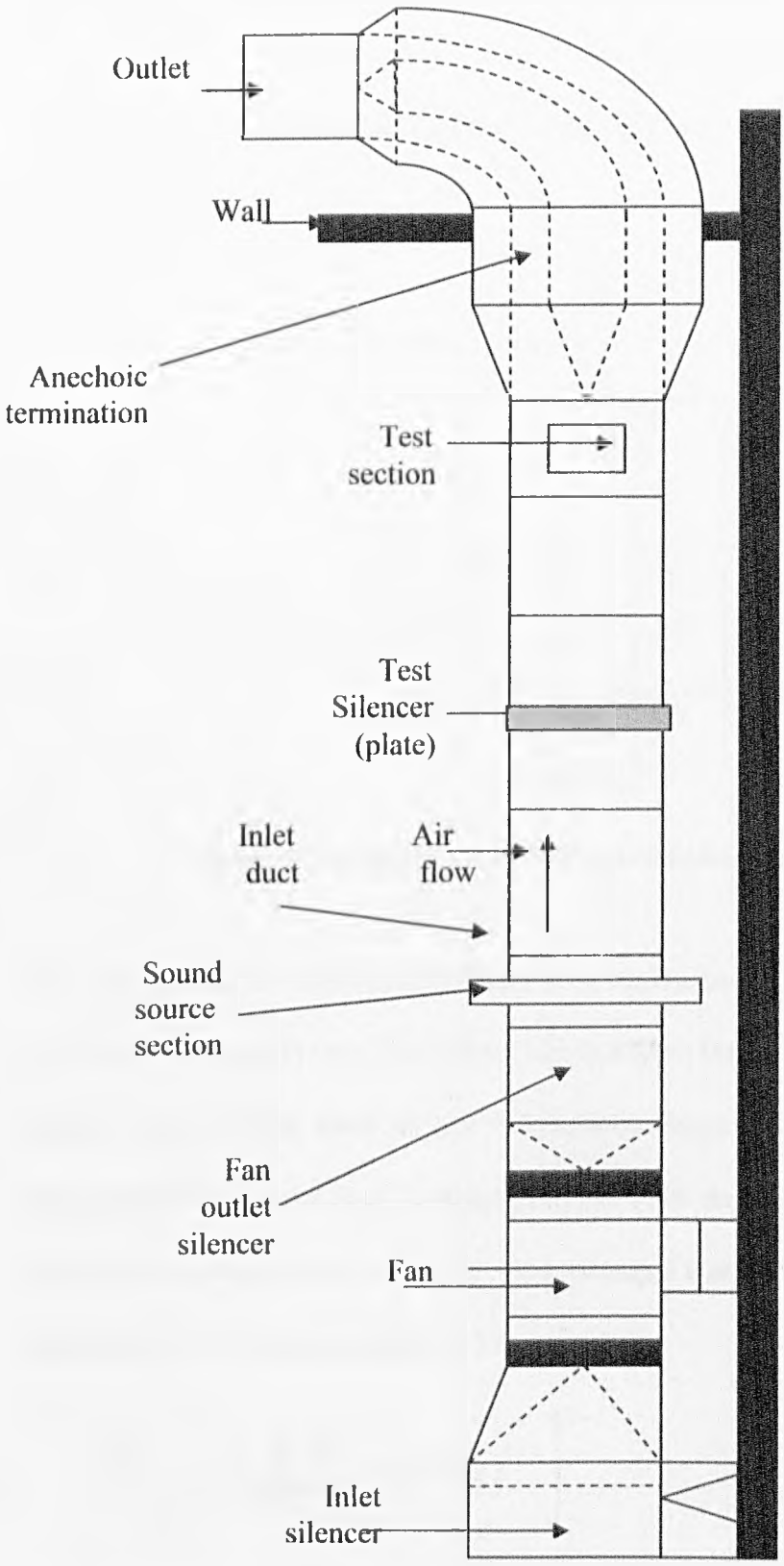

Figure.4.5: A diagram of the flow duct test arrangement.

4.4.2 Aerodynamic test of the duct

Flow calibration test has been carried out in the duct by using four Pitot static tubes that were vertically fixed in the top of the duct. The Pitot static tube is used to measure the stream velocity and consists of L-shape tube facing into the oncoming flow.

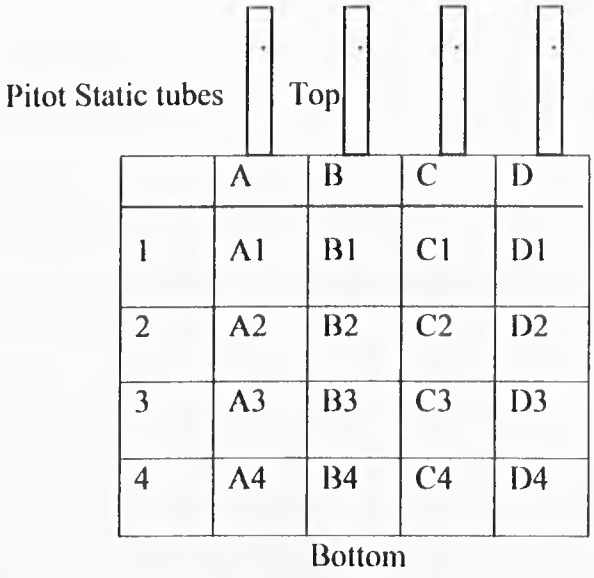

Figure.4.7: A diagram of the Pitot static tube locations in the duct.

For each pressure the difference of head at the downstream of the fan outlet in the test section was measured at the four points for each Pitot static tube across duct section i.e. sixteen points for four tubes. Figure 4.7 shows a diagram of the Pitot static tubes test arrangement in the flow duct. A diagram of the Pitot static tube is given in Figure 4.8. The measured pressures at each point were averaged and corrected for the effects of the boundary layer by using equation (4.27).

$$\Delta H_{ij} = \left[\frac{1}{16} \sum_{i=1}^{n} \sum_{j=1}^{m} \omega_{ij} (\Delta h_{ij})^{1/2} \right]^2 \tag{4.27}$$

where ω_{ij} is the correction factor, Δh_{ij} is the difference of head measured in terms of the fluid flowing (mmH_2O), n and m are 4. The correction factor taken from [23] is 0.97 for positions A2, A3, D2, and D3. It is 0.96 for locations B1, C1, B4, and C4. It is 0.94

for locations A1, A4, D1, and D4. It is 1 for locations B2, B3, C2, and C3. The standard errors in measured pressures for Figure4.9-4.10, from lower corrected pressure to higher corrected pressure, are 0.0787, 0.151, 0.359, 0.528, and 0.686, respectively. The unit of the standard errors is given in mmH_2O. The estimated error in static pressure differential is 0.25 mmH_2O. The pressure difference ΔP_{ij} can be found by using equation (4.28) [22];

$$\Delta P_{ij} = P_0 - P_{st} = \rho_m g \Delta H_{ij} \tag{4.28}$$

where P_0 is the stagnation pressure, P_{st} is the static pressure, ρ_m is the density of water (10^3 kg/m^3), and g is the gravitational acceleration (9.81 m/s^2).

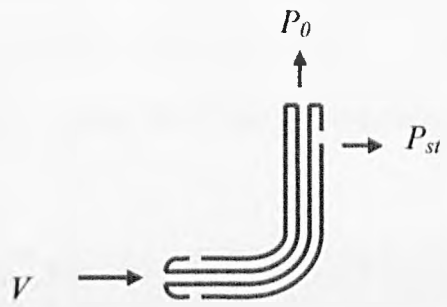

Figure.4.8: A diagram of the Pitot static tube.

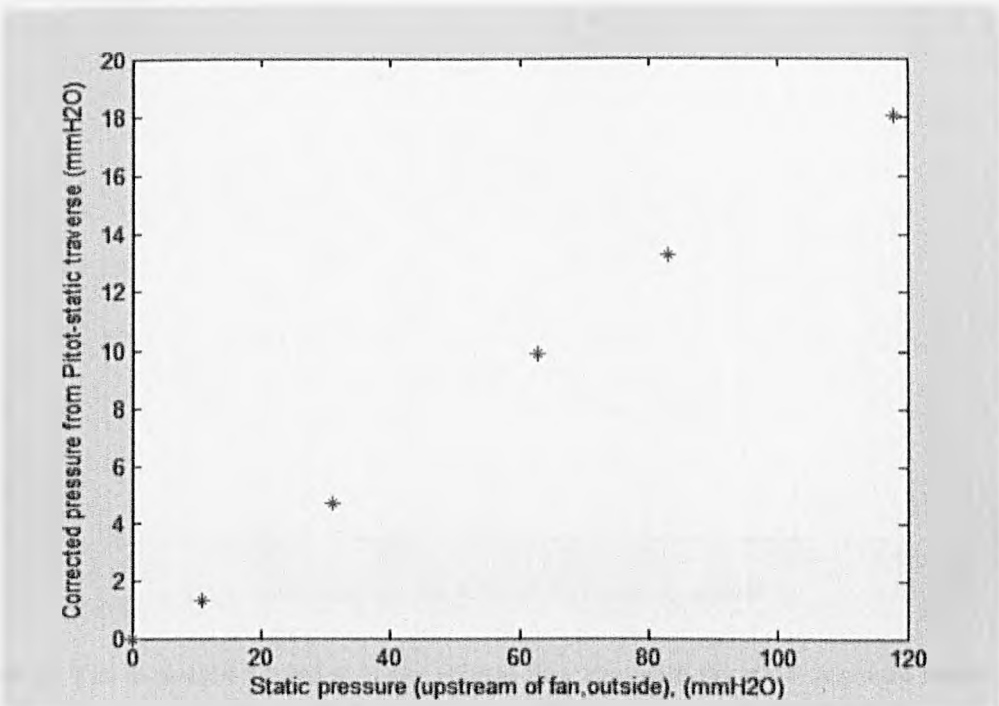

Figure4.9: The variation of the pressure in the duct to static pressure across fan inlet

The velocity of the flow in the duct is given by [22];

$$V_{ij} = \sqrt{\frac{2\Delta P_{ij}}{\rho_0}} \tag{4.29}$$

The measured variation of the pressure difference in the duct according to static pressure across fan inlet upstream is shown in Figure 4.9. Once the velocity of the flow is calculated, the volume flow rate in the duct can easily be predicted by

$$Q_{ij} = A_D \sum_{i=1}^{4} \sum_{j=1}^{4} V_{ij} \tag{4.30}$$

where A_D is the area of the test section in the duct. During the flow calibration test, the temperature, and the density of the air were equal to 18^0C and 1.19 kg/m^3 at 1 bar pressure, respectively. The measured variation of the volume flow rate with the static pressure across fan inlet upstream is shown in Figure 4.10. The curve is parabolic indicating that the volume flow rate is proportional to the square root of the static pressure.

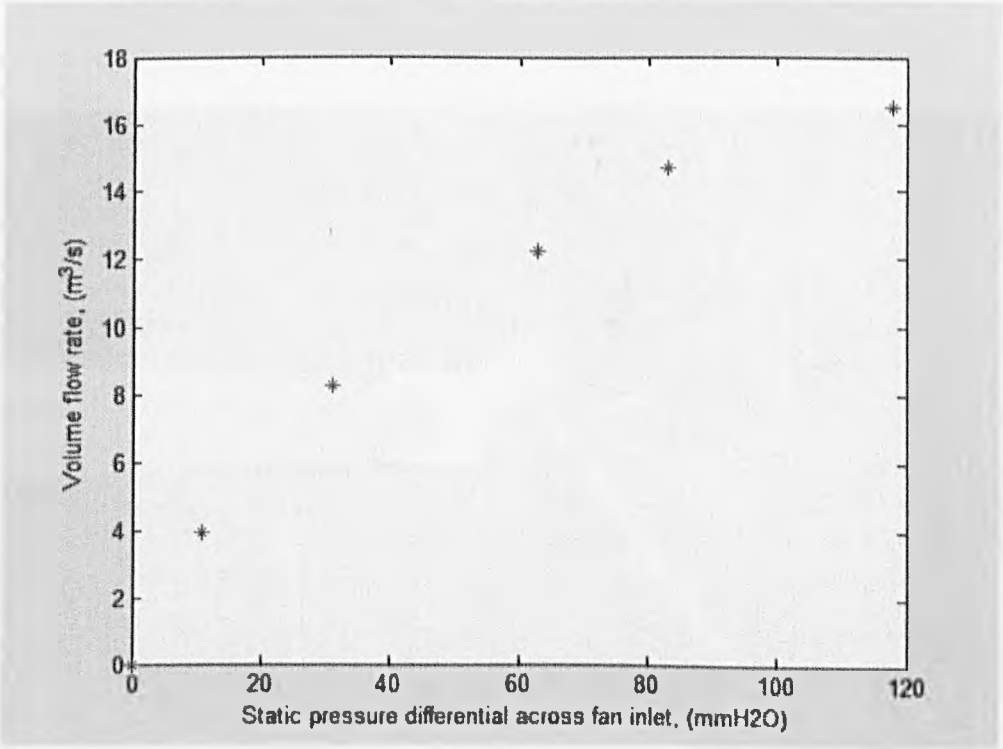

Figure4.10: The measured variation of the volume flow rate with the static pressure across the fan inlet

4.4.3 *Insertion loss measurements in a porous plate due to the presence of air flow*

The insertion loss can be determined from (4.31) [21]:

$$IL = \bar{L}_{pII} - \bar{L}_{pI} \tag{4.31}$$

where $\bar{L}_{pI}$ is the spatial average sound pressure level in the frequency band in the test duct, when the test silencer is installed, and $\bar{L}_{pII}$ is the spatial average sound pressure level in the frequency band in the test duct, when the silencer is out.

X - Key positions

O -Additional positions

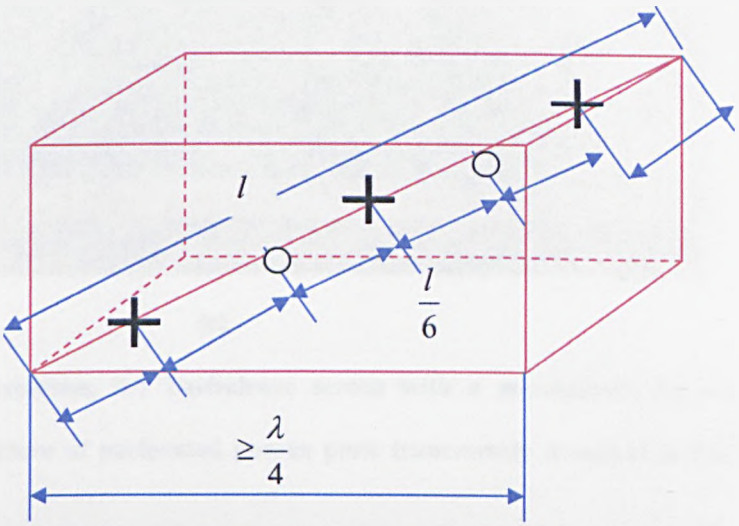

(a)

(b)

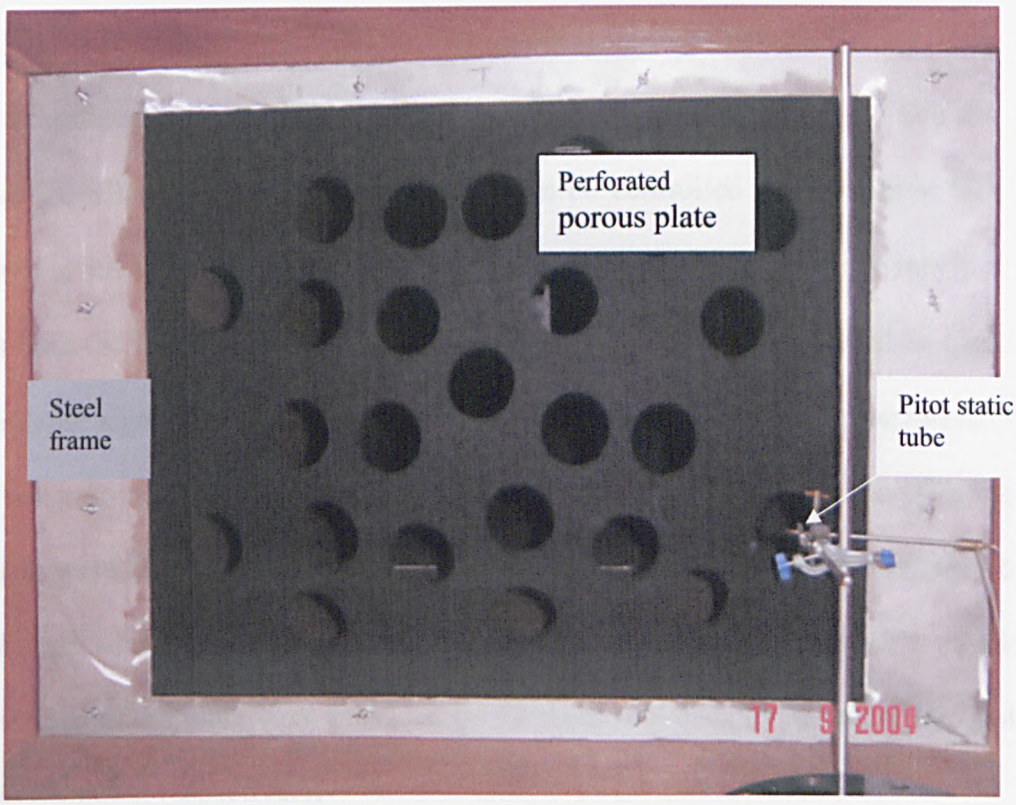

(c)

Figure4.11: a-) Microphone positions, b-) Turbulence screen with a microphone fitted on a longitudinal rail, and c-) A picture of perforated porous plate transversely mounted in the flow duct.

The spatial averaged sound pressure level, $\overline{L}_p$, should be calculated by measuring the local sound pressure levels at least at three key positions equally spaced on the diagonal line shown in Figure 4.11a. The local sound pressure levels are measured by a ½ in B&K microphone which is fitted in a B&K turbulence cancelling tube as shown in Figure4.11b.

The length of this line should be at least equal to a quarter of wavelength or bigger than a quarter of wavelength. The spatial average sound pressure level, $\overline{L}_p$, in dB, can be determined from the local sound pressure levels, L_{pi}, using (4.32) [21] :

$$\overline{L}_p = 10\log\left[\frac{1}{n_m}\sum_{i=1}^{n_m} 10^{\frac{L_{pi}}{10}}\right] \tag{4.32}$$

where n_m is the number of measurements.

The background noise produced by the air flow at each measurement position should be at least 10 dB below the test signal. This can be controlled by measuring the sound pressure levels with the loudspeaker unit turned on and off. The air flow rate in the test series with the test silencer installed and without the test silencer should be same. The microphone signal should be analyzed in one-third octave bands. The perforated Black plate was transversely mounted in the flow duct as shown in Figure4.11c. The edges of the plate were clamped by using two steel frames. The area of the plate affected by the sound was reduced to 0.9m x 0.7m because of the steel frame. The 1.8% and 14.4% perforations of the plate were provided by 10 holes of 44mm diameter, and 25 holes of 84 mm diameter, respectively.

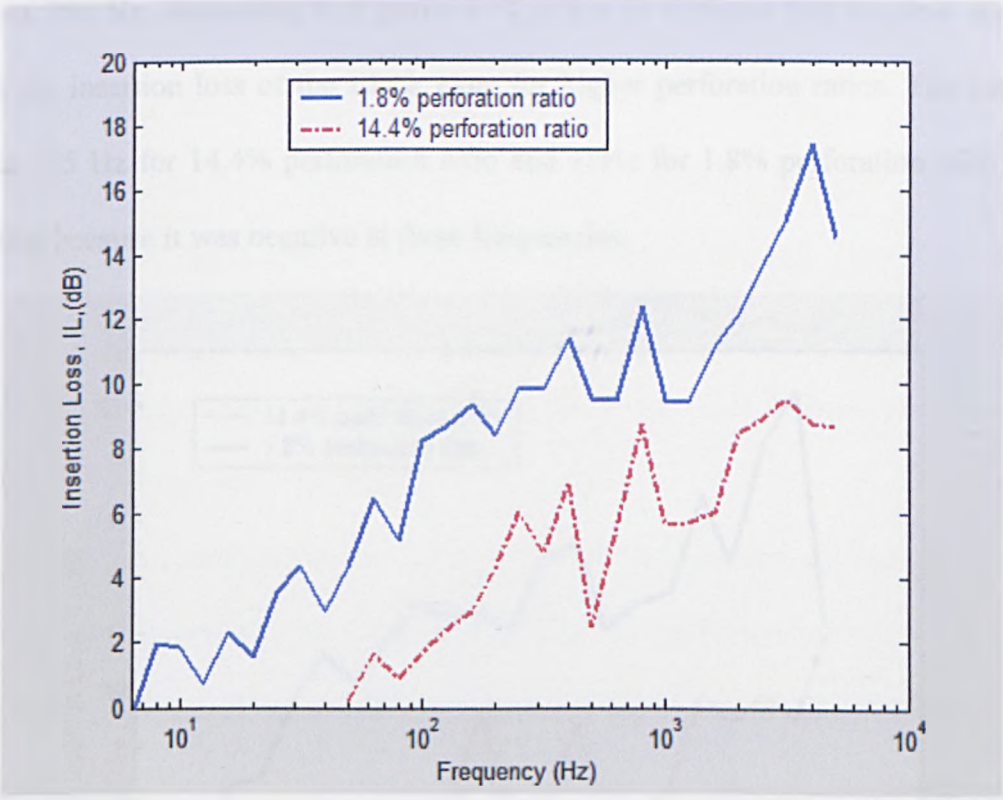

Figure.4.12: The measured insertion loss of the perforated Black plate without air flow

Figure 4.12 shows the measured insertion loss data for the perforated Black plate without air flow. For 1.8% perforation the insertion loss is higher throughout the frequency range due to the narrower air ways, and has maximum values between 1000

Hz and 5000 Hz. For 14.4% perforation, the insertion loss at 50 Hz is not plotted, being negative due to the undulations in the measured insertion loss or measurements error at low frequency. Figure 4.12 shows that increasing the perforation ratio decrease the measured insertion loss by about 6 dB. The results of measuring the insertion loss of the Black plate in presence of air flow are shown in Figure 4.13. The air flow speed in front of the hole at the receiver side of the plate is 52.37 m/s for 1.8% perforation ratio, and is 30.24 m/s for 14.4% perforation ratio, corresponding to Mach numbers of 0.153 and 0.088, respectively. The air flow speed on source side of the plate is 5.39 m/s. For 1.8% perforation the presence of air flow increases the measured insertion loss throughout the frequency range by about 3 dB. But the measured *IL* of the black plate for 14.4% perforation ratio is not affected by air flow except for a very small change between 200 Hz and 700 Hz. According to Figures 4.12 and 4.13 it seems that air flow does not affect the insertion loss of the Black plate for higher perforation ratios. The insertion loss at 125 Hz for 14.4% perforation ratio and 15Hz for 1.8% perforation ratio is not recorded because it was negative at these frequencies.

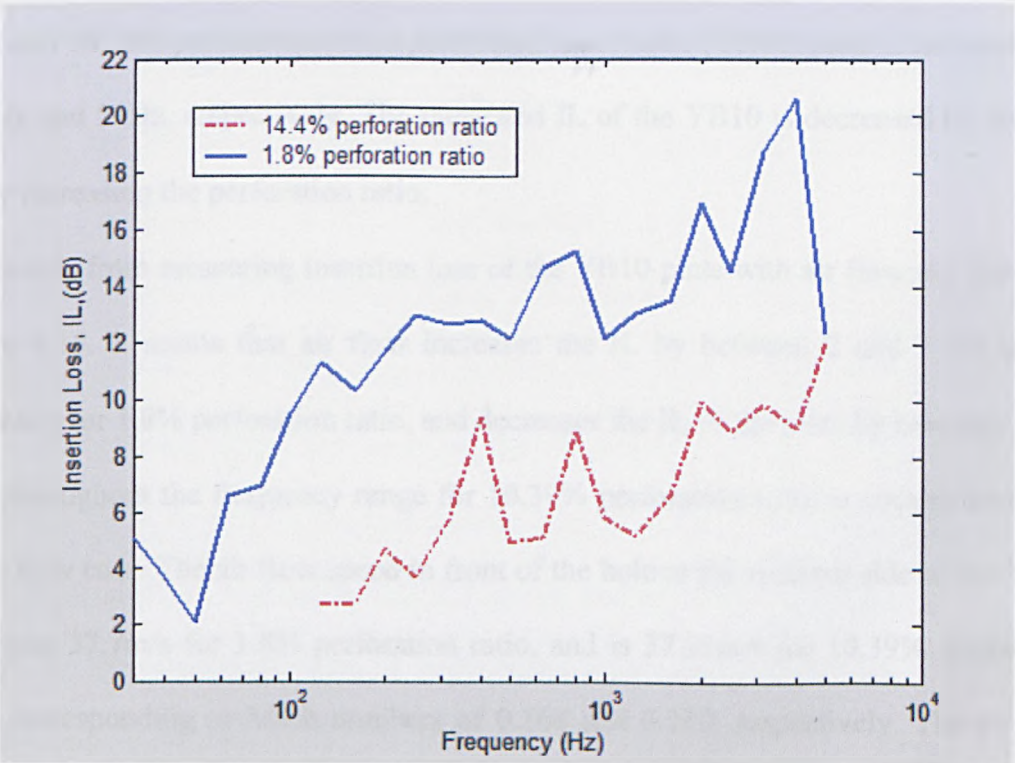

Figure.4.13: The measured insertion loss of the perforated Black plates with air flow

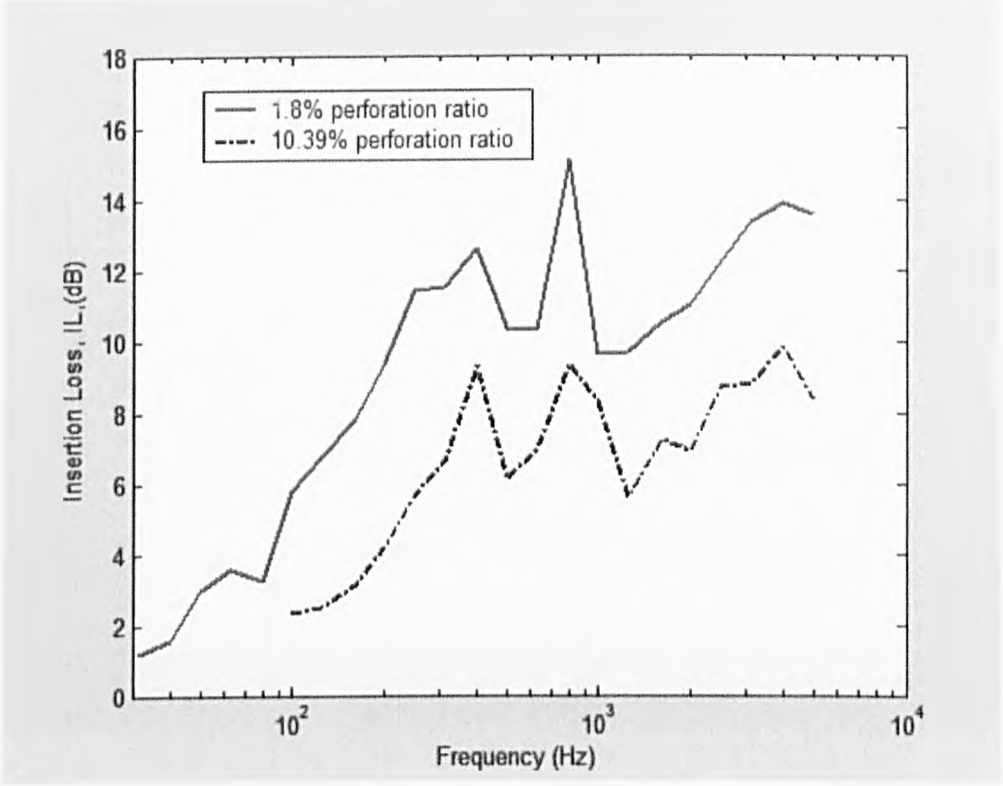

Figure.4.14: The measured insertion loss of the perforated YB10 plates without air flow

The results from measuring the insertion loss of two perforated YB10 plates with different perforation ratios in the absence of air flow are shown in Figure 4.14. For both perforation ratios, the IL curves exhibit peaks between 315Hz and 1000Hz. The IL for 1.8% and 10.39% perforation ratios perforated peroelastic (YB10) plate is not plotted at 31.5Hz and 50Hz, respectively. The measured IL of the YB10 is decreased by about 4 dB by increasing the perforation ratio.

The results from measuring insertion loss of the YB10 plate with air flow are shown in Figure 4.15. It seems that air flow increases the IL by between 2 and 5 dB at low frequency for 1.8% perforation ratio, and decreases the IL of the plate by between 1 and 2 dB throughout the frequency range for 10.39% perforation ratio in comparison with no air flow case. The air flow speed in front of the hole at the receiver side of the YB10 plate was 57.7m/s for 1.8% perforation ratio, and is 37.71m/s for 10.39% perforation ratio, corresponding to Mach numbers of 0.168 and 0.110, respectively. The air flow speed on source side of the plate is 5.69 m/s

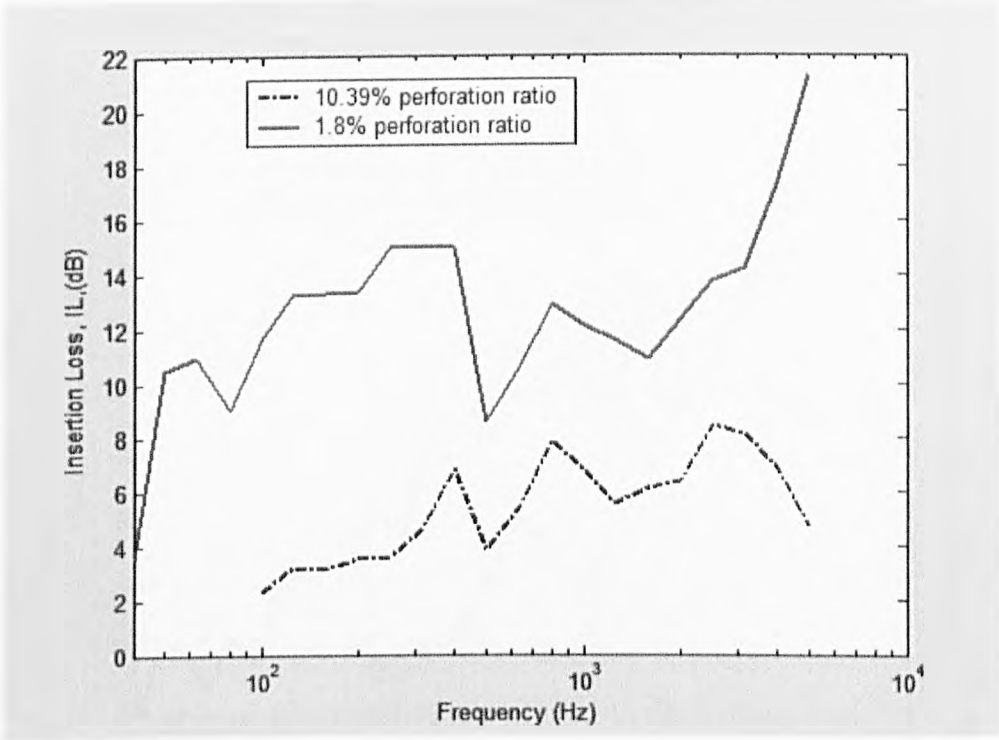

Figure4.15: The measured insertion loss of the perforated YB10 plates with air flow

4.4.4 The measured IL of the porous plates at different locations in the duct

To assess the affects of inserting perforated plates on the uniformity of the flow in the duct, the insertion loss has been measured with different plate locations. The plates which were previously mounted at a distance of 4.5 m from the microphone were brought to the distance of 2.5 m to microphone. The perforated poroelastic plate was excited by the acoustic sound field without air flow.

The measured insertion loss of the Black plate mounted at different locations in the duct, in the absence of air flow, is compared in Figure 4.16. It seems that mounting the plate at different locations does not affect the measured *IL* very much in the absence of air flow. In the case of 1.8% perforation ratio the *IL* of the Black plate (when distance between Microphone and plate was 2.5 m) is not recorded at 50 Hz, since it was negative at this frequency. This *IL* only changes between 100 Hz and 300 Hz with different plate positions. For 14.4% perforation the measured *IL* data at both locations shows about same effects, even though there is a small difference at 50 Hz.

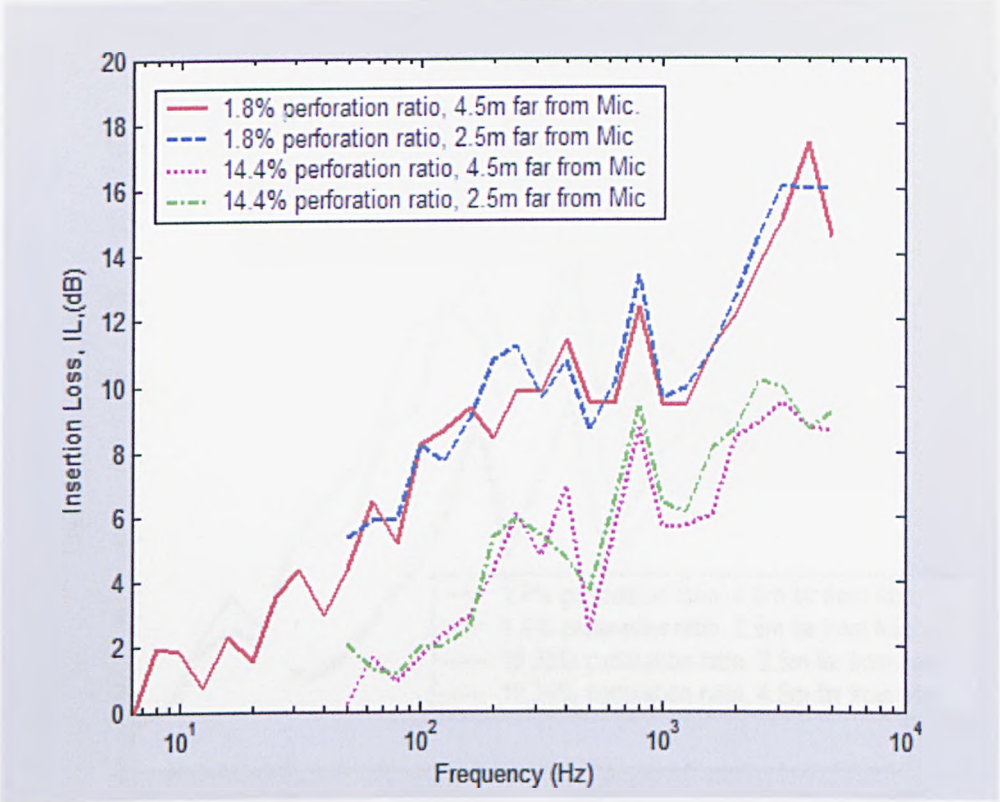

Figure4.16: The measured insertion loss of the Black plates with the plate at different locations in the duct without air flow.

Figure 4.17 shows comparisons between the measured *IL* of the YB10 plate at different locations in the duct without mean air flow. For 1.8% perforation ratio the *IL* data are not completely similar, and are changed between 0.5 and 2 dB throughout frequency range. The peak *IL* is decreased by about 2 dB when mounting the plate closer to microphone.

For the higher perforation, the *IL* results are similar at low frequency, and are changed little between 1000 Hz and 2500 Hz. The peak insertion loss is definitely similar at both locations. The *IL* data are not plotted at below 100 Hz. They were negative due to the undulations in the measured insertion loss or measurements error at low frequency.

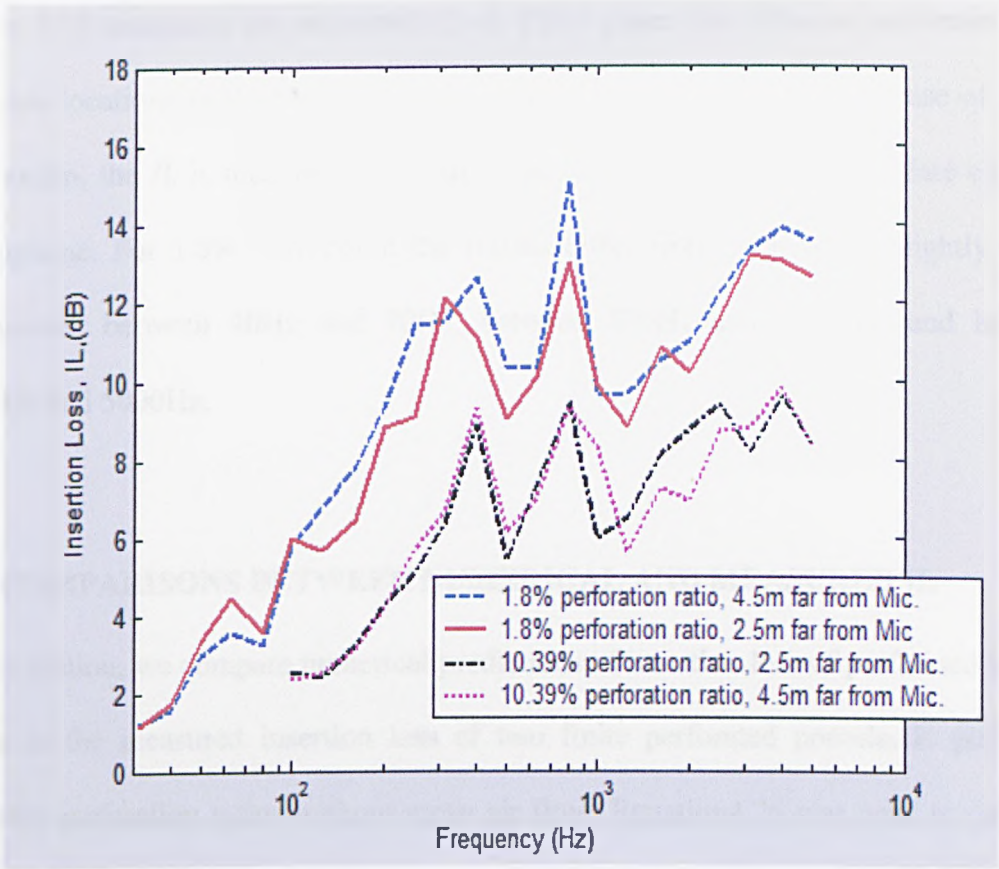

Figure4.17: The measured insertion loss of the YB10 plates with the plates at different locations in the duct without air flow.

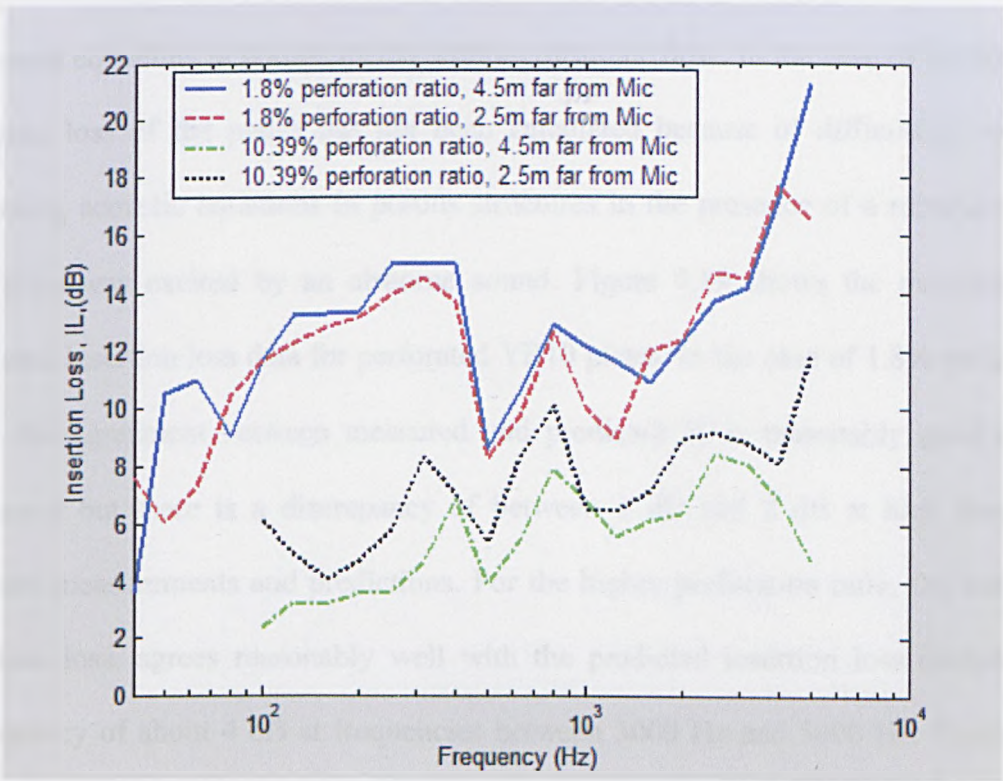

Figure4.18: The measured insertion loss of the YB10 plates at different locations in the duct with air flow.

Figure 4.18 compares the measured *IL* of YB10 plates for different perforations and different locations in the duct in the presence of mean air flow. In the case of higher perforation, the *IL* is increased along frequency range by mounting the plate closer to microphone. For 1.8% perforation the results differ from each other, slightly in the frequencies between 40Hz and 70Hz, between 800Hz and 1250Hz, and between 4000Hz and 5000Hz.

4.5 COMPARISONS BETWEEN NUMERICAL AND MEASURED IL

In this section, we compare numerical predictions of insertion loss of perforated infinite plates to the measured insertion loss of two finite perforated poroelastic plates for different perforation ratios without mean air flow. Equation4.26 was used to calculate the insertion loss of clamped rectangular perforated plates. The insertion loss of the plate changes with the perforation ratio. In the present work the numerical calculation of the sound field in the duct is limited to the equations of a vibrated poroelastic plate and the sound equations in porous media without mean air flow. In the case of air flow, the insertion loss of the plates has not been calculated because of difficulties with the governing acoustic equations in porous structures in the presence of a mean air flow. The plate was excited by an airborne sound. Figure 4.19 shows the measured and predicted insertion loss data for perforated YB10 plates. In the case of 1.8% perforation ratio, the agreement between measured and predicted *IL* is reasonably good at low frequency but there is a discrepancy of between 1 dB and 2 dB at high frequency between measurements and predictions. For the higher perforation ratio, the measured insertion loss, agrees reasonably well with the predicted insertion loss except for a discrepancy of about 4 dB at frequencies between 3000 Hz and 5000 Hz. Figure 4.19 shows that the perforation has a little effect on the *IL* at very low frequency.

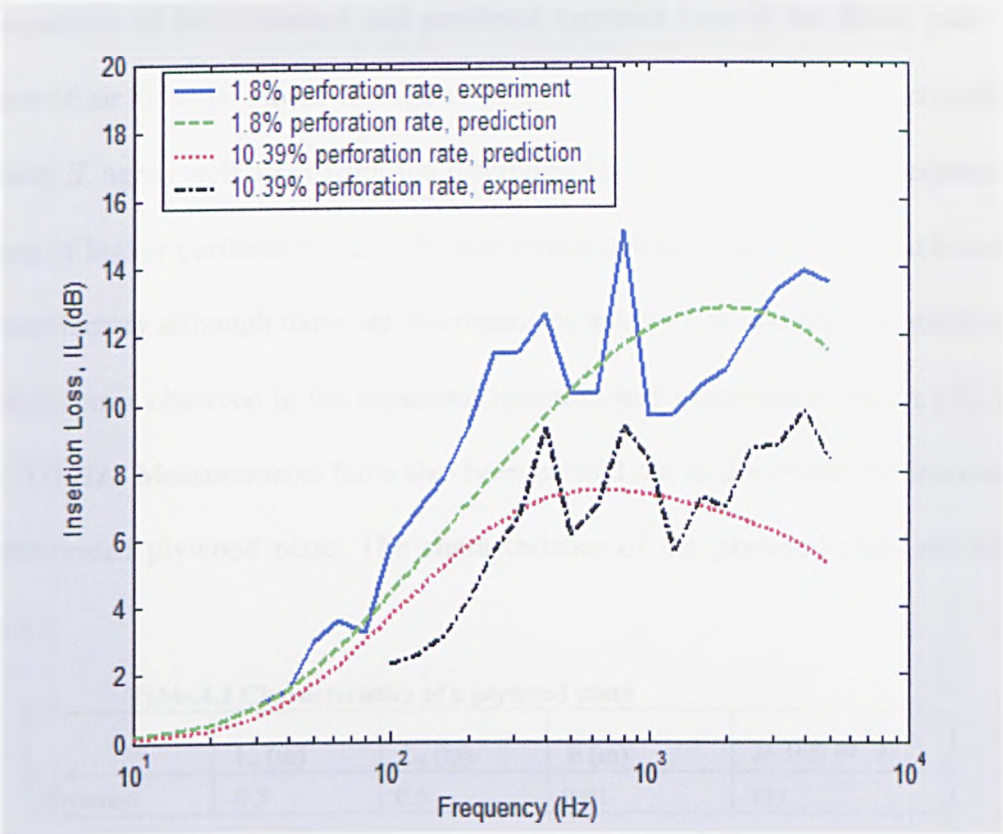

Figure.4.19: Predicted and measured insertion loss of perforated YB10 plates without air flow.

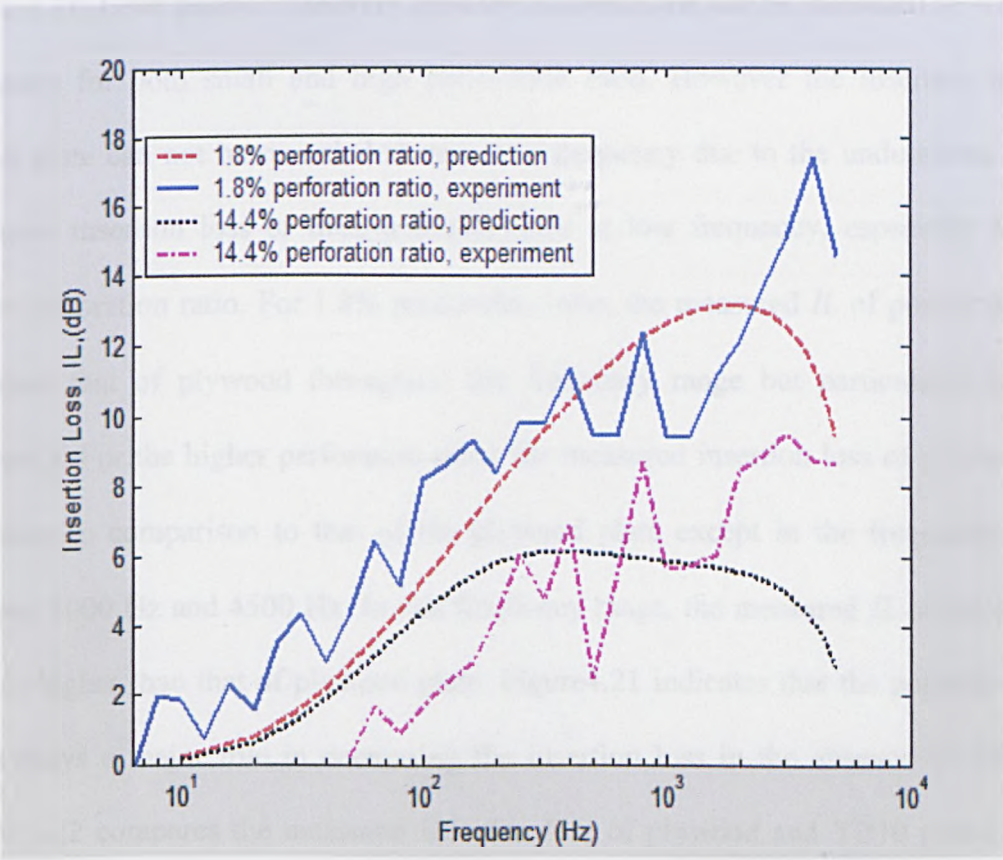

Figure.4.20: Predicted and measured insertion loss of perforated Black plates without air flow.

A comparison of the measured and predicted insertion loss of the Black plate in the absence of air flow is shown in Figure 4.20. For 1.8% perforation the measured and predicted *IL* agree well apart from the discrepancies observed at higher frequencies. In the case of higher perforation ratio, the agreement between the predicted and measured *IL* is satisfactory although there are discrepancies at very low and high frequencies. The maximum error observed in the measured insertion loss presented in Figure4.20 is 1.43 dB at 500 Hz. Measurements have also been carried out to determine the insertion loss of a perforated plywood plate. The characteristics of the plywood plate are given in Table 4.2.

Table.4.2 Characteristics of a plywood plate

	L_x (m)	L_y (m)	h (m)	ρ (kg/m^3)
Plywood	0.5	0.5	0.01	737

The measured insertion loss of a plywood plate is compared to that of the YB10 plate in Figure 4.21. If the plate is relatively rigid the insertion loss can be measured at very low frequency for both small and high perforation ratio. However the insertion loss of porous plate can not be recorded at very low frequency due to the undulations in the measured insertion loss or measurements error at low frequency, especially for the higher perforation ratio. For 1.8% perforation ratio, the measured *IL* of porous plate is less than that of plywood throughout the frequency range but particularly at high frequency. For the higher perforation ratio, the measured insertion loss of porous plate decreases in comparison to that of the plywood plate except in the frequency range between 3000 Hz and 4500 Hz. In this frequency range, the measured *IL* of the porous plate is higher than that of plywood plate. Figure4.21 indicates that the porosity of the plates plays a major role in decreasing the insertion loss in the absence of air flow. Figure 4.22 compares the measured insertion loss of plywood and YB10 plates in the presence of air flow. In the presence of air flow the insertion loss of the plywood plate is

not recorded below 31.5 Hz and above 2000 Hz as shown in Figure4.22. The *IL* of the plywood plate is higher than that measured for theYB10 plate with air flow at low frequency. The maximum error observed in the measured insertion loss presented in Figure4.21 is 1.43 dB at 500 Hz for the YB10 plate, and is 1.85 dB at 400 Hz for the plywood plate.

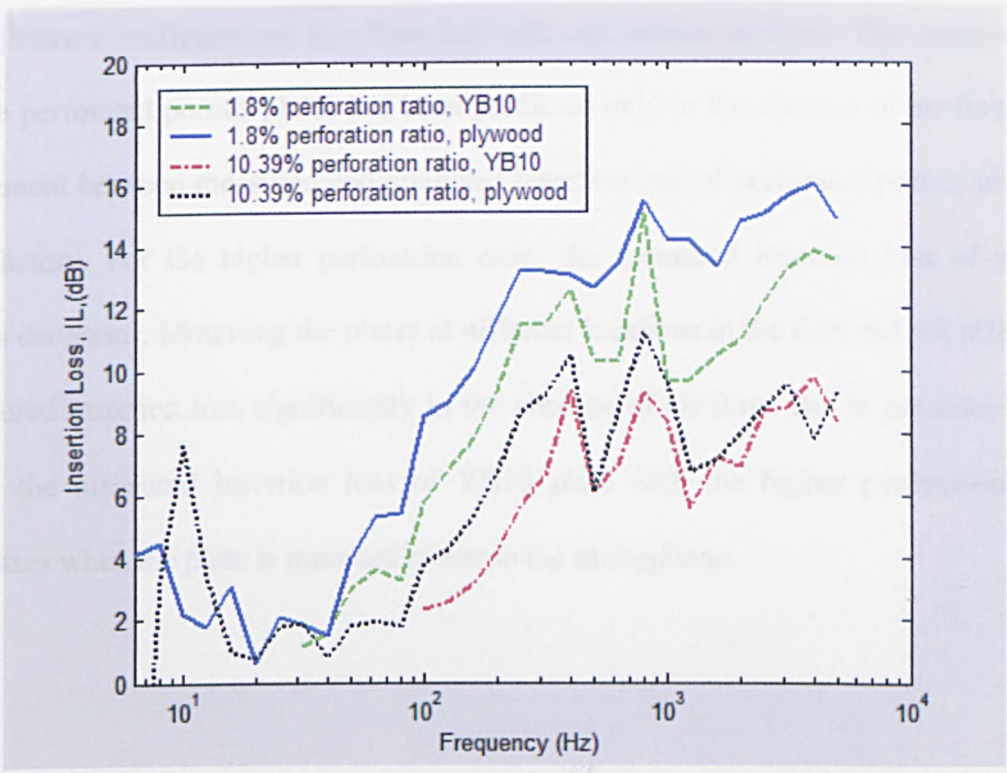

Figure.4.21: The measured insertion loss of a plywood and YB10 plates without air flow.

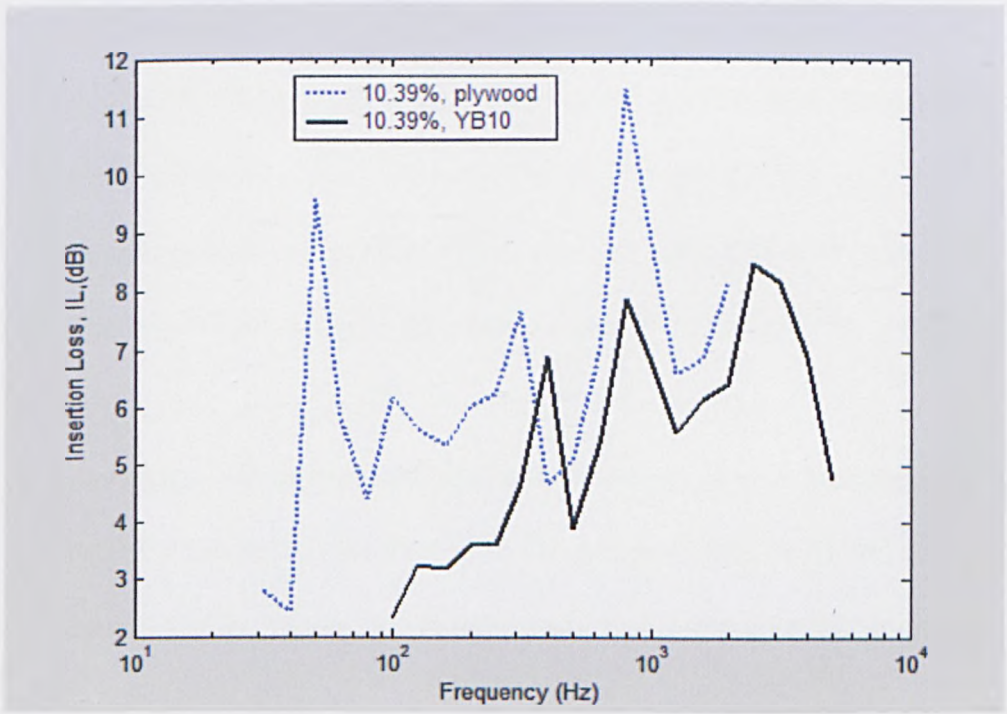

Figure.4.22: The measured insertion loss of a plywood and YB10 plate with air flow.

4.6 CONCLUSION

An analytical model that takes into account the effect of perforations in plates and the effect of the flexural vibrations of plates has been presented and used to calculate the insertion loss and absorption coefficient of plates. The insertion losses of two different types of perforated porous plates have been measured for different perforation ratios in two different configurations in a flow duct with and without air flow. The insertion loss of the perforated porous plates has been predicted only in the absence of air flow. The agreement between measured and predicted insertion loss of perforated porous plates is satisfactory. For the higher perforation ratio, the measured insertion loss of porous plates decreases. Mounting the plates at different locations in the duct did not affect the measured insertion loss significantly in the absence of air flow. But in presence of air flow, the measured insertion loss of YB10 plate with the higher perforation ratio increases when the plate is mounted closer to the microphone.

References:

1. Lord Rayleigh, "*Theory of Sound*" (London, 1926) Vol.(I), and (Dover, New York, 1945), Vol.(II).
2. K. V. Horoshenkov and K. Sakagami, "A method to calculate the acoustic response of a thin, baffled, simply supported poroelastic plate," J. Acoust. Soc. Am. 110, 904-917 (2001).
3. D. Takahashi, M. Tanaka, "Flexural vibration of perforated plates and porous elastic materials under acoustic loading," J. Acoust. Soc. Am. 112(4), 1456-1464 (2002).
4. D. Takahashi, K. Sakagami, and M. Morimoto, "Acoustic properties of permeable membranes," J. Acoust. Soc. Am. 99, 3003-3020 (1996).
5. A. Cummings, "Low frequency acoustic transmission through the walls of rectangular ducts," J. Sound Vib. 61, 327-345 (1978).
6. A. Cummings, "Low frequency acoustic radiation from duct walls," J. Sound Vib. 71, 201-226 (1980).
7. A. Cummings, "Stiffness control of low frequency acoustic transmission through the walls of rectangular ducts," J. Sound Vib. 74, 351-380 (1981).
8. A. Cummings, "Design charts for low frequency acoustic transmission through the walls of rectangular ducts," J. Sound Vib. 78, 269-289 (1981).
9. A. Cummings and R. J. Astley, "Finite element computation of attenuation in bar-silencers and comparison with measured data," J. Sound Vib. 196(3), 351-369 (1996).
10. A Cummings, "Transient and multiple frequency sound transmission through perforated plates at high amplitude," J. Acoust. Soc. Am. 79(4), 942-951 (1986).
11. U. Ingard, "On the theory and design of acoustic resonators," J. Acoust. Soc. Am. 25(6), 1037-1061 (1953).

12. C. L. Morfey, "Sound transmission and generation in ducts with flow," J. Sound Vib. 14(1), 37-55 (1971).

13. J. C. Wendoloski, "Sound absorption by an orifice plate in a flow duct," J. Acoust. Soc. Am. 104(1), 122-132 (1998).

14. P. Leclaire, K. V. Horoshenkov, M. J. Swift and D. C. Hothersall, "The vibrational response of a clamped rectangular porous plate," J. Sound Vib. 247(1), 19-31 (2001).

15. D. Y. Maa, "Microperforated-panel wideband absorbers," Noise Control Eng. J., 29, 77-84 (1987).

16. J. F. Allard (1993), "Propagation of sound in porous media, Modelling sound absorbing materials". Elsevier, New York, pp-20.

17. K. Attenborough, "On the acoustic slow wave in air-filled granular media," J. Acoust. Soc. Am. 81, 93-102(1987).

18. K. V. Horoshenkov, K. Attenborough, and S. N. Chandler-Wilde, "Padé approximants for the acoustical properties of rigid frame porous media with pore size distributions," J. Acoust. Soc. Am. 104(3), 1198-1209(1998).

19. D. Takahashi, "Sound transmission through single plates with absorptive facings: Improved theory and experiment," J. Acoust. Soc. Am. 88(2), 879-882(1990).

20. D. Takahashi, "Sound transmission through single plates with absorptive facings," J. Acoust. Soc. Am. 83(4), 1453-1457(1988).

21. *International Standard ISO* 7235 1991 Acoustics-measurement procedures for ducted silencers-insertion loss, flow noise and total pressure loss.

22. J. F. Douglas, J. M. Gasiorek, and J. A. Swaffield (1997), "Fluid mechanics". Longman, Singapore, pp-158.

23. A. Cummings, private archives.

Chapter 5

MEASUREMENTS OF ACOUSTIC INSERTION LOSS DUE TO A POROUS PLATE SILENCER IN THE FLOW DUCT

5.1 INTRODUCTION

The aim was to investigate the effectiveness of introducing structures based on a poroelastic plate into the flow duct for attenuating noise. Measurements were made of the acoustic insertion loss along a flow duct due to a porous plate 'silencer'. A poroelastic plate was mounted in the flow duct and separated from the walls by an air cavity in order to allow bending vibration. The plate was excited by lateral components of the air flow and by the acoustic plane wave. The acoustic insertion loss was calculated from sound pressure measurements in flow duct.

Huang [1, 2] has carried out theoretical and experimental work on structural sound noise control devices. Ramamoorthy *et al* [3] used experimental and theoretical methods to investigate the use of a passive device, a structural acoustic silencer, to calculate transmission loss. He has taken the effect of external fluid into account, and also presented a practical relationship between the transmission loss and plate dispersion. Tang and Lin [4] have studied the resonant mass-spring behaviour of a stiff light composite panel absorber, and investigated its applicability as an alternative means of noise reduction.

Panneton and Atalla [5] have presented a three dimensional finite element formulation to predict the vibro-acoustic behaviour of multilayer structures. Their approach is based on a coupled finite element formulation. Astley *et al* [6] has examined some of the effects of wall flexibility on sound propagation and attenuation in a duct with a bulk liner and negligible mean flow.

5.2 GEOMETRY FOR ACOUSTIC SILENCER

The design of the mounting for the porous plate in the flow duct is shown in the Figure 5.1. A 20mm thick poroelastic plate with dimensions of 1m x 0.8m is mounted on one side of the flow duct, and separated from the wall by an air cavity. The plate is parallel to the direction of the air flow. The length and width of the cavity are the same as those of the porous plate, and the cavity height is 60 mm. A steel frame having 0.7 m x 0.9 m internal dimension with 3 mm thickness is used to hold the plate. The plate dimensions are reduced to 0.9 m x 0.7 m as a result of using a steel frame. Two steel fairings are attached to edges of the plate in order to ease the aerodynamic loading of the plate. There are two fluid/plate interfaces.

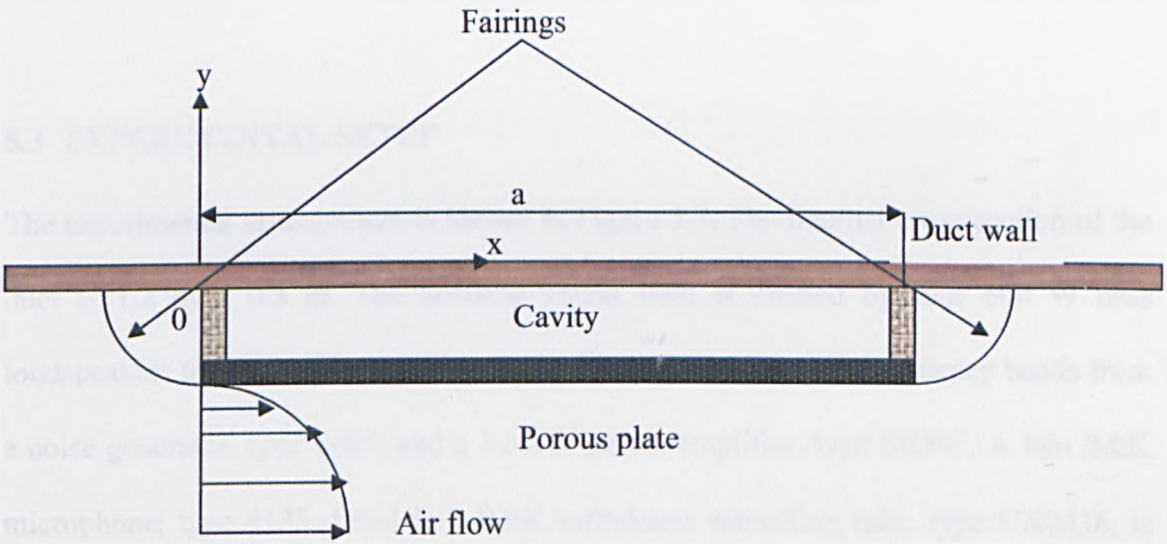

Figure5.1: Porous plate mounted along the duct wall with air cavity.

The excitation forces are provided by the incoming acoustic plane wave and the lateral components of the air flow. Plane waves propagate only in the region of $x < 0$ and $x > a$, which is the length of the plate as shown in Figure5.2. A picture of the porous plate attached to the duct, and separated from the wall by a cavity is shown in Figure5.2.

Figure5.2: Picture of the porous plate mounted on side of the duct wall.

5.3 EXPERIMENTAL SETUP

The experimental arrangement is shown in Figure 5.3. The internal cross-section of the duct is 1.2 m x 0.8 m. The acoustic sound field is created by four 600 W bass loudspeakers that are fed with random noise filtered in 1/3 octave frequency bands from a noise generator, type 1405, and a 1.6 kW power amplifier, type SR707. A ½in B&K microphone, type 4133, fitted in a B&K turbulence cancelling tube, type UA0436, is used to sample the acoustic sound field. The distance between the microphone and the nearest side of the plate is 4.5 m.

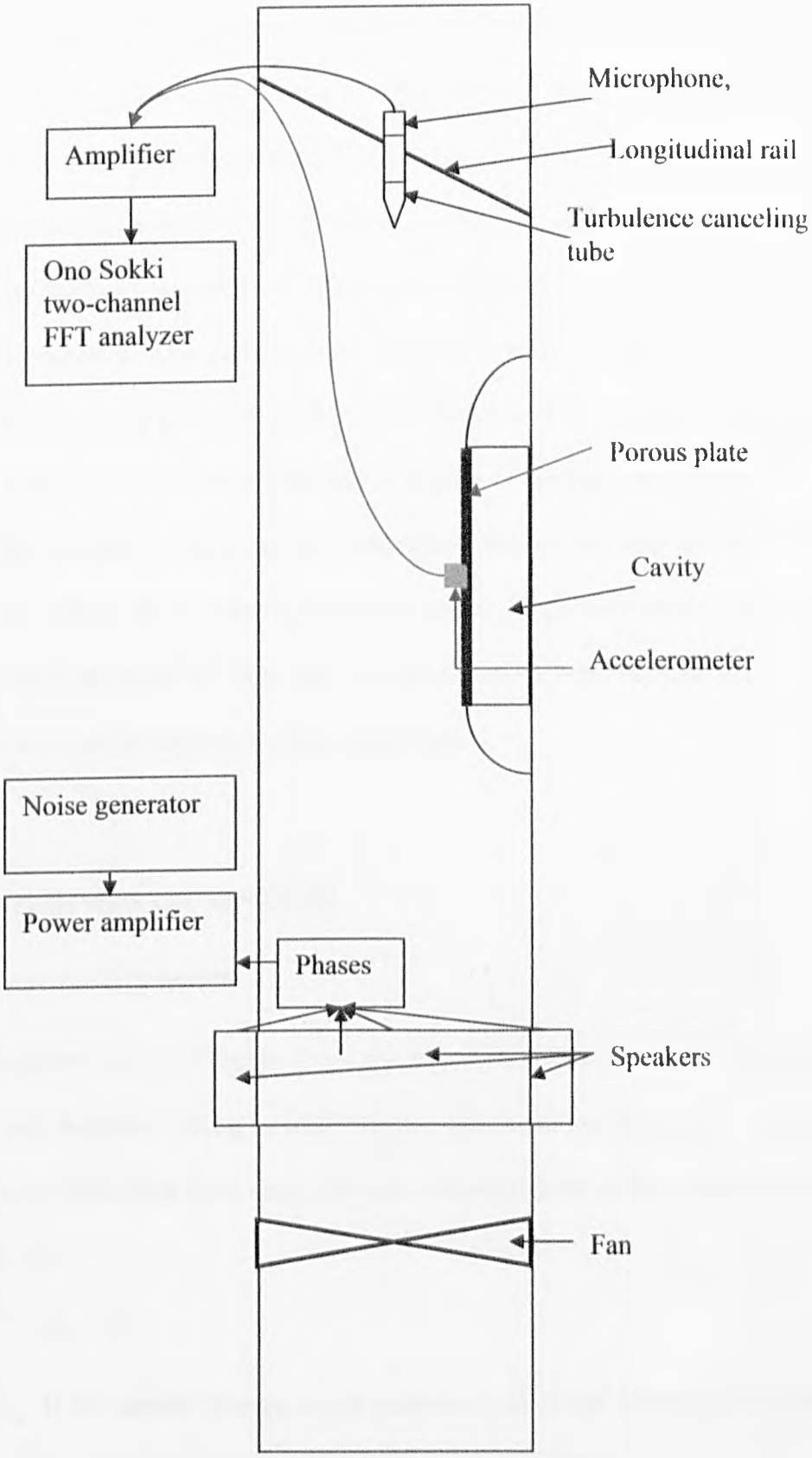

Figure5.3: Experimental setup; dimensions in the figure are not to scale.

The microphone is attached to a preamplifier that is connected to a B&K measuring amplifier, type 2609. The output of the measuring amplifier is fed to a two channel FFT analyzer, type CF350Z. The signal to noise ratio for the measurements made in the presence of the silencer is between 12 dB and 17 dB. The signal to noise ratio for the measurements made without the silencer is between 12.5 dB and 16.5 dB.

The plate made of recycled car dashboard is clamped between a steel frame and a wooden supporter. The properties of this Black plate are given in Table 4.1. The insertion loss results given here is for a plate mounted on one vertical wall of the duct. If the plate were to be mounted at the top or bottom of the duct, the plate would bend due to gravity. Because of bending, the aerodynamic movements will not be parallel to the plate. This effects the insertion loss measurements. The results for the plate mounted at the top and bottom of the flow duct are not shown in here, because the insertion loss was not recorded throughout the frequency range.

5.4 EXPERIMENTAL RESULTS

5.4.1 Insertion loss results

The procedure used in Chapter 4 and the recommendations in ISO standard 7235 [7] have been followed during measurements. The insertion loss due to porous plate 'silencer' is calculated from sound pressure measurements in the duct by the following formula [7]:

$$IL = \bar{L}_{pII} - \bar{L}_{pI} \tag{5.1}$$

where $\bar{L}_{pI}$ is the spatial average sound pressure level in the frequency band in the test duct, when the test silencer is installed, and $\bar{L}_{pII}$ is the spatial average sound pressure level in the frequency band in the test duct, when the silencer is not present.

The sound pressure level, $\overline{L}_p$, is calculated by measuring the local sound pressure levels at least at three key positions equally spaced on the longitudinal span of the line shown in Figure4.11a. The spatial average sound pressure level, $\overline{L}_p$, in dB, is determined from the local sound pressure levels, L_{pi}, using the equation (4.32).

The insertion loss (*IL*) of the black porous plate in the absence of the air flow is given in Figure 5.4. The *IL* is not recorded at 125 Hz, and is maximum at 800 Hz. The *IL* is by about 1 dB for low frequency, but it is increasing up to 3.7 dB for high frequency. Separating the plate from the wall by an air cavity causes an increase in the resonance frequency of the plate because stiffness of the system is increased by an air cavity.

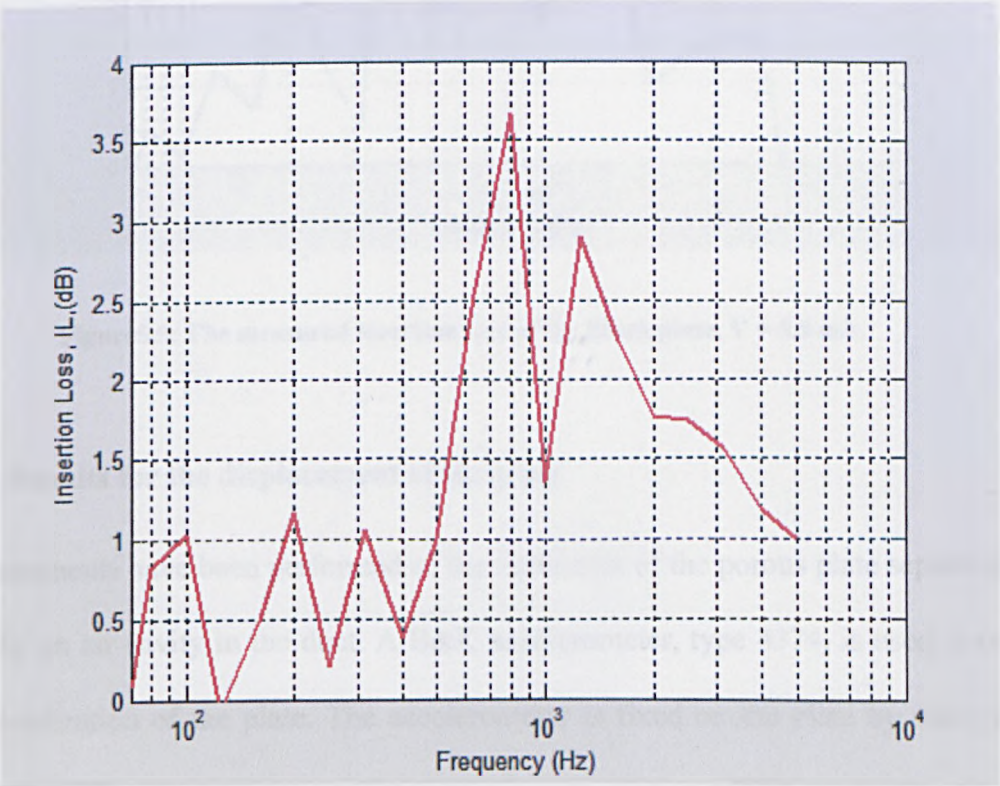

Figure5.4: The measured insertion loss of the Black plate, zero mean flow.

The insertion loss measurements have been carried out for the porous plate in the presence of air flow with an average air flow speed of 5.5 m/s in the duct, corresponding to a Mach number of 0.016. The result is shown in Figure 5.5. The presence of air flow

results in an increase in the maximum *IL* and a shift in the frequency of the peak from 800 Hz to 400 Hz. The maximum *IL* shown in Figure 5.4 is increased by about 3.3 dB in the case of air flow as shown on Figure 5.5.

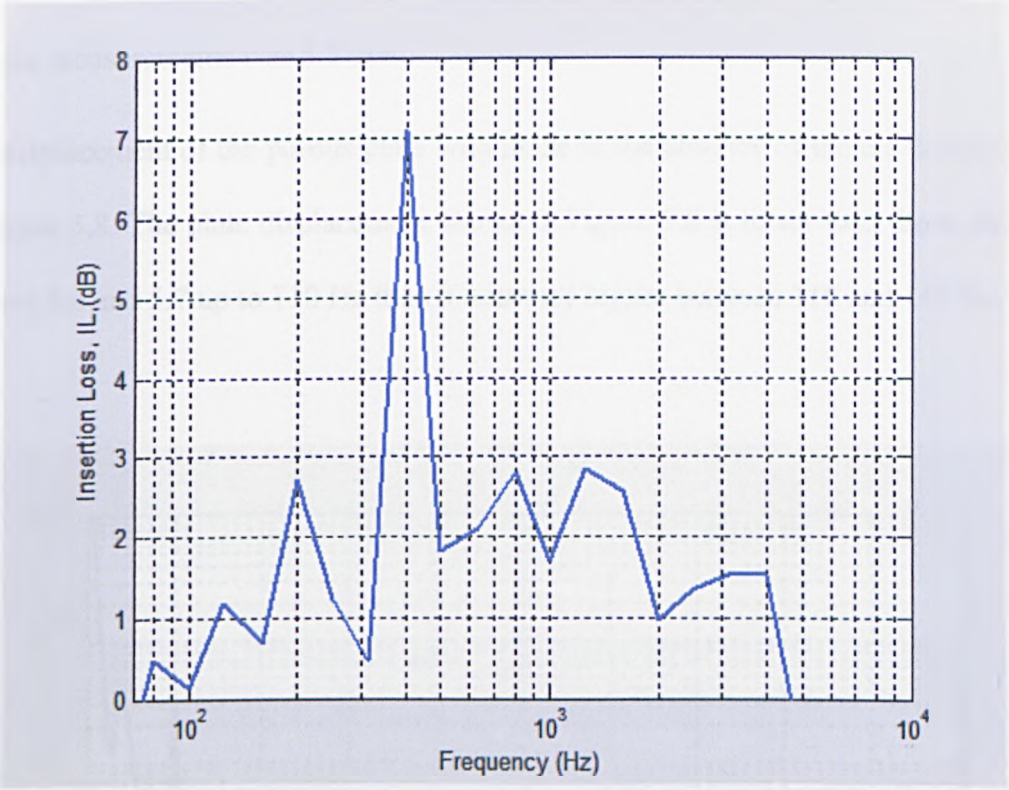

Figure5.5: The measured insertion loss of the Black plate, V = 5.5 m/s.

5.4.2 Results for the displacement of the plate

Measurements have been performed of the deflection of the porous plate separated from wall by an air cavity in the duct. A B&K accelerometer, type 4374, is used to monitor the acceleration of the plate. The accelerometer is fixed on the plate by using double sided tape. The output of the accelerometer is connected to a B&K measuring amplifier, type 2609, as shown in Figure 5.3. The measured plate displacements are plotted versus frequency in Figures 5.6 to 5.8 for three different cases. The Figure 5.6 and Figure 5.7 show that the displacements of the porous plate with and without noise, in the presence of air flow, are not similar to each other. This means that in the presence of air flow for

a plate mounted on a duct wall inside the duct parallel to the direction of the flow, and separated from the wall by an air cavity, turning on and off the noise generator will increase the displacement of the plate. The resonant peak observed at 50 Hz in Figure5.6 is shifted to 72 Hz in Figure5.7, and is increased. The velocity of the air flow in these measurements was 5.5 m/s.

The displacement of the porous plate with noise in the absence of the air flow is shown in Figure 5.8. The plate displacement shown in Figure 5.8 is lower than those shown in Figures 5.6 and 5.7 up to 110 Hz then it becomes higher between 110 and 143 Hz.

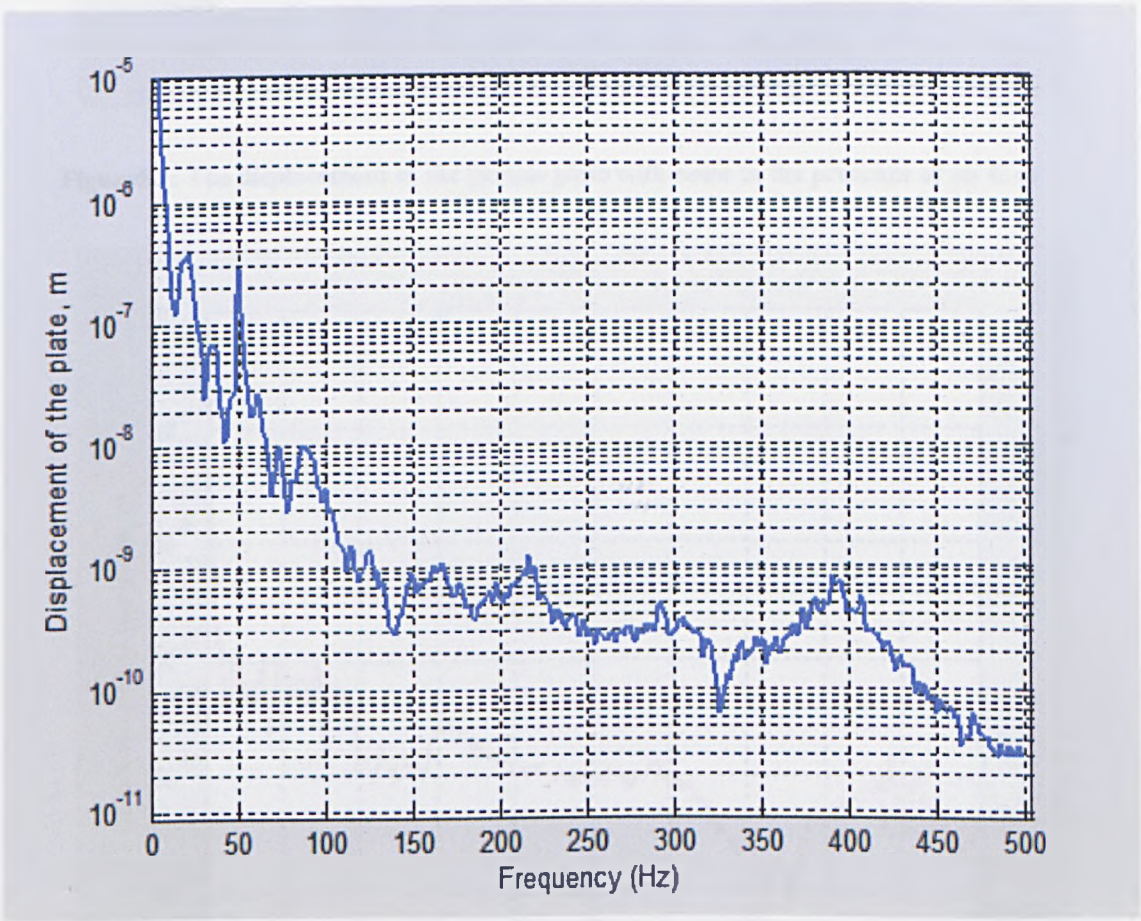

Figure5.6: The displacement of the porous plate in presence of the air flow without noise.

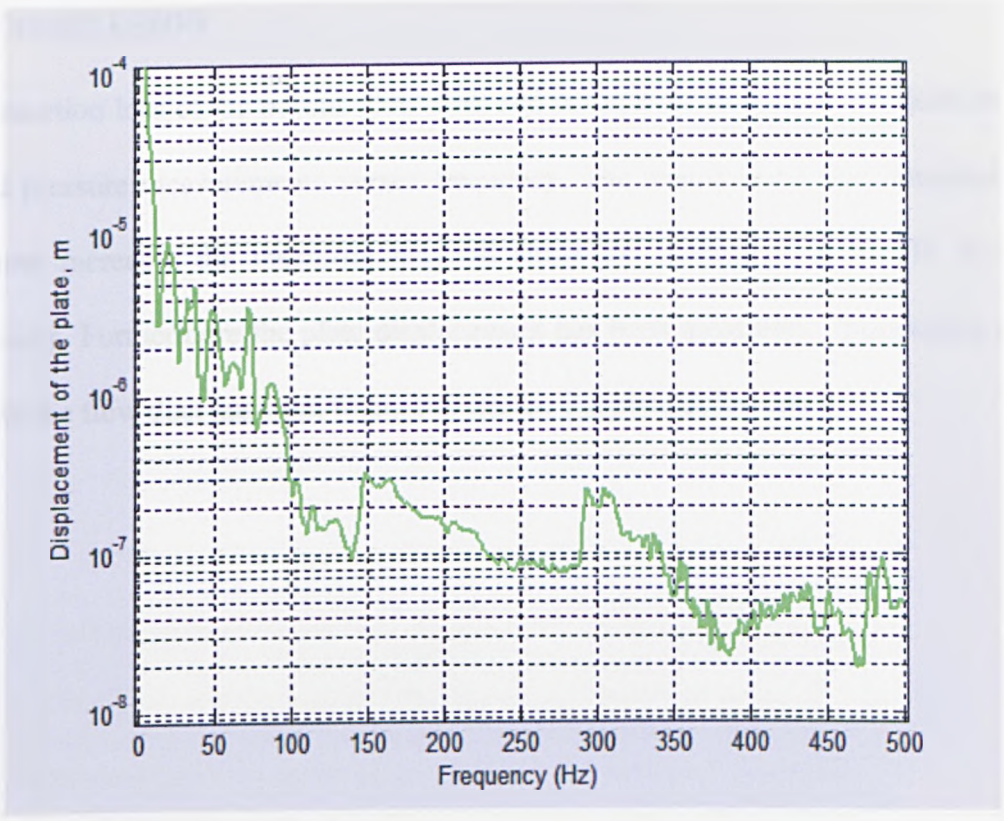

Figure5.7: The displacement of the porous plate with noise in the presence of air flow

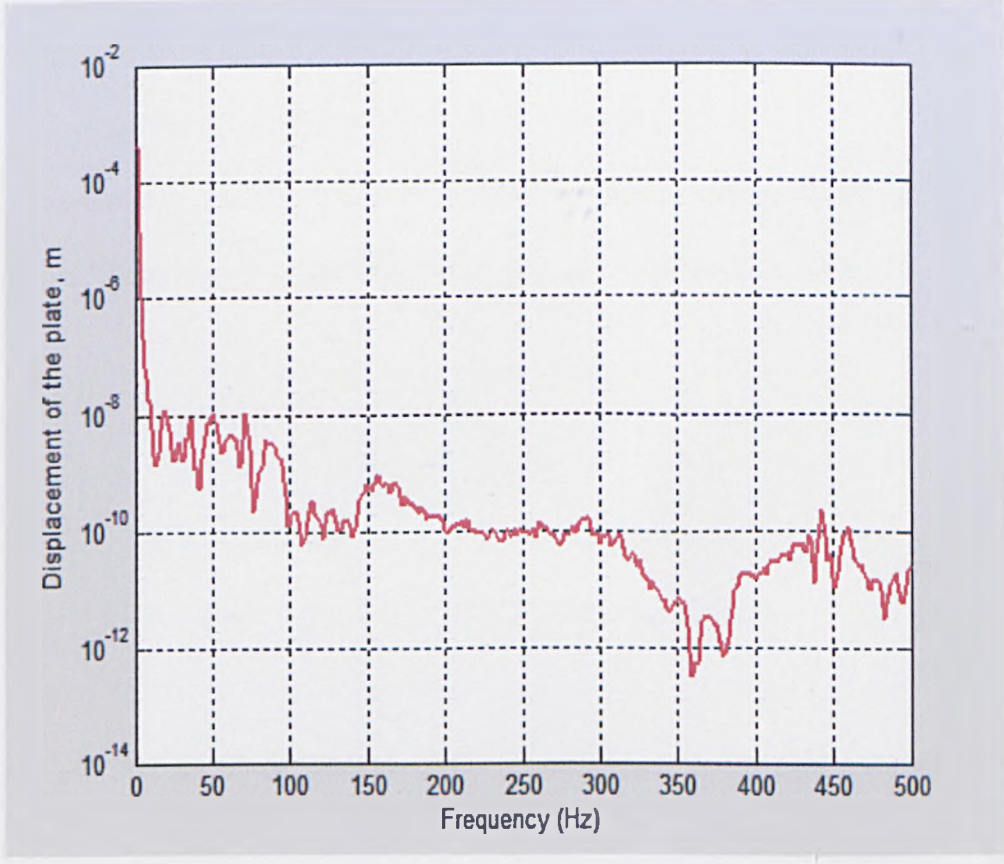

Figure5.8: The displacement of the porous plate with noise in the absence of the air flow.

5.5 CONCLUSION

The insertion loss of the porous plate with and without air flow has been deduced from sound pressure measurements versus frequency. The results show that introduction of air flow increases the insertion loss and shifts the maximum in the TL to lower frequency. Furthermore the plate displacement has been measured. Introducing the air flow in the flow duct has been found to increase the plate deflection.

References:

1. L. Huang, "A theoretical study of duct noise control by flexible panels," J. Acoust. Soc. Am. 106, 1801-1809 (1999).
2. L. Huang, "Experimental study of sound propagation in a flexible duct," J. Acoust. Soc. Am. 108, 624-631 (2000).
3. S. Ramamoorthy, K. Grosh, and T. G. Nawar, "Structural acoustic silencers-Design and experiment," J. Acoust. Soc. Am. 114, 2812-2824 (2003).
4. W. C. Tang, and W. Z. Lin, "Stiff light composite panels for duct noise reduction," Applied acoustics, 64, 511-524 (2003).
5. R. Panneton, and N. Atalla, "Numerical prediction of sound transmission through finite multilayer systems with poroelastic materials," J. Acoust. Soc. Am. 100, 346-354 (1996).
6. R. J. Astley, A. Cummings, and N. Sormaz, "A finite element scheme for Acoustic propagation in flexible-walled ducts with bulk-reacting liners, and comparison with experiment," J. Sound Vib. 150(1), 119-138 (1991).
7. *International Standard ISO* 7235 1991 Acoustics-measurement procedures for ducted silencers-insertion loss, flow noise and total pressure loss.

Chapter 6

QUALIFICATION TEST OF THE IMPEDANCE TUBE

6.1 INTRODUCTION

A large impedance tube has been built to study the effects of vibration on the acoustic properties of the poroelastic plates in the Acoustic Research Centre at the University of Hull. Calibrations have been carried out for three different configurations of the empty impedance tube with a rigid backing. The aim of doing these calibrations is to determine relative pressure against distance (in the x direction) at the plane wave frequency [1-2] and at the standing wave frequency [3], and also, to make sure we get plane waves in the duct.

Chung [4] has presented a theory to measure acoustical properties at normal incidence in the impedance tube. He has decomposed a broadband stationary random acoustic wave into its incident and reflected components by using a simple transfer-function relation between the acoustic pressures at two locations on the tube wall. Chung [5] has presented experimental results to demonstrate the accuracy and the general usefulness of the theory.

Pyett [6] has calculated the specific normal impedance of a layer of anisotropic porous material for a plane wave in terms of two propagation parameters of the material, the characteristic impedance and the propagation constant. Swift [7] has presented an experimental study on the effect of bending vibration on the acoustic properties of thin porous plates. He has also studied a coupling between the solid motion and the fluid motion. Allard [8] has presented methods for impedance measurements in a Kundt's tube and in the free field and obtained the real and imaginary parts of the measured impedance.

6.2 CONSTRUCTION OF THE IMPEDANCE TUBE

A large impedance tube of 6m long with a rectangular internal cross section of 50 cm x 50 cm and a rectangular external cross section of 65 cm x 65 cm (i.e. the thickness of the tube walls is 75mm) has been constructed from concrete to increase the rigidity and mass. The impedance tube is straight with a uniform cross-section and with smooth, non-porous, rigid walls in the test section. Inside of the tube is painted by a high solids epoxy coating (resin component).

The walls of the tube are sufficiently thick and heavy that they are assumed not to vibrate during acoustic measurements. 30 holes of 20mm diameter and of 75mm depth have been made in the top wall of the impedance tube to enable measurements of sound pressure at several places in the tube and hence to evaluate the sound absorption coefficient and acoustical surface impedance of sound absorbing materials. The holes can be closed by aluminium tabs. The design of the impedance tube is shown in Figure 6.1. A rigid steel door of 40 mm thickness is mounted at the one end of the impedance tube. The door is sealed with an adhesive. A loudspeaker is located at the opposite end of the tube from the rigid door.

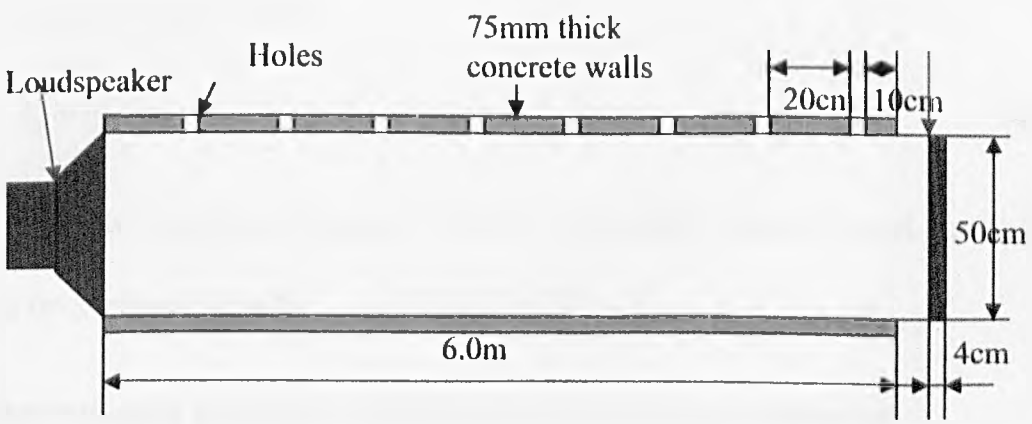

Figure6.1: Design of the impedance tube: dimensions in the figure are not to scale.

6.3 TEST PROCEDURE

6.3.1 Determination of the sound speed

The temperature in the impedance tube is measured by a thermometer. Hence the speed of sound is calculated from the tube air temperature using Eq.(6.1) [1]

$$c_0 = 343{,}2\sqrt{\frac{T}{293}} \tag{6.1}$$

where T is the temperature, in Kelvin.

For a measured temperature, 19°C, the sound speed is 342.7 m/s.

6.3.2 Determination of the cut-off frequency

The cut-off frequency of a rectangular tube is given by [1]

$$f_c < \frac{c_0}{2d} \tag{6.2}$$

where d is the maximum side length of the tube.

For the rectangular impedance tube and a temperature of 19°C, the cut-off frequency, f_c, is below 342.7Hz.

6.3.3 Determination of the wavelength

The wavelength is given by [1];

$$\lambda_0 = \frac{c_0}{f} \tag{6.3}$$

where f is the operating frequency between the cut-off frequency and the lower working frequency of the tube.

6.3.4 Determination of the density of the air and characteristic impedance

The density of the air is calculated from [1]

$$\rho = \rho_0 \frac{P_a}{P_0} \frac{T_0}{T} \tag{6.4}$$

where P_a is the atmospheric pressure in kPa, $T_0 = 293$K, $P_0 = 101{,}325$kPa and $\rho_0 = 1{,}186$ kg/m^3.

The atmospheric pressure of the tube is measured by a barometer. The characteristic impedance of the air is the product of the density of the air and the velocity of sound.

6.4 TESTS FOR PLANE WAVES

Measurements have been carried out in the impedance tube to calculate the relative pressure against distance in the tube for a single input frequency. The end of large impedance tube is closed by a rigid backing. Calibration was carried out for rigid-backing. The relative pressure has been calculated along the x-direction (normal to the tube axis). The reason for these measurements was to make sure that plane waves are produced in the tube. For plane waves the relative pressure along the x-direction should be constant. The experimental arrangement used for the measurement is shown in Figure 6.2.

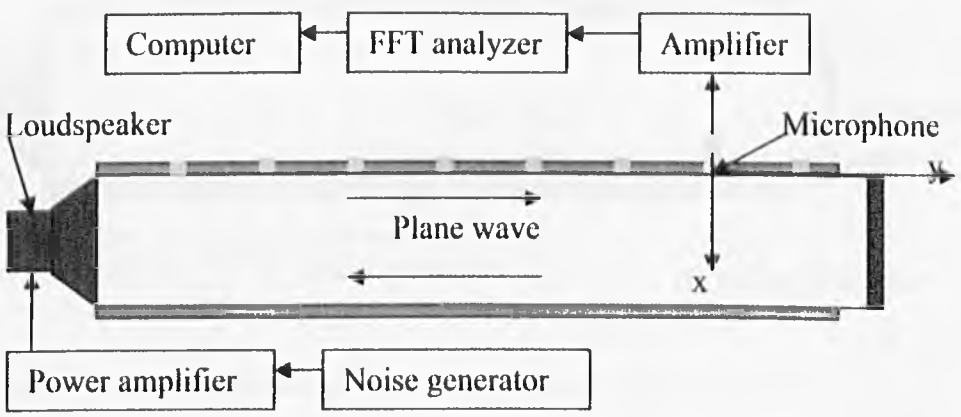

Figure6.2: Experimental set-up of the impedance tube

The acoustic sound field was created by a loudspeaker that is fed with a noise generator, type 1405, and a 600 W power amplifier. A ½in B&K microphone, type 4133, was

mounted with its diaphragm flush with the end of the tube. The microphone grid was sealed tight to the microphone housing. The microphone was supported by a preamplifier which was connected to a B&K measuring amplifier, type 2609. The output of the measuring amplifier was fed to a two channel FFT analyzer, type CF350Z, which was connected to a computer.

Measurements have been carried out also using a probe tube parallel to the axis of the impedance tube. The aim of performing this measurement was to make sure we get constant peak levels. The impedance tube with a probe tube is shown in Figure 6.3. The probe tube has 2mm internal diameter, 4mm external diameter and is 1700mm long. The probe tube was connected to a coupling chamber. A ½in B&K microphone with 50m*V/Pa* sensitivity, type 4190, was fixed to the coupling chamber, and the circumference of the microphone was sealed by adhesive tape. The arrangement and procedure were similar to that shown in Figure 6.2 except for the probe tube.

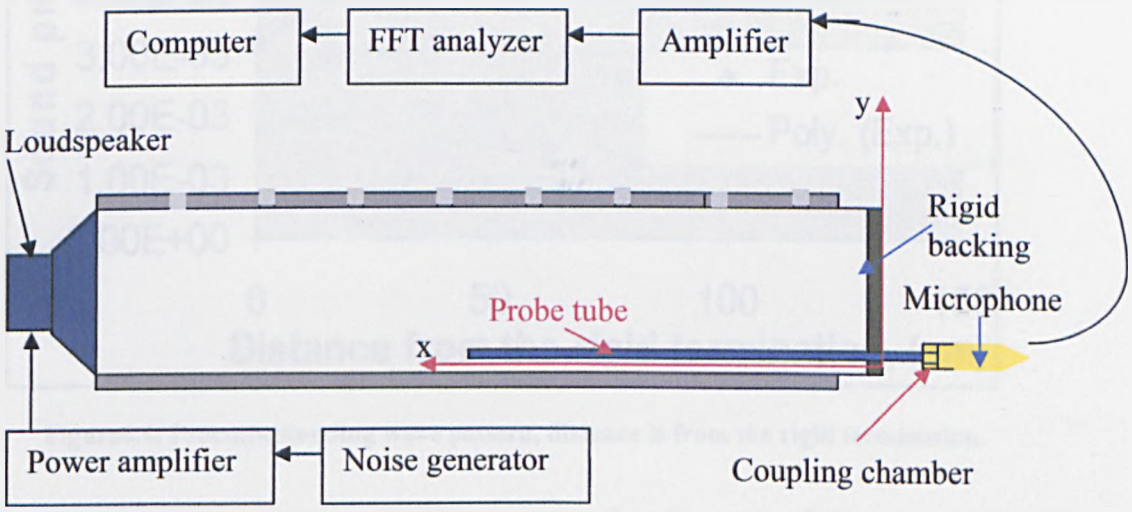

Figure6.3: Experimental set-up of the impedance tube with a probe tube

6.5 RESULTS

The concrete and steel impedance tube has been calibrated according to the recommendation in EN ISO 10534-2:2001 [1]. The pressure standing wave pattern measured in the impedance tube by means of a probe tube is shown in Figure 6.4. The

measurements have been carried out at forty six points on probe tube spaced at 25 mm intervals. 16 averages were carried out on the spectra measured at each microphone positions in order to cancel out interfering noise. The sound pressure was calculated at each position. The half-wavelength, frequency, and the speed of sound that were used are 0.77 m, 222.5 Hz, and 342.7 m/s respectively. The resulting data are shown in Figure 6.4. The dashed line in Figure 6.4 shows the approximation by the 6^{th} degree polynomial trend-line for the results. The two relative pressure peaks in the plot against distance parallel to the tube axis seem to have more or less the same values i.e. although the relative sound pressure standing wave pattern shown in Figure 6.4 is not perfect, it is good enough to support the use of the impedance tube for subsequent measurements.

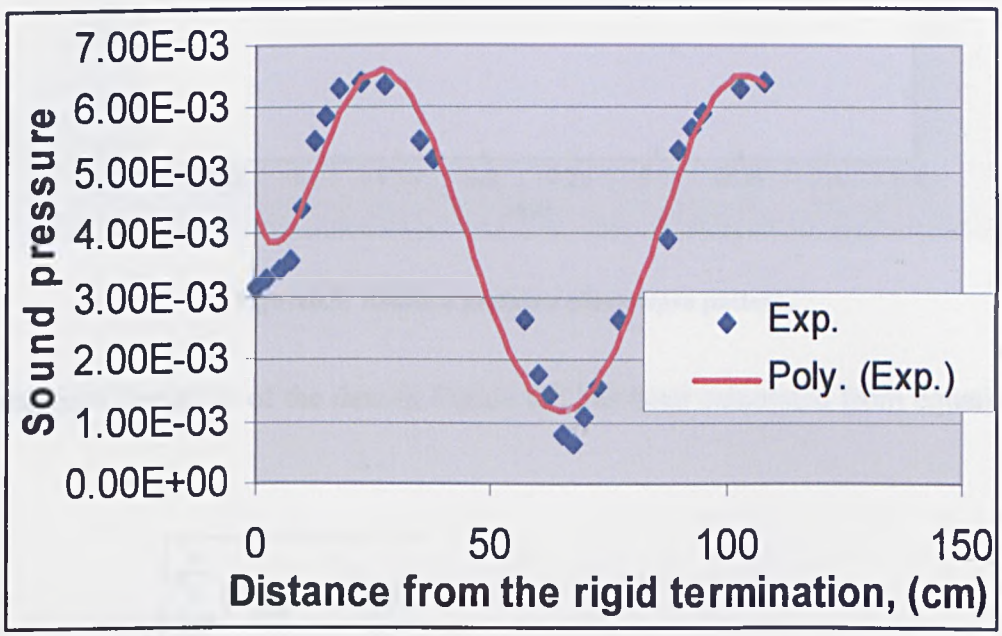

Figure6.4: Pressure standing wave pattern, distance is from the rigid termination.

The results of measurements made along a normal to the axis of the impedance tube using the arrangement shown in Figure 6.2 are shown in Figure 6.5. During the measurements the signal amplitude was chosen to be at least 10 dB higher than the background noise at all frequencies below cut-off frequency. The microphone was inserted through the top surface of the impedance tube at a distance of 50 cm from the rigid termination. Figure 6.5 shows the sound measured pressure plotted against

distance in the x-direction at 138.75 Hz. The relative pressure is more or less constant with distance normal to the tube axis which indicates that plane waves are produced in the impedance tube.

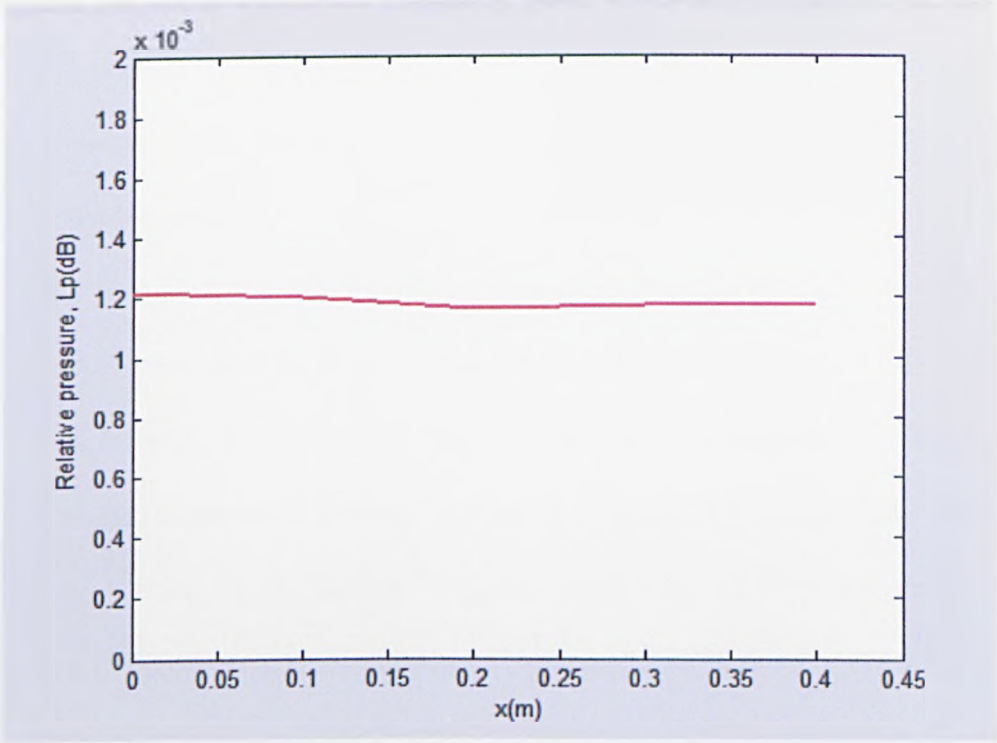

Figure6.5: Relative pressure plane wave pattern.

The standard deviation of the data in Figure 6.5 has been calculated from equation(6.5) [9]:

$$\sigma_{sd} = \sqrt{\frac{\sum_{i=1}^{n}(P_{init} - \overline{P}_{av})^2}{n-1}} \tag{6.5}$$

where n is the number of measurements, P_{init} is the measured relative pressure, and $\overline{P}_{av}$ is the averaged relative pressure by using equation (6.6):

$$\overline{P}_{av} = \frac{\sum_{i=1}^{n} P_{init}}{n} \tag{6.6}$$

The calculated standard deviation is 2.41e-5 dB, i.e. a negligible value.

6.6 CONCLUSION

Qualification tests have been performed on a large rectangular impedance tube using two different configurations. The results obtained from these tests support the assumption that below the cut-off frequency, plane waves are produced in the tube.

References:

1. British Standard EN ISO 10534-2:2001. "Acoustics-Determination of sound absorption coefficient and impedance in impedance tubes. Part 2: Transfer-function method."
2. ISO Standard: E 1050-90. "Standard test method for impedance and absorption of acoustical materials using a tube, two microphones, and a digital frequency analysis system."
3. ISO Standard: C 384-58 (1972). "Standard method of test for impedance and absorption of acoustical materials by the tube method."
4. J. Y. Chung, D. A. Blaser, "Transfer function method of measuring in-duct acoustic properties. I. Theory," J. Acoust. Soc. Am. 68(3), 907-913 (1980).
5. J. Y. Chung, D. A. Blaser, "Transfer function method of measuring in-duct acoustic properties. II. Experiment," J. Acoust. Soc. Am. 68(3), 914-921 (1980).
6. J. S. Pyett, "The acoustic impedance of a porous layer at oblique incidence," Acoustica. Vol.3, 375-382(1953).
7. M. J. Swift, K. V. Horoshenkov, P. Leclaire, D. C. Hothersall, K. Fujiwara, and H. Torihama, "On the effect of the bending vibration on the acoustic properties of thin poroelastic plates," J. Acoust. Soc. Am. 107(3), 1786-1789(2000).
8. J. F. Allard, and B. Sieben, "Measurements of acoustic impedance in a free field with two microphones and a spectrum analyzer," J. Acoust. Soc. Am.; Letters to the Editor. 77(4), 1617-1618(1985).
9. A. Biran, and M. Breiner (1999), "Matlab-5 for engineers," Addison-Wesley, Harlow, England, pp42.

Chapter 7

THE INFLUENCE OF VIBRATION ON THE ACOUSTIC IMPEDANCE

7.1 INTRODUCTION

Measurements in a large impedance tube have been carried out to calculate the absorption coefficient and the acoustic surface impedance, and in order to obtain better understanding of the effects of structural vibration and sound radiation from a clamped poroelastic panel on its surface impedance.

Leissa [1] has carried out an investigation on the vibration of nonporous plates. A widely detailed study of behaviours of plates can be found in [1].

Swift *et al* [2] has presented an experimental study on the effect of bending vibration on the acoustic properties of thin porous plates. The experimental result shows that the surface acoustic impedance is more affected in porous plates with higher values of the flow resistivity as a result from a better coupling between airborne sound and bending vibration in the elastic frame.

Horoshenkov *et al* [3, 4] has studied acoustic response of porous plates and the effect of plate vibration. He has introduced a simple boundary condition as a coupling condition between the plate and surrounding air at the plate surface.

Bies and Hansen [5] have presented a systematic review of the use of flow resistance information and demonstrated the utility of its use for the solution of a wide range of acoustical problems.Takahashi and Tanaka [6] have developed an analytical model by introducing flow continuity at the plate surface in a spatially mean sense and air-solid interaction within the plate material. A detailed work about sound propagation in porous materials can be found in [7].

Chung [8] has presented a theory to measure acoustical properties at normal incidence in the impedance tube. He has decomposed a broadband stationary random acoustic wave into its incident and reflected components by using a simple transfer-function relation between the acoustic pressures at two locations on the tube wall. Chung [9] has presented experimental results to demonstrate the accuracy and the general utility of the theory.

7.2 EXPERIMENTAL SETUP

Experimental measurements have been carried out in the large impedance tube detailed in the previous chapter. General information about the construction of the impedance tube is given in chapter 6. A porous plate (YB10) was used for this measurement. The edges of the plate are clamped in the impedance tube by using a steel frame. All the gaps between the plate and steel frame were sealed by using double sided tape and frame sealant. Porous plate is separated from rigid steel door by an air gap of 60 mm in order to allow bending vibration. Experimental setup is shown in Figure7.1.

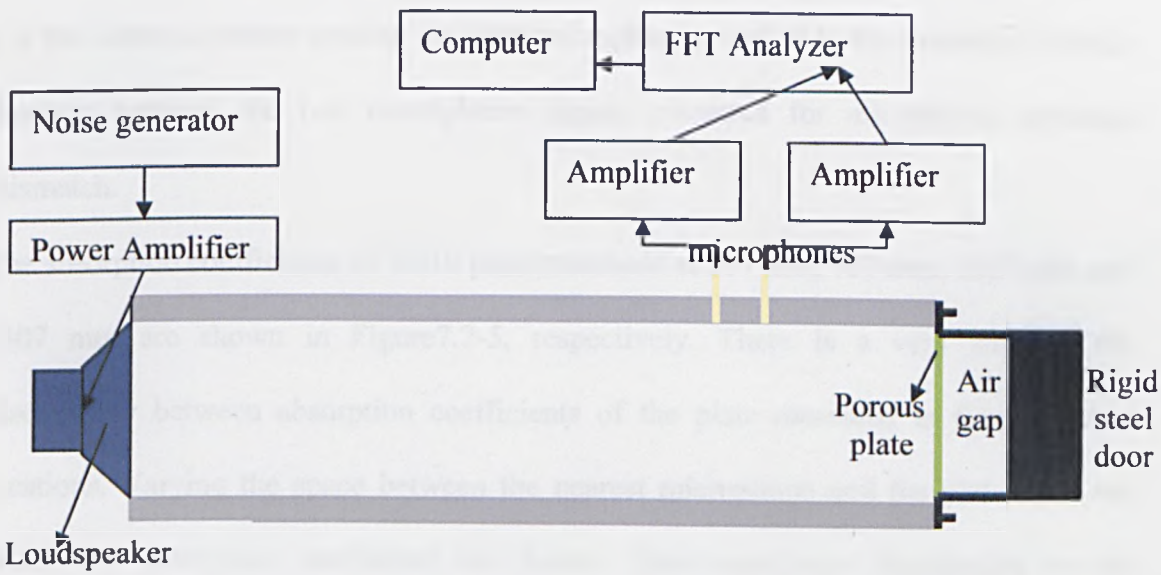

Figure7.1: Experimental setup.

The acoustic sound field was created by a loudspeaker that was fed with a noise generator via a 600 W power amplifier. Two ½in B&K microphones were mounted into microphone grid at positions along the length of the impedance tube. The microphone grid was sealed tight to the microphone housing. The microphones were supported by two preamplifiers which were connected to two B&K measuring amplifiers. The outputs of the measuring amplifiers were connected to a two-channel FFT analyzer which was connected to a computer.

7.3 EXPERIMENTAL RESULTS

7.3.1 Absorption coefficient

Normal incidence sound absorption coefficient of YB10 plate was calculated by;

$$\alpha = 1 - \left|R_c\right|^2, \tag{7.1}$$

where R_c is the complex reflection coefficient which was given by [10]:

$$R_c = \frac{H - e^{iks}}{e^{-iks} - H} e^{j2k(l+s)}, \tag{7.2}$$

where l is the distance from the test sample to the centre of the nearest microphone, and s is the centre-to-centre spacing between microphones, and H is the measured transfer function between the two microphone signals corrected for microphone response mismatch.

The absorption coefficients of YB10 plate measured at 507 mm, 707 mm, 1307 mm and 2307 mm are shown in Figure7.2-5, respectively. There is a very small, 0.03, discrepancy between absorption coefficients of the plate measured at four different locations. Varying the space between the nearest microphone and the plate does not affect the absorption coefficient too much. Three resonance frequencies in the impedance spectrum are observed as shown in Figure7.2-5.

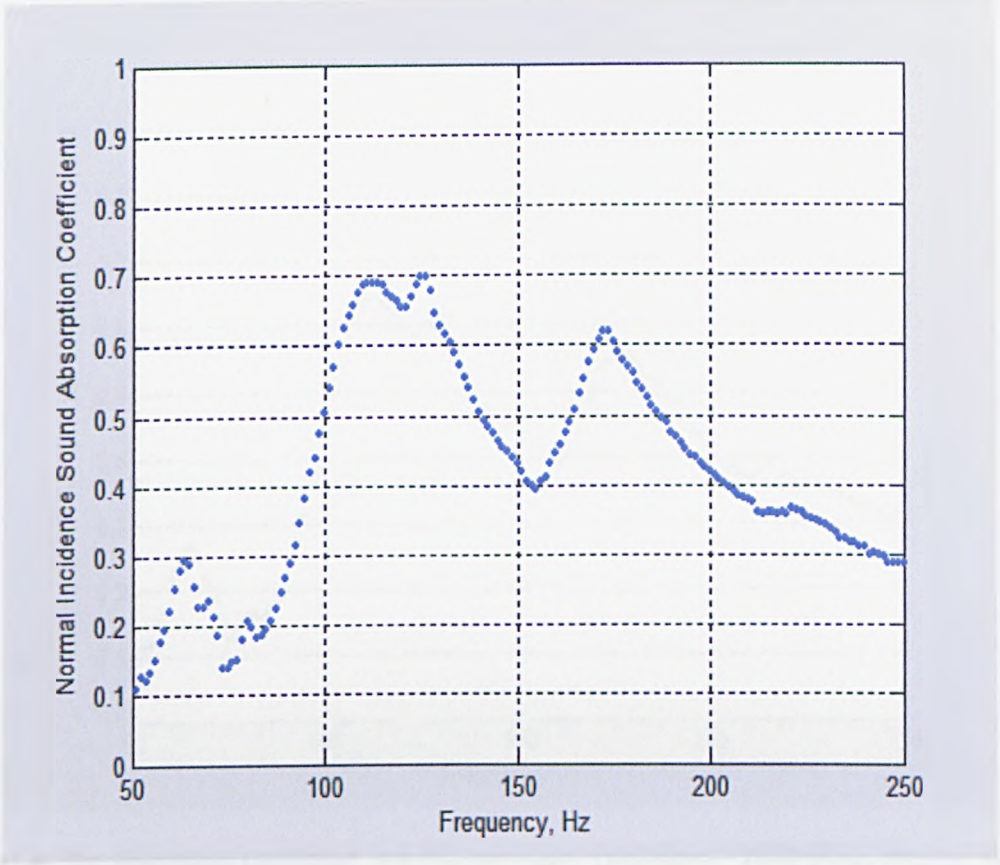

Figure7.2: The absorption coefficient of a 10.7 mm thick rectangular YB10 plate, distance between plate and nearest microphone = 507 mm.

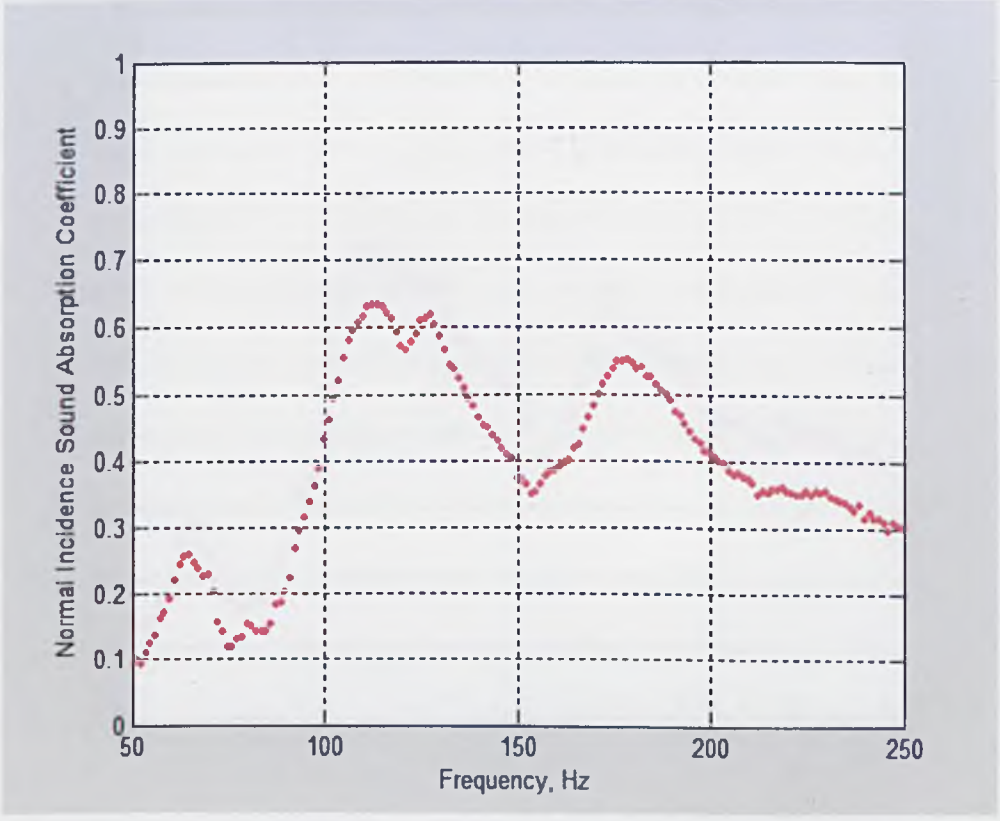

Figure7.3: The absorption coefficient of a 10.7 mm thick rectangular YB10 plate, distance between plate and nearest microphone = 707 mm.

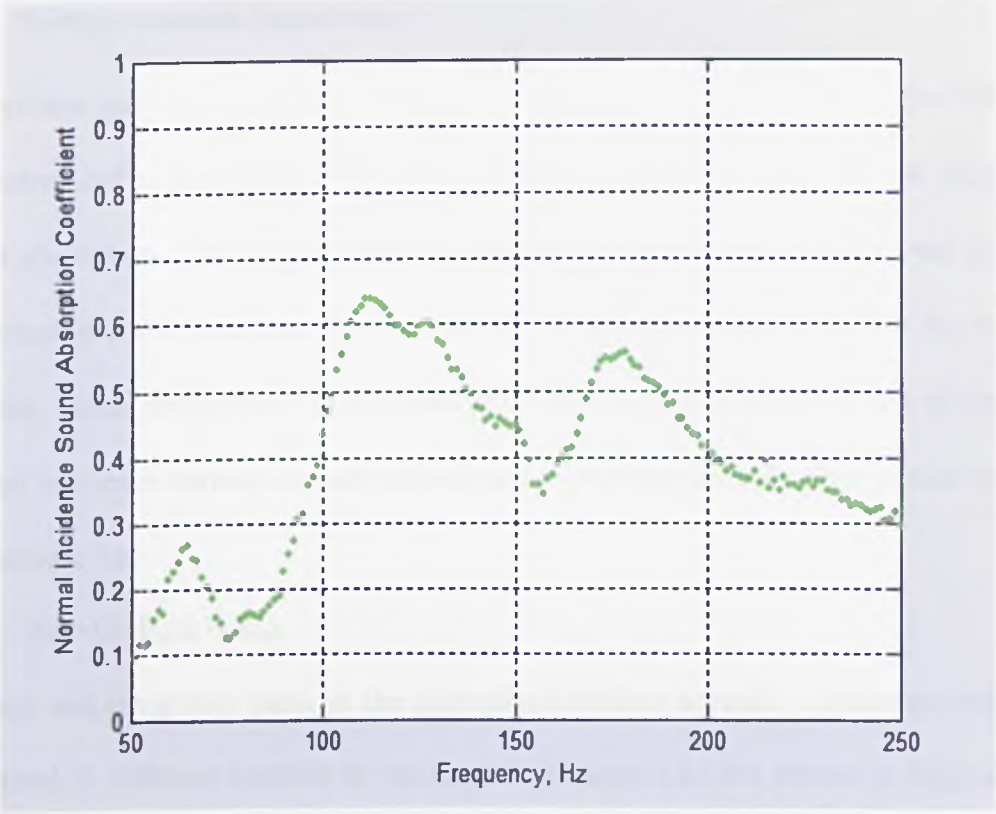

Figure7.4: The absorption coefficient of a 10.7 mm thick rectangular YB10 plate, distance between plate and nearest microphone = 1307 mm.

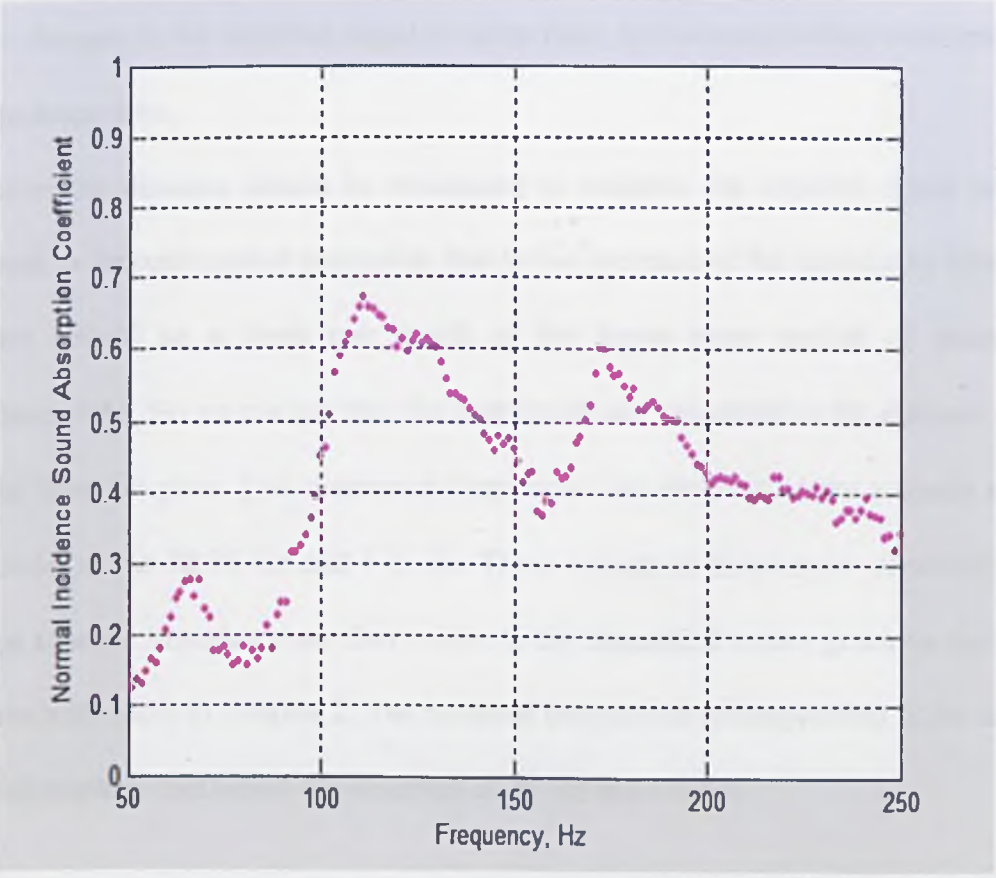

Figure7.5: The absorption coefficient of a 10.7 mm thick rectangular YB10 plate, distance between plate and nearest microphone = 2307 mm.

7.3.2 Surface acoustic impedance

The surface acoustic impedance is an important parameter in calculating the reflection coefficient and in determining the effectiveness of a porous medium for the purpose of sound absorption. The surface acoustic impedance depends on thickness and physical properties of porous material. It also depends on the acoustic impedance of the backing medium. Sound propagation in the impedance tube is normal to the surface of the plate. Normal incidence surface acoustic impedance at the front surface of the porous medium is calculated by;

$$Zs = (1+R_c)/(1- R_c) \tag{7.3}$$

The real and imaginary parts of the normalized surface acoustic impedance which are calculated at different location in the large impedance tube are shown in Figures7.6-9. There is big difference between results at low frequency below 100 Hz. As shown in Figures7.6-9 increasing the distance between the nearest microphone and the plate causes changes in the required signal to noise ratio, is increasing added absorption due to impedance tube.

Therefore the distance should be minimized to maintain the required signal to noise ratio and to decrease added absorption due to the presence of the impedance tube. This distance should be at least one length of the larger cross section of rectangular impedance tube. So we can say that the best results are calculated at the distance of 507 mm far from the plate. Two resonance frequencies are observed in the acoustic surface impedance at the 88.75 Hz and 155 Hz. These resonance frequencies observed in the surface acoustic impedance are fairly close to the theoretical values given by the theory of poroelastic plate in Chapter 2. The resonant frequencies corresponding to the minima in the absorption coefficient are observed at 75 Hz and 155 Hz.

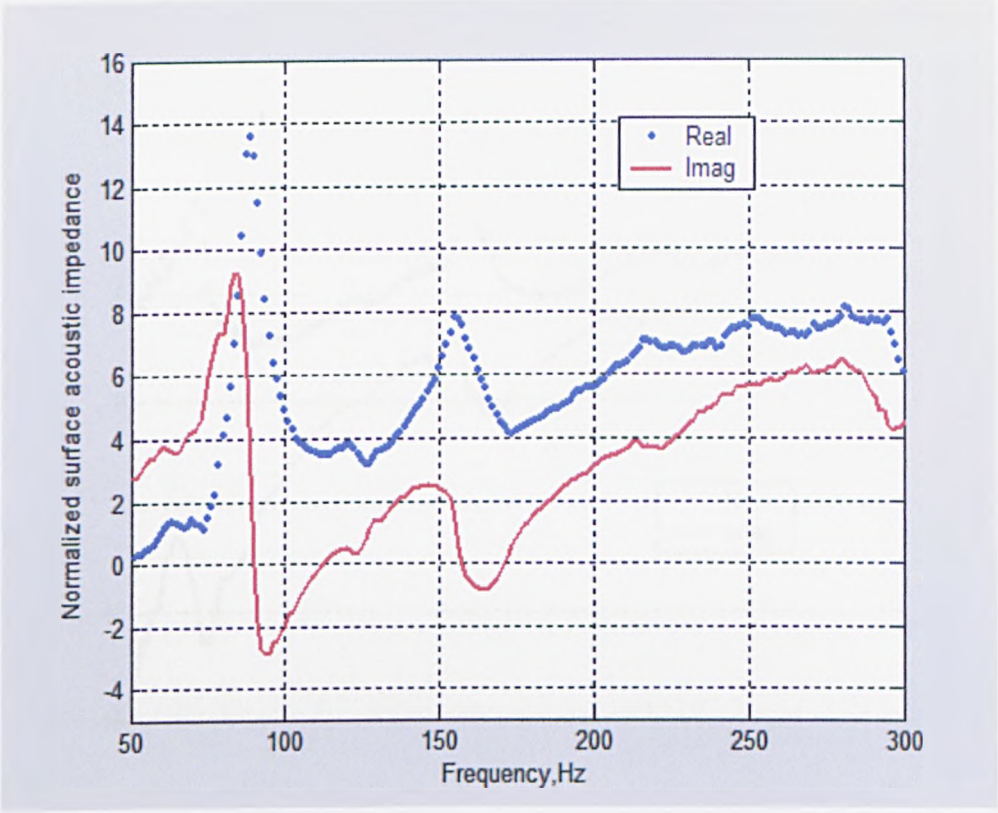

Figure7.6: The real and imaginary parts of the normalized surface impedance of a 10.7 mm thick rectangular YB10 plate, distance between plate and nearest microphone = 507 mm.

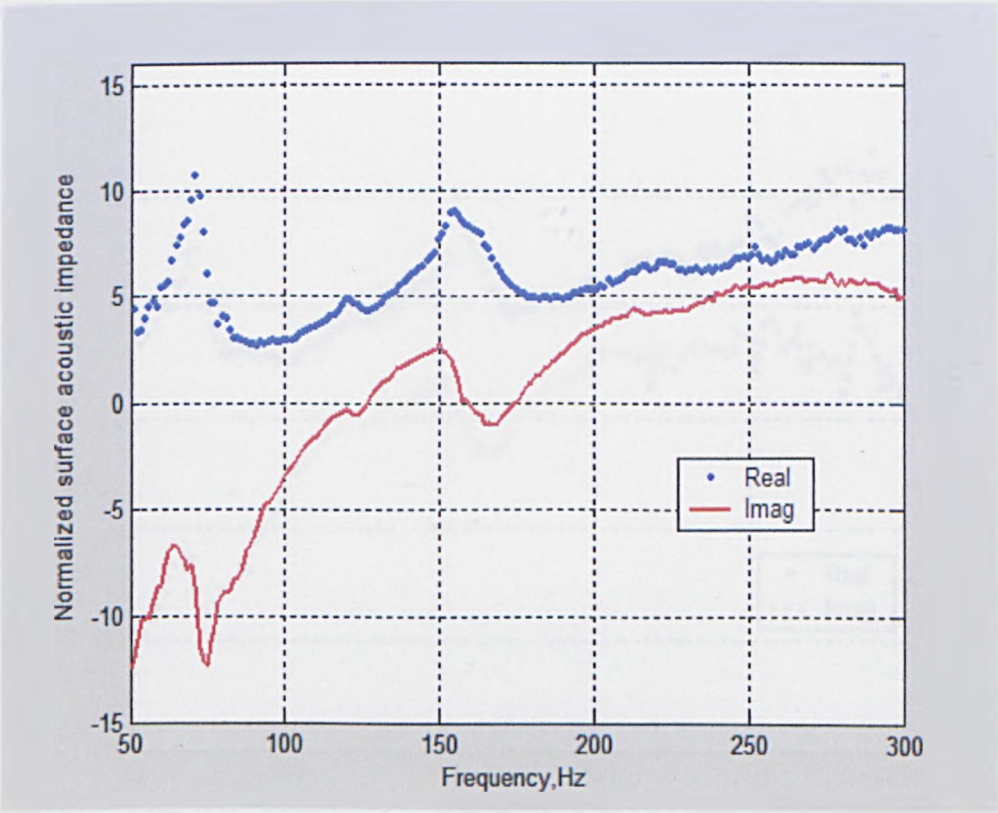

Figure7.7: The real and imaginary parts of the normalized surface impedance of a 10.7 mm thick rectangular YB10 plate, distance between plate and nearest microphone = 707 mm.

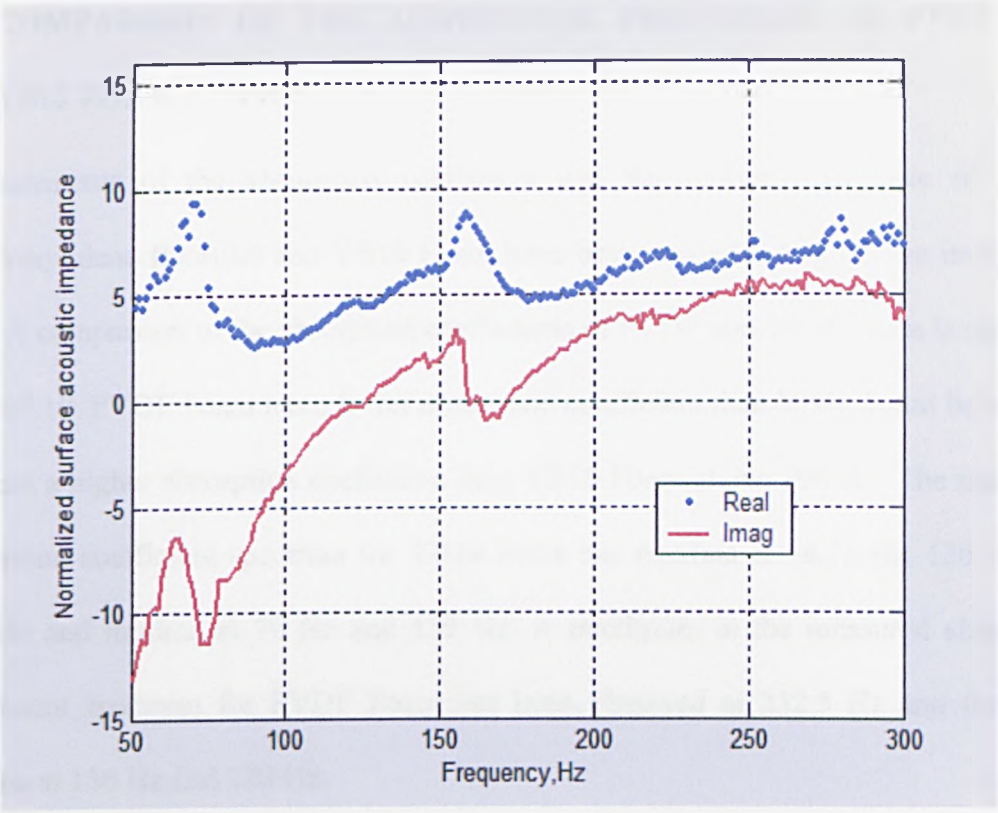

Figure7.8: The real and imaginary parts of the normalized surface impedance of a 10.7 mm thick rectangular YB10 plate, distance between plate and nearest microphone = 1307 mm.

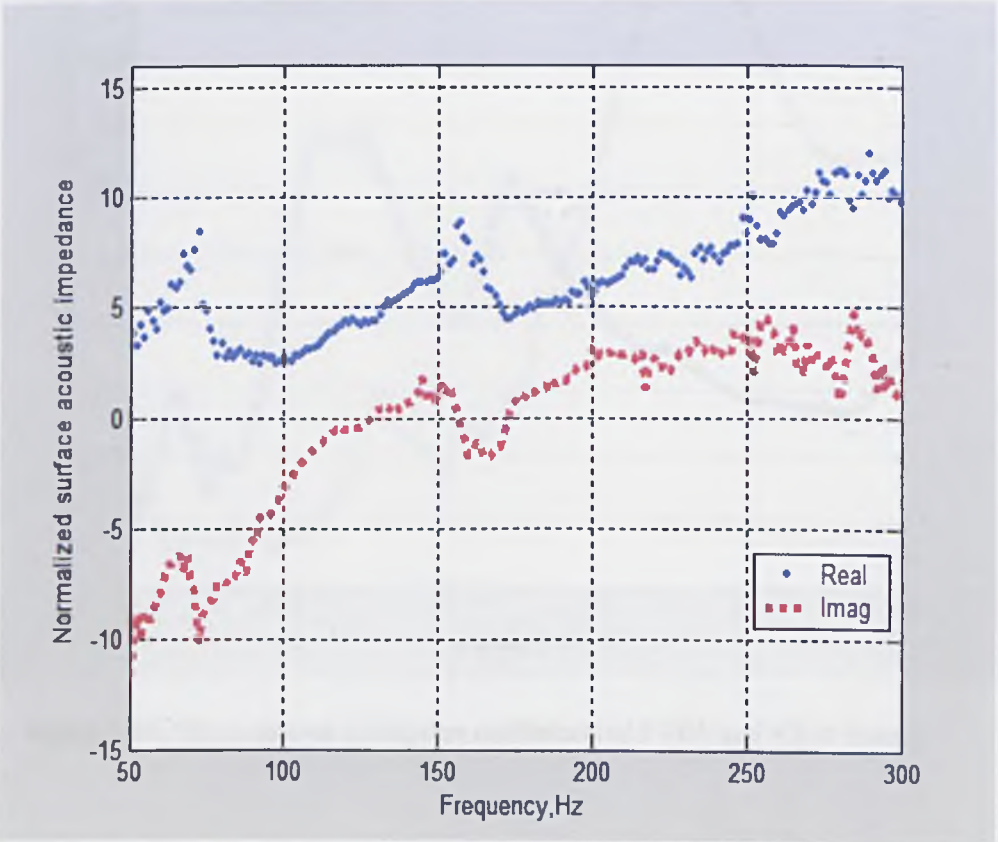

Figure7.9: The real and imaginary parts of the normalized surface impedance of a 10.7 mm thick rectangular YB10 plate, distance between plate and nearest microphone = 2307 mm.

7.4 COMPARISON OF THE ACOUSTICAL PROPERTIES OF PVDF AND YB10 FOAM PLATES

Measurements of the absorption coefficient and the surface impedance of PVDF (polyvinylidene fluoride) and YB10 Foam have been carried out in a large impedance tube. A comparison of the absorption coefficients of PVDF and YB10 Foam is shown in Figure7.10. PVDF Foam has a lower absorption coefficient than YB10 Foam below 190 Hz, and a higher absorption coefficient than YB10 Foam above 190 Hz. The measured absorption coefficient spectrum for YB10 Foam has maxima at 58.75 Hz, 130 Hz and 170 Hz and minima at 70 Hz and 155 Hz. A maximum in the measured absorption coefficient spectrum for PVDF Foam has been observed at 232.5 Hz and there are minima at 150 Hz and 280 Hz.

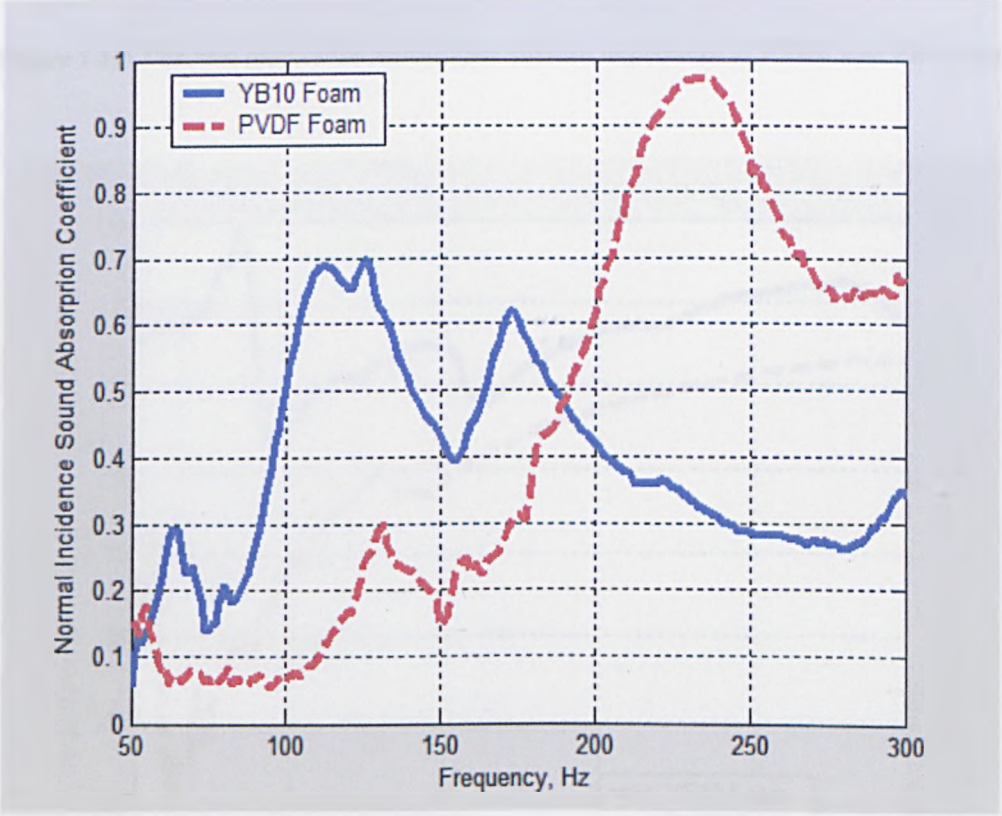

Figure 7.10: The measured absorption coefficients of PVDF and YB10 Foam.

A comparison of the real and imaginary part of the surface acoustic impedance of PVDF Foam and YB10 Foam are shown in Figure 7.11 and Figure 7.12.

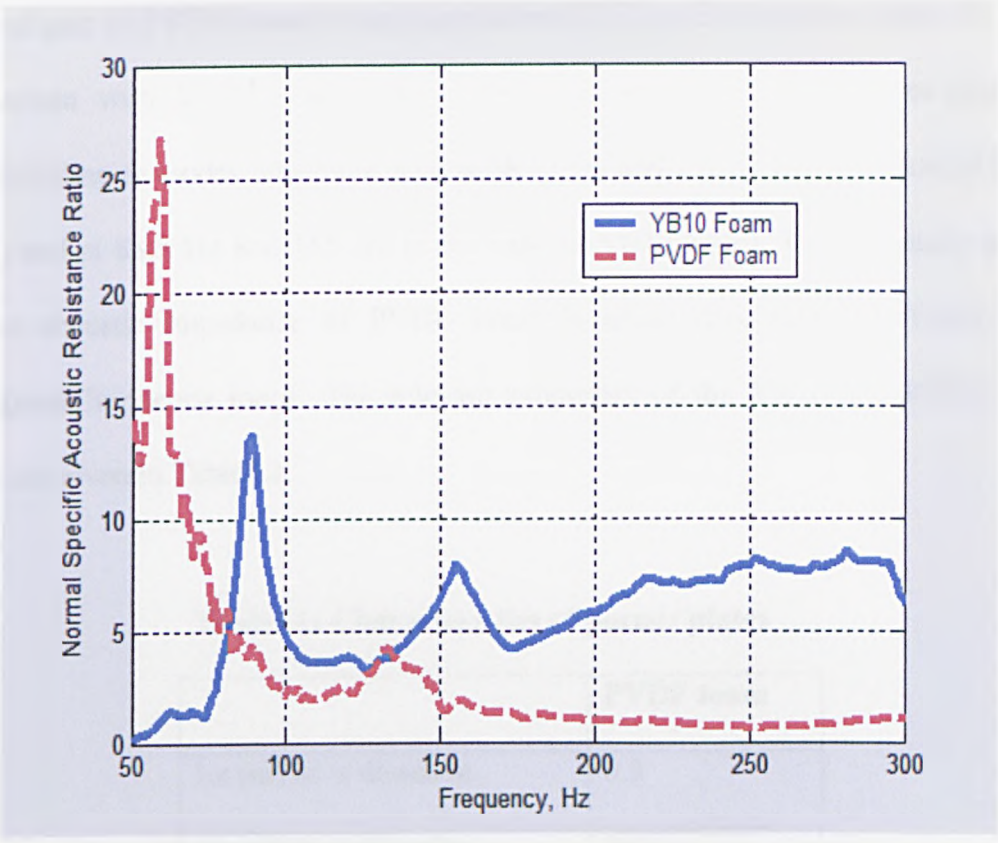

Figure 7.11: The real part of the normalized surface impedance of PVDF and YB10 Foam.

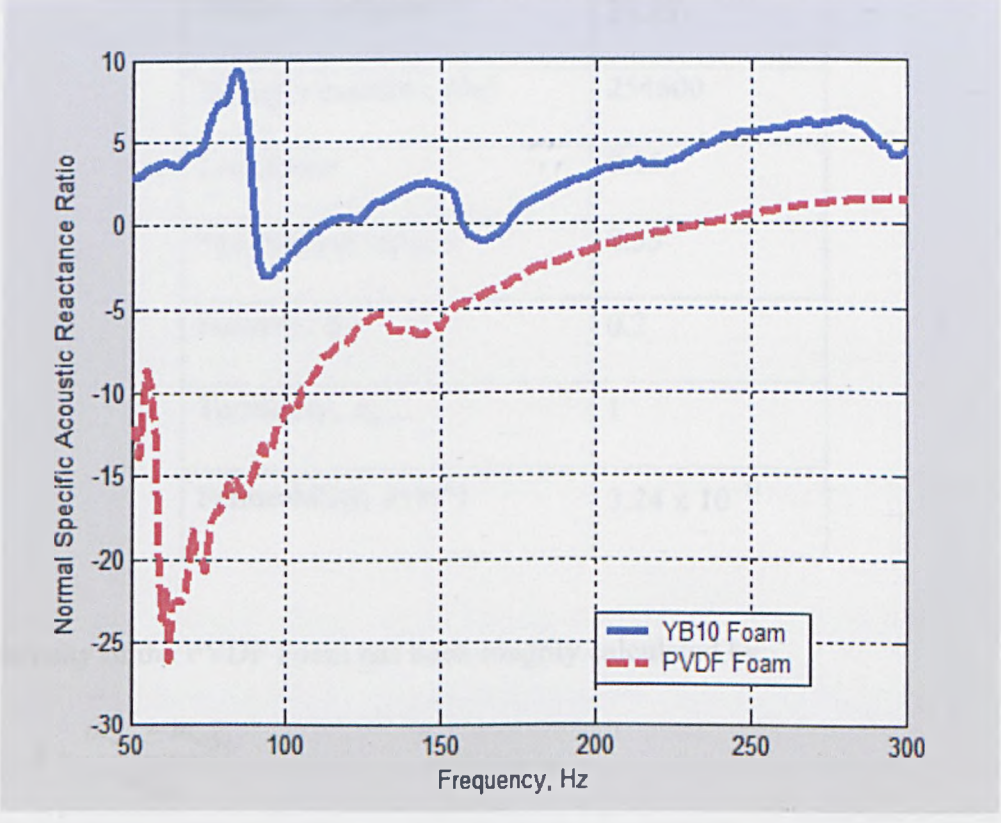

Figure 7.12: The imaginary part of the normalized surface impedance of PVDF and YB10 Foam.

The real part of PVDF Foam is very high below 82 Hz and is very low above 82 Hz in comparison with YB10 Foam. There are resonances in the impedance spectrum corresponding to modes which are seen at 58.75 Hz and 133.5 Hz in the case of PVDF Foam, and at 88.5 Hz and 155 Hz in the case of YB10 Foam. The imaginary part of surface acoustic impedance of PVDF Foam is lower than those of YB10 Foam throughout frequency range. The relevant properties of the YB10 and PVDF Foam plates are given in Table7.1.

Table7.1: Characteristics of porous plates

	PVDF foam
Lx (m) in x direction	0.5
Ly (m) in y direction	0.5
Thickness (m)	0.025
Density, ρ (kg/m^3)	25.15
Young's modulus, (Pa)	254600
Loss factor	0.15
The Poisson ratio, ν	0.35
Porosity, ϕ	0.2
Tortuosity, τ_∞	1
Permeability, $\kappa(m^2)$	3.24×10^{-11}

The porosity of the PVDF Foam has been roughly calculated by;

$$\phi = \frac{m_{wet} - m_{dry}}{m_{wet}} \tag{7.4}$$

Where m_{wet} is the wet mass, and m_{dry} is the dry mass.

The loss factor and tortuosity have been assumed to be equal to 0.15 and 1 respectively. The permeability has been calculated from the measured value of flow resistivity (567700 mks rayls/m). The modulus of elasticity has been deduced from data [11].

The values in Table7.1 have been used to predict the spectra of dynamic deflection response of the PVDF Foam and YB10 Foam plates subject to a harmonic point force excitation (the magnitude of the force is 1 N) applied at x_0 = 0.1 m and y_0 = 0.09 m from a corner of the foam plate. The results are shown in Figure7.13.

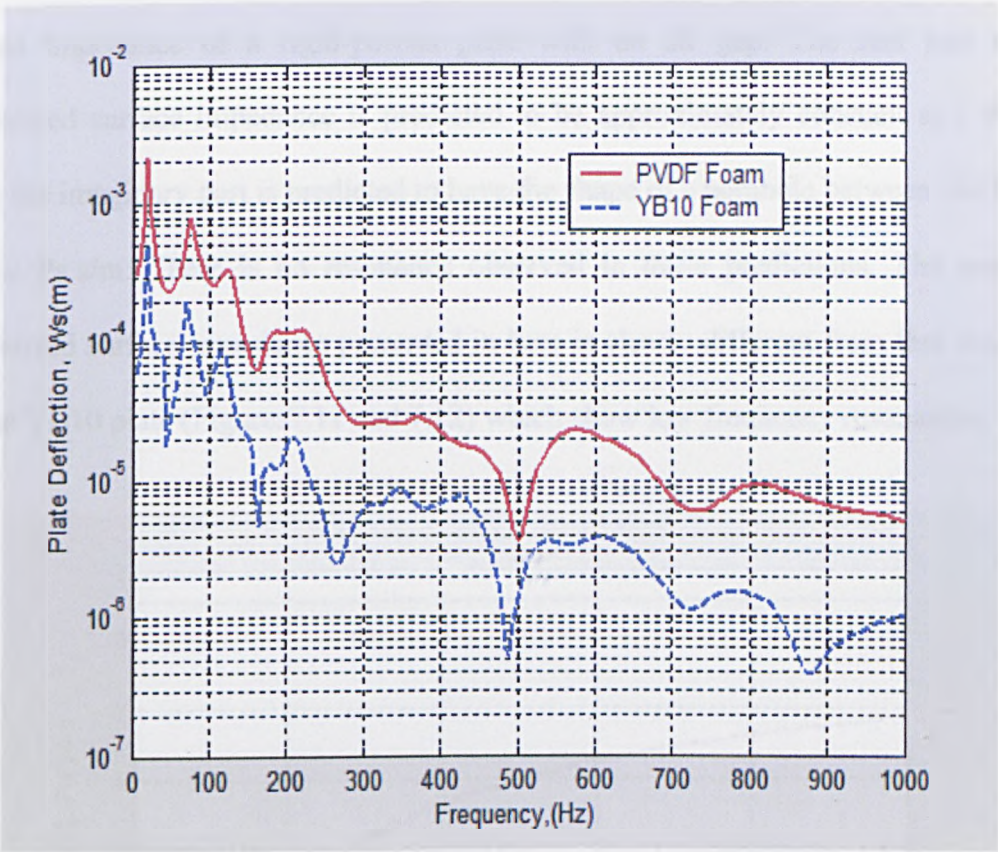

Figure 7.13: A comparison of the predicted deflections of PVDF Foam and YB10 Foam.

By comparing Figures 7.10 and 7.13, it can be seen that the low frequency maxima in the measured normal incidence absorption coefficient spectra are related to deflection minima. The resonance frequencies observed in the surface acoustic impedance are close to the predicted minima in the deflections of the PVDF foam and YB10 foam.

7.5 COMPARISON WITH PREDICTIONS FOR A RIGID-POROUS PLATE

To emphasize the importance of the elasticity of the clamped porous plate calculations have been made of the surface impedance and normal incidence absorption coefficient of a rigid-porous plate with the same pore-related properties as the YB10 plate. Equation4.9 has been used to calculate the surface impedance of the rigid-porous version of the YB10 plate. Allard's methods [7] have been used to calculate the parameters of the rigid-porous plate. Characteristics of the rigid-porous plates are given in Table1.2. Figure7.14 shows the predicted real and imaginary part of the normalized surface impedance of a rigid-porous plate with an air gap. The real part of the normalized surface impedance is predicted to be approximately constant at 1 Pa.s/m, while the imaginary part is predicted to have the shape of a parabola between -14 Pa.s/m and -2 Pa.s/m. There is no resonance observed in these predictions. The predicted normalized surface impedance presented in here is clearly different from that measured for the YB10 plate (Figures7.11 and 7.12) which show low frequency resonances.

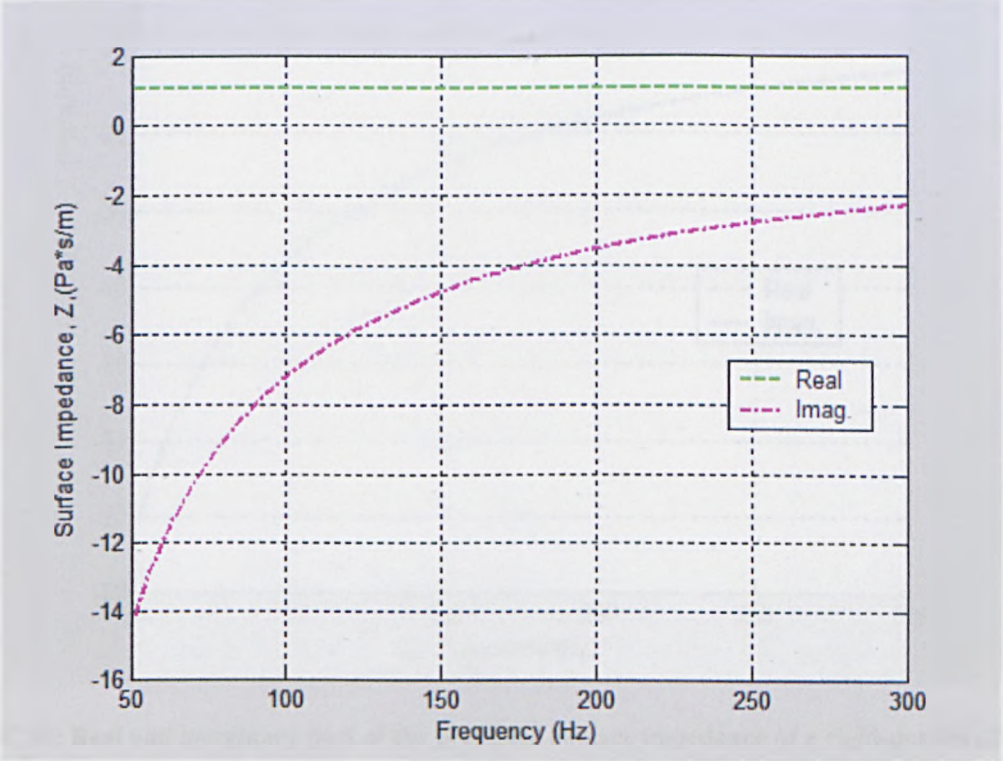

Figure7.14: Real and imaginary part of the predicted surface impedance of a rigid-porous plate with an air gap

The predicted real and imaginary part of the predicted normalized surface impedance of a rigid-porous plate without an air gap is shown in Figure7.15. The real part of the surface impedance is predicted to be constant at about 0.9 Pa.s/m, while the imaginary part of the surface impedance is predicted to have the shape of a parabola between -70 Pa.s/m and -12 Pa.s/m. The predicted normal incidence absorption coefficients of a rigid-porous plate with the same pore-related properties as the YB10 plate with and without an air gap are shown in Figure7.16. The predicted absorption coefficient of a rigid-porous plate with an air gap is increases uniformly up to 0.44, whereas the absorption coefficient of a rigid-porous plate without an air gap is predicted to vary between 0 and 0.023.

According to the results shown in Figures7.10-7.12 and 7.14-7.16 it can be said that the low frequency absorption is determined by the elasticity of the plate.

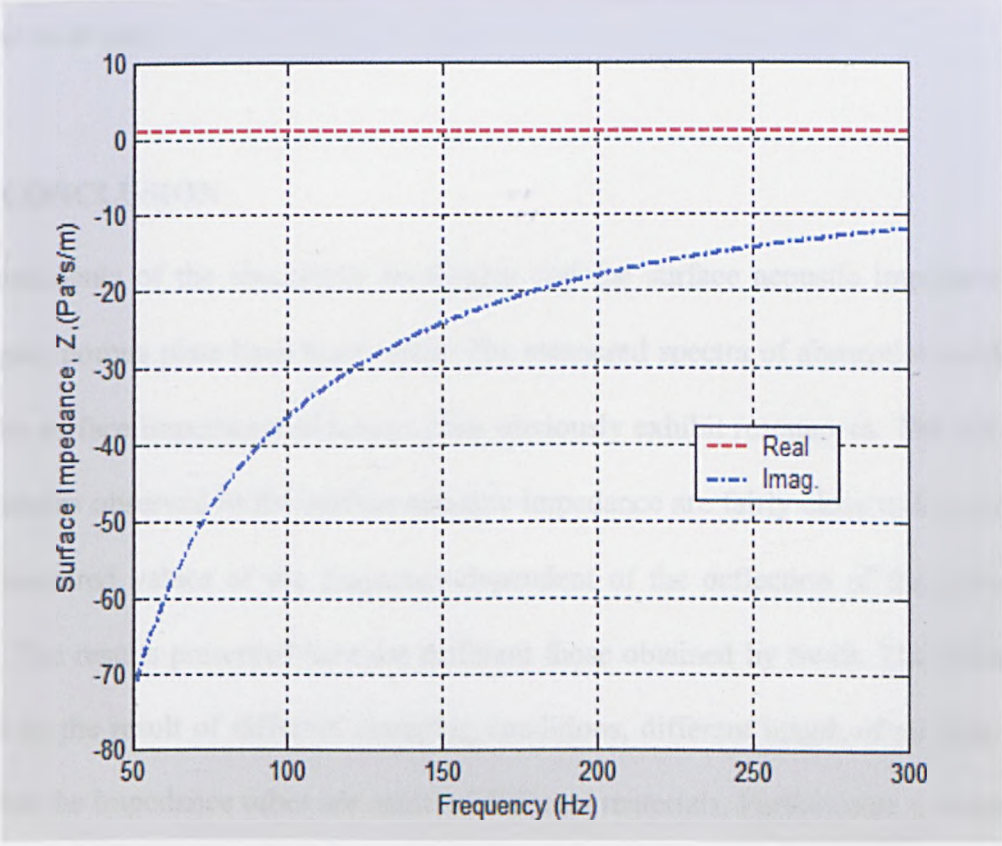

Figure7.15: Real and imaginary part of the predicted surface impedance of a rigid-porous plate without an air gap.

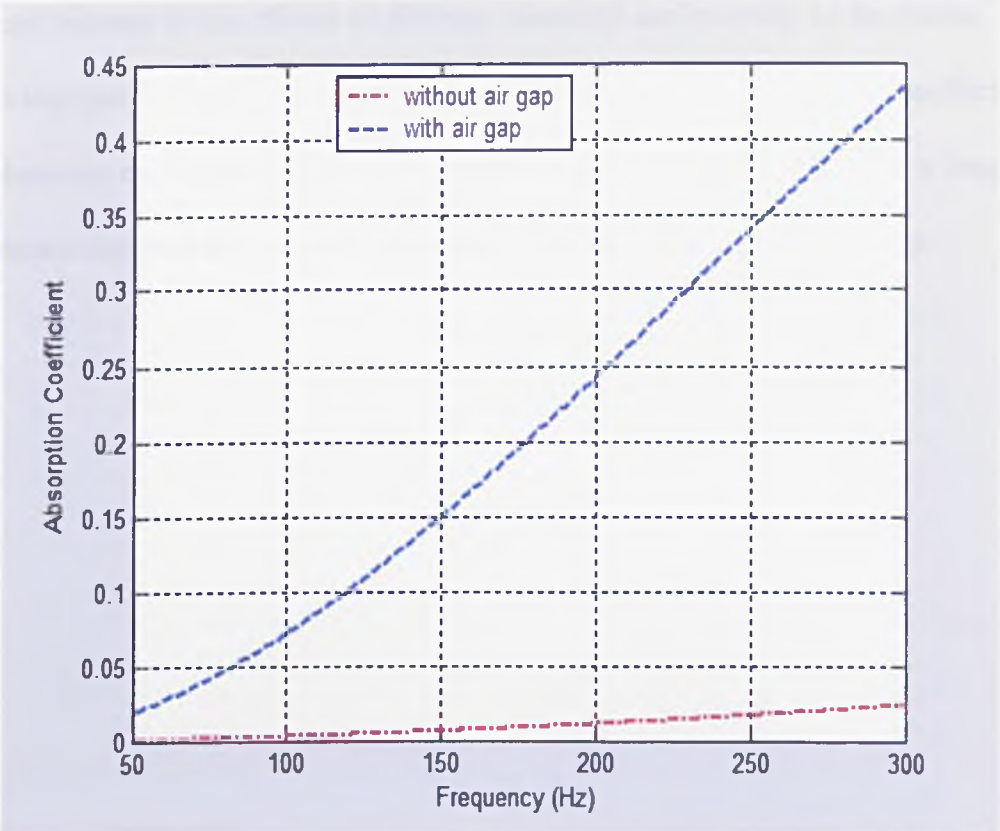

Figure7.16: The predicted normal incidence absorption coefficients of a rigid-porous plate with and without an air gap

7.6 CONCLUSION

Measurements of the absorption coefficient and the surface acoustic impedance of a clamped, porous plate have been made. The measured spectra of absorption coefficient and the surface impedance of porous plate obviously exhibit resonances. The resonance frequencies observed in the surface acoustic impedance are fairly close to the predicted and measured values of the frequency-dependent of the deflection of the poroelastic plate. The results presented here are different those obtained by Swift. The differences might be the result of different clamping conditions, different length of air gap, or the fact that the impedance tubes are made of different materials. Furthermore a comparison of the acoustical properties of PVDF foam and YB10 foam has been presented. The results of the acoustical properties of PVDF foam and YB10 foam are significantly

different because of the effects of different elasticity and porosity of the foams. These results together with predictions of the surface impedance and absorption coefficient of a rigid-porous equivalent of the YB10 plate with air gap suggest that the low frequency resonances observed are primarily the result of the poroelastic plate elasticity.

References:

1. A. Leissa, "Vibration of Plates," J. Acoust. Soc. Am, New York, 1993.
2. M. J. Swift, K. V. Horoshenkov, P. Leclaire, D. C. Hothersall, K. Fujiwara, and H. Torihama, "On the effect of the bending vibration on the acoustic properties of thin poroelastic plates," J. Acoust. Soc. Am. 107(3), 1786-1789(2000).
3. K. V. Horoshenkov and K. Sakagami, "A method to calculate the acoustic response of a thin, baffled, simply supported poroelastic plate," J. Acoust. Soc. Am. 110, 904-917 (2001).
4. K. V. Horoshenkov and K. Sakagami, "Acoustic response of a thin poroelastic plate," in Proceedings of the 16th International Congress on Acoustics (1998), pp. 1897-1898.
5. D. A. Bies and C. H. Hansen, "Flow resistance information for acoustical design," Applied Acoustics 13(1980), pp. 357-391.
6. D. Takahashi, M. Tanaka, "Flexural vibration of perforated plates and porous elastic materials under acoustic loading," J. Acoust. Soc. Am. 112(4), 1456-1464 (2002).
7. J. F. Allard, "Propagation of Sound in Porous Media: Modelling Sound Absorbing Materials," (Elsevier, London, 1993).
8. J. Y. Chung, D. A. Blaser, "Transfer function method of measuring in-duct acoustic properties. I. Theory," J. Acoust. Soc. Am. 68(3), 907-913 (1980).
9. J. Y. Chung, D. A. Blaser, "Transfer function method of measuring in-duct acoustic properties. II. Experiment," J. Acoust. Soc. Am. 68(3), 914-921 (1980).
10. ISO Standard: E 1050-90. "Standard test method for impedance and absorption of acoustical materials using a tube, two microphones, and a digital frequency analysis system."
11. F.L. Scarpa, Aerospace Eng. Bristol. Personal Communication.

8.1 CONCLUSION

The deflection of a non-porous (aluminium) plate has been studied theoretically and numerically for clamped and simply supported boundary conditions. The responses of the clamped and simply supported plate have been calculated at different locations. Furthermore the deflection of clamped poroelastic plates made from recycled automobile dashboards (of two types YB10 foam and G foam) has been measured and predicted. There is a fairly good agreement between the general shapes of the predictions and data as a function of frequency for both plates. The quantitative agreement is best for the YB10 foam plate. The vibroacoustic indicators of a simply supported plate and of clamped porous plates have been predicted. The mean square velocity and the radiated sound power of stiff plates are predicted to be lower than those of the other plates. But the radiation efficiency of stiff plates is predicted to be higher than those of non-stiff plates. The predicted radiation impedance matrix is found to exhibit a smooth variation in terms of frequency.

The fluid-loaded vibration of a clamped porous plate has been investigated through the solution of the governing equations of flexural vibrations. The fluid-loaded deflections of porous elastic plates have been calculated and compared to the predicted in-vacuo deflections. The effect of fluid loading looks more important in porous plates because the porous plates are fairly light and relatively flexible by comparison with an aluminium plate. The predicted frequency responses of the fluid-loaded plate vibration and radiation have been investigated. The location and magnitude of the force during point excitation have been predicted to be very important.

An analytical model that takes into account the effect of perforations in plates and the effect of the flexural vibrations of plates has been presented and used to calculate the

insertion loss and absorption coefficient of plates. The insertion losses of two different types of perforated porous plates have been measured for different perforation ratios in two different configurations in a flow duct with and without air flow. The insertion loss of the perforated porous plates has been predicted only in the absence of air flow. The agreement between measured and predicted insertion loss of perforated porous plates has been found to be tolerably good. For the higher perforation ratio, the measured insertion loss of porous plates was found to be generally decreased. Mounting the plates at different locations in the duct did not affect the measured insertion loss very much in the absence of air flow. But in presence of an air flow, the measured insertion loss of YB10 plates with the higher perforation ratio is increased by mounting the plate closer to microphone.

The transmission loss of the porous plate mounted in the flow duct and separated from the walls by an air cavity with and without air flow has been deduced from sound pressure measurements versus frequency. The results show that introduction of air flow increases the transmission loss and shifts the maximum in the TL to lower frequency. Furthermore the plate displacement is calculated. Introducing the air flow in the flow duct has been found to increase the plate deflection.

Qualification tests have been performed on a large rectangular impedance tube using two different configurations. The results obtained from these tests support the assumption that below the cut-off frequency, plane waves are produced in the tube. Measurements of the absorption coefficient and the surface acoustic impedance of a clamped, porous plate have been made. The measured spectra of absorption coefficient and the surface impedance of porous plate obviously exhibit resonances. The resonance frequencies observed in the surface acoustic impedance are fairly close to the predicted and measured values for the frequency-dependence of the deflection of the poroelastic plate.

8.2 SUGGESTIONS FOR FURTHER WORK

There are still many things to be done in order to understand the acoustical behaviour of poroelastic plates and their potential noise control applications. The effects of fluid loading on the vibration of porous plate have been studied theoretically and numerically. However the effects of fluid loading on the vibration of porous plate should be investigated experimentally also and compared with the predictions. Moreover the fluid-loaded deflections and vibroacoustic indicators of porous elastic plates should be measured and compared with predictions presented in Chapter 3. Furthermore a sensitivity analysis should be done for the effects of fluid loading on vibroacoustic indicators.

A theoretical and numerical study of the acoustical response of a poroelastic plate mounted in a flow duct and separated from wall by an air cavity should be investigated. The radiation and vibration should have the greatest effect at low frequencies while the visco-thermal effect should be significant at higher frequencies. The triple combination of the bending vibration, the presence of the air gap and the higher frequency visco-thermal sound attenuation in porous media is should enable useful acoustic performance over a wide frequency range. Fully numerical methods should be used in the prediction scheme for the acoustic attenuation of the porous plate. Also the use of approximate analytical methods and variational techniques such as Rayleigh-Ritz formulations should be investigated. The results should be compared with the experimental results presented in Chapter 5.

Theory for the acoustical surface impedance, and the absorption coefficient of a porous plate separated from a rigid surface by an air gap and clamped in a large impedance tube should be performed in order to increase the domain of validity of the existing model, and to allow comparisons with the experimental results presented in Chapter 7. Furthermore measurements of absorption coefficient in large impedance tube should be

carried out with 80 mm air gap on the yellow plate for comparison with those obtained by Swift in order to give a more precise understanding of the effects of structural vibration and radiation from a porous plate on its acoustic surface impedance.